UNIVERSITY OF OKLAHOMA

GRADUATE COLLEGE

A COMPREHENSIVE INVESTIGATION ON MICROSCALE PROPERTIES AND MACROSCOPIC BEHAVIOR OF NATURAL EXPANSIVE SOILS

A DISSERTATION

SUBMITTED TO THE GRADUATE FACULTY

in partial fulfillment of the requirements for the

Degree of

DOCTOR OF PHILOSOPHY

By

BOTAO LIN
Norman, Oklahoma
2012

A COMPREHENSIVE INVESTIGATION ON MICROSCALE PROPERTIES AND MACROSCOPIC BEHAVIOR OF NATURAL EXPANSIVE SOILS

A DISSERTATION APPROVED FOR THE
SCHOOL OF CIVIL ENGINEERING AND ENVIRONMENTAL SCIENCE

BY

_____
Dr. Amy Cerato, Chair

_____
Dr. Kanthasamy Muraleetharan

_____
Dr. Gerald Miller

_____
Dr. Kianoosh Hatami

_____
Dr. Megan Elwood Madden

This Dissertation is dedicated to my beloved

Mom and Dad (Qingxiu & Shanke), Wife (Shanshan) and Son (Wilson)

Whose Love and Support contributed to this Achievement

Acknowledgements

I would like to express my sincere gratitude to my advisor, Dr. Amy Cerato, for her continuous support for this study. I deeply appreciate her guidance that brings me into the field of geoengineering, and all of her valuable, insightful discussion and revision of the materials shaping up this dissertation. She is always ready to help with ideas and laboratory supports even when her schedule is packed with numerous teachings and meetings. None of the works in this dissertation could have been accomplished without her remarkable supervision. I also greatly appreciate my committee members, Dr. Kanthasamy Muraleetharan, Dr. Gerald Miller, Dr. Kianoosh Hatami and Dr. Megan Elwood Madden for their fantastic teaching and advising through the past five years, and valuable reviews and comments that helped improve the quality of this dissertation.

Special thanks are given to Mr. Mike Schmitz for his exceptional skills in helping design the laboratory tests; Dr. Andy Madden for his expert guidance in mineralogy and geochemistry; and Mrs. Susan Williams for her patient assistance with all the graduate paperwork. To Rory Victor, Amanda Adams, Juan Pinilla, Wassim Tabet, Nick Hussey, Michaela Campbell, Zach Thompson, Karim Saadeddine, Hoda Soltani, Colin Osborne, Jaime Granados, Chunyang Liu and Charbel Khoury, I want to thank you for the help with my research work and the comic relief you provided.

I would like to extend gratitude to my friends of best acquaintance: thank you for all the wonderful moments we have been sharing through all these years. Most importantly, I want to thank my family--it is your understanding, support and love that sustained me throughout the years to finally make this achievement.

Table of Contents

List of Tables

List of Figures

Abstract

Understanding the complicated behavior of expansive soil requires in-depth exploration of microscopic phenomena under varying situations, especially when the soil stays unsaturated and experiences swell-shrink cycles. This study is dedicated to a comprehensive investigation of eleven micro-scale properties that function as revealing factors of these electro-physico-chemical mechanisms and the associated surface forces. These microscale properties include: specific surface area (S_a), cation exchange capacity (CEC), surface conductance (λ_{ddl}), soil acidity (pH), mineralogy (from X-ray diffraction), structure (from scanning electron microscopy), elemental composition (from energy-dispersive X-ray spectrometry), diffuse double layer thickness (t), real relative permittivity (κ'), effective conductivity (σ) and suction (s). Four naturally collected and two laboratory stabilized expansive soils were selected as the study objects. The roles of some microscale properties in determining the macroscopic behavior of volume change and shear strength have been thoroughly examined through experimental work including three dimensional water content-volume-suction studies and a triaxial test program on unsaturated specimens along three capillary paths. The effects of chemical stabilization by fly ash have also been extensively evaluated from a microscopic point of view.

Some innovative testing and analysis approaches were proposed; highlights include (1) constructing a two-terminal electrode system integrated in conventional oedometer equipment and performing dielectric measurements on natural expansive soils at various hydromechanical stages; (2) quantifying diffused double layer (DDL) in terms of thickness and surface conductance; (3) establishing an unsaturated triaxial test

program based on the predetermined hysteretic soil water characteristic curves (HSWCCs) and the chilled mirror hygrometer tests after shear. Additional newly developed approaches were applied in the studies of soil mineralogy, structure and pore fluid (e.g., assessment of the degree of interfacial polarization and the electrical anisotropy).

This research establishes a comprehensive framework of expansive soil behavior based on experimental efforts and analysis founded in geology, geochemistry, electronics and geomechanics. The outcome will not only help field engineers explain and find solutions for natural threats on civil infrastructure caused by expansive soils, but also provide evidence and a database for verification or improvement of the present geophysical and mechanical constitutive models. Some potential research efforts, especially the imaging of intact soil structure and the adoption of dielectric testing as a common geotechnical practice, are suggested based on the findings of this study.

Chapter 1: Introduction

1.1 Engineering Problems Associated with Expansive Soils

Expansive soil, the type of clayey soil that experiences volumetric swelling or shrinkage with adsorption or desorption of water, covers one-fourth of the United States, and is also distributed worldwide in semi-arid or arid regions in China, Brazil, and the Middle East. Expansive soil poses potential damage to foundations of structures, bridges and roads or induces potential landslides along transportation corridors. On the other hand, expansive soil can be beneficial when used as impervious lining material for canals or irrigation ducts, engineered clay barrier (ECB) material for nuclear waste repositories (NWR) or other types of pollutant containments and disposal sites such as landfills, due to its extremely low hydraulic permeability.

The macroscopic behavior (mechanical properties and responses at the macroscale) of expansive soil in terms of volume change and shear strength is difficult to physically predict because of the high composition of clay platelets/aggregates that are governed by surface physicochemical forces rather than mechanical forces due to their micron size (~2 μm) and the diffuse double layer formed around clay platelets. Consequently, an innovative approach to fully understand expansive soil identification and quantitative movement prediction lies in understanding the ***surface phenomena*** of individual clay platelets (or aggregates) within the soil matrix and the interaction of contacting particles (or aggregates) under the influences of various surface forces. The impact of incorporating such physicochemical fundamental material properties into unsaturated soil mechanics research will provide more accurate parameters for physical models to better predict the macroscopic behavior of unsaturated clays.

Above all, it is necessary to clarify the concepts of microscale properties and macroscopic behavior of expansive soils. Microscale properties are defined in this research project as the soil properties that are determined by the particle/aggregate level electro-physico-chemical mechanisms and indicative of the effects of three independent variables as mineralogy, structure and pore fluid. A group of microscale properties will be introduced later and chosen for detailed exploration. Macroscopic behavior comprises engineering level properties related to volume change or shear strength of an entire soil sample during laboratory tests or in-situ. Common engineering level properties include Atterberg limits (LL, PL and PI), activity (A), density (ρ), void ratio (e), water content (w), dry density (ρ_d, or dry unit weight, γ_d), grain size-distribution, hydraulic conductivity (k), percent of swell (δh), coefficient of linear extensibility (COLE), swell pressure (p_s), wetting/drying-caused and shear-induced volume changes (δv), linear shrinkage (LS), unconfined compressive strength (q_u), saturated/unsaturated drained/undrained shear strength (q) and modulus (E) that represents soil stiffness.

1.2 Conventional Study Methods on Expansive Soils

1.2.1 Common Geotechnical and Physicochemical Properties

The conventional study of expansive soil characteristics can be divided into two categories, namely, the study of microscale properties like clay mineralogy and soil fluid chemistry, and the investigation on macroscopic features such as plasticity and density (Nelson and Miller 1992).

Many researchers have developed empirical relationships to estimate the swelling characteristics of expansive soils based on simple geotechnical properties, including Atterberg Limits, water content, dry density and grain size distribution (Holtz

and Gibbs 1956, Seed et al. 1962, Van der Merwe 1964, Raman 1967, Richards et al. 1984, Chen 1988, McKeen 1992, Lytton 1994, 1995&1997, Puppala et al. 2006a). For example, Seed et al. (1962) presented the equation $SP = KC^x$, where SP is swell potential, K and x are constants depending on clay type and C is clay size fraction (%).

Although these studies were useful in understanding some aspects of expansive soils, there are several problems associated with relationships that depend solely on properties like water content and Atterberg Limits. The first is that Atterberg Limits have high variability (Hammitt 1966, Johnston and Strohm 1968, Ledbetter and Krinitzsky 1982, Koester 1992, Cerato and Lutenegger 2004, Gutiérrez 2006), meaning that a wide range of results for a given soil are typical. Another problem is that the Atterberg plasticity index (PI) is not a fundamental soil property because soils with similar PI's have been shown to exhibit different shrink-swell behavior (Buhler and Cerato 2007) and shear strength characteristics (Puppala et al. 2006a), while soils with similar specific surface area (S_a) and cation exchange capacity (CEC) behave alike (Cerato and Lutenegger 2005). It is the ***surface area*** and ***mineral composition*** of the soil solid phase, and ***available cations*** of the external pore fluid that largely determine the nature and behavior of the soil, namely its internal geometry and porosity, its mineralogy and geochemical composition, its interactions with fluids and solutes as well as its compressibility, strength in the thermodynamic regime. An innovative and fresh aspect to fully understand expansive soil identification and quantitative prediction lies in understanding the ***surface phenomena*** of individual clay particles/aggregates within the soil matrix.

For a given clay species, S_a and CEC are two commonly investigated physicochemical properties that dominate the fine-grained soil behavior. Specific surface area (S_a) is defined as the surface area (m^2) per unit mass (g). It has long been recognized as one of the most important factors controlling many physical and chemical properties of fine-grained soils (Peterson et al. 1996). S_a consists of total S_a, external S_a and internal S_a, with the first being the sum of the last two. The external S_a represents the surface area of clay particles and aggregates exclusive of the areas in the interlayer zones of phyllosilicate unit cell layers whereas the internal S_a comprises areas of interlayer surfaces only (Mitchell and Soga 2005). In this study, the term S_a points to the total one unless otherwise specified. The CEC is the quantity of exchangeable cations required to balance the negative charge on the surface of the clay particle and expressed in milliequivalents per 100 grams of dry soil (Nelson and Miller 1992). CEC reflects surface activity and high CEC values indicate high swell potential of expansive soils (Mitchell and Soga 2005). Combined with the study of CEC is the investigation of pH as a measure of acidity of the soil solute.

Efforts were carried out to correlate the physicochemical properties of S_a and CEC with some macroscopic characteristics. A good example is the previous research in the soil science arena that uses the coefficient of linear extensibility (COLE) to determine the swelling index of a soil. COLE values measure soil swelling using saran-coated natural samples and was first designed for studies of soil classification and genesis; however, it has been translated over the years for engineering evaluation. COLE has been directly related to potential volume change (PVC) and swell index (SI) in tables (Hallberg 1977) and in the form $PVC = 0.12 + 61\ COLE$ (Franzmeier and Ross

1968). There have also been several empirical correlations between CEC and S_a to COLE on soils from Israel reported by Smith et al. (1985) which are $COLE = 0.0007\ S_a + 0.0264$ and $COLE = 0.0034\ CEC + 0.0271$, while Ross (1978) presented different empirical correlations as $COLE = 0.0018CF - 0.0047$ and $COLE = 0.0006\ S_a + 0.0259$ using micaceous soils from Canada (CF = clay size fraction). Even though the S_a is an intrinsic property and should absorb all the mineralogy and geologic differences within the measured value, when using the aforementioned COLE correlations, there would be a 16 % discrepancy in the COLE, and subsequent swelling index predictions for a highly expansive soil (S_a = 800 m^2/g). This is possibly because the linear extensibility is not a simple 1-parameter prediction. Grabowska-Olszewska (1988) presented one of the only correlations between swelling and S_a as δh (%) = $6.1\times10^{-2}\ S_a$ + 10 %, however, this relationship seems to be only valid for certain illitic clays (specific geology and pore fluid chemistry) with S_a values between 146-163 m^2/g.

1.2.2 XRD, SEM, EDXS Approaches

X-ray diffraction (XRD) provides a means to reveal the mineralogical makeup of expansive soils, while scanning electron microscope (SEM) can directly image soil structure. Studying combined results of the XRD and SEM results provides an insightful view of the microscopic nature of expansive soil from which the macroscopic behavior, especially swell potential, can be qualitatively assessed. The volume change and water retention behavior vary with the differences in the mineralogical properties of the clays (Fleureau et al. 1993, Tripathy et al. 2010), while the swelling of natural expansive soils correlates well with percentage of montmorillonite (Al-Rawas 1999, Lin and Cerato 2012a). Meanwhile, the particle/aggregate configuration and alignment

affect the expansive soil behaviors such as water retention (Cui et al. 2006), swelling/shrinkage/consolidation (Ito and Azam 2010), anisotropic swelling (Avsar et al. 2009) and drainage conditions (Langroudi and Yasrobi 2009).

X-rays are high-energy electromagnetic radiation waves with usable wavelengths ranging from 0.25 nm to 0.05 nm (Suryanarayana and Norton 1998). It is possible to utilize X-rays to measure the distance between successive atomic planes (d-spacing) based on Bragg's law and positions of atoms or ions within a crystal. Therefore, the crystal structure can be determined and the corresponding mineral identified. There have been a large amount of investigations on clay mineralogy with the aid of the XRD technique (e.g. Brown and Brindley 1980, Wilson 1987, Moore and Reynolds 1997, Last 2001, Poppe et al. 2001). Several researchers also proposed quantitative mineral analysis methods from the XRD results (Snyder and Bish 1989, McManus 1991, Srodon et al. 2001, Hillier 2003, Omotoso 2006, Dermatas et al. 2007). The United States Geological Survey (USGS) provides an open report on the quantification of mineralogy (USGS 2001), which was adopted in this research project related to the XRD analyses.

Scanning electron microscopy (SEM) has been widely used in the fields of geology, geochemistry, material sciences and biology. The significantly shorter wavelength of the electrons compared to that of visible light enables a much higher resolution in terms of magnifications from 10 X or less to around 200,000 X on most commercial SEMs (England 1991). Applications of SEM have been seen in the field of civil engineering in revealing the effects of structure on the engineering behavior of expansive soils, or vice versa. Al-Rawas and McGown (1999) proposed a qualitative

approach to analyze the SEM images of Omani expansive soil. Al-Rawas (1999) also combined SEM and XRD to investigate the factors controlling the expansive nature of the soils and rocks in northern Oman. Shi and Jiang (2002) used SEM to study the engineering geological characteristics of expansive soils in China. Komine and Ogata (1999), Katti and Shanmugasundaram (2001) made use of SEM to disclose the structure change of expansive soils in response to swelling. Avsar et al. (2009) evaluated the relationship between swelling anisotropy and structure of Ankara clay by obtaining vertical and lateral swell pressures in a thin wall oedometer and by performing SEM observations on undisturbed samples. Langroudi and Yasrobi (2009) elucidated the impact of various drainage conditions on the swelling behavior of unsaturated expansive clay soils through the application of a drainage-controlled uniaxial oedometer cell and the SEM observation. In the meantime, the structure information based on SEM aided in proposing conceptional (Zhang et al. 2004) or constitutive models (Man and Graham 2010) for highly plastic clay. Applications of SEM were also reported in investigations of the structure alterations related to lime/cement or sludge ash stabilizations (Choquette et al. 1987, Lin et al. 2007, Shi et al. 2007).

Several researchers attempted to develop quantitative relationships between SEM micrographs and soil characteristics such as porosity, average particle size, water activity, permeability, and aggregate orientation (Smart and Leng 1993, Frost and Wright 1993, Tovey and Hounslow 1995, Shi and Li 1995, Frost and McNeil 1998, Shi et al. 1998, Martinez-Nistal et al. 1999, Katti and Shanmugasundaram 2001, Montes-H et al. 2003a&b, Liu et al. 2005); mostly through image digitization, binarization and isolation of target objects. However, all of these approaches require significant

simplification of the micrograph complexity that has a resolution down to the aggregate scale while information about the inter-platelet or platelet-aggregate connections is depleted. Moreover, the digitization process is highly dependent on the grayscale of each pixel which is sensitive to the angle the studied object aligned relative to the direction of the electron beam. The methodologies underlying the quantification of SEM images remain immature and subjective. In this regard, the SEM micrographs in this study are subject to qualitative assessment only.

Energy dispersive X-ray spectrometer (EDXS) is usually integrated in an SEM instrument providing qualitative analysis on elemental composition of certain points or regions on a focused image area. The technique was most frequently used to detect chemical formation either naturally occurred (Azam et al. 1998, Zhang et al. 2004) or as a result of soil treatment /stabilization (Lin et al. 2007, Shi et al. 2007).

1.2.3 The Role of Suction

In most cases, in-situ or as-compacted expansive soils remain unsaturated; before soil expansion ever takes place, their behavior is highly affected by surface tension forces at the air-water interface (Nelson and Miller 1992, Fredlund and Rahardjo 1993). Therefore, the examination of hydraulic and mechanical behavior of expansive soil lies mostly within the unsaturated soil mechanics framework. Soil suction is a quantified property descriptive of the free energy of soil water and can be measured in terms of the partial vapor pressure of soil water. McKeen (1992) created a classification model of swell potential based on suction by correlating the soil volume response to suction change with the slope of the suction-water content relationship. Garbulewski and Zakowicz (1995) presented a classification scheme of swell potential

by evaluating the relationship between swell pressure and suction. Lin and Cerato (2012a) evaluated the swell potential of four naturally collected expansive soils based on the matric suction values at their initially compacted states. Some other researchers (Delage et al. 1998, Alonso et al. 1990, Alonso et al. 1995, Alonso et al. 1999, Romero et al. 1999, Alonso et al. 2005, Nowamooz and Masrouri 2008) worked on volume evolutions of expansive soils during wetting-drying (or swell-shrink) cycles under constrained suction values. A variety of test methods and applications of soil suction in the heave prediction were covered in the book of Nelson and Miller (1992).

Soil suction consists of three components (Fredlund and Rahardjo, 1993): matric suction, which is the capillary force at the air-water interface and defined as the difference between pore air pressure and pore water pressure; osmotic suction, which arises from the forces on water molecules as a result of the chemical composition of the soil, and total suction, the sum of the former two. Matric suction has been widely believed to be the crucial component in determining the hydraulic and mechanical behavior of unsaturated soils while osmotic suction was commonly assumed as constant for a specific soil regardless of varying hygroscopic conditions and most often dismissed for its role as a component of total suction (Fredlund and Rahardjo 1993). The effects of matric suction on the hydraulic and mechanical behavior of unsaturated soils have been thoroughly discussed in the book of Fredlund and Rahardjo (1993) and some more recent works will be reviewed in later sections.

1.3 Recent Experimental Advances

Besides the abovementioned microscale properties including physicochemical properties (S_a, CEC, pH), mineralogical and structural characteristics (XRD pattern,

SEM micrograph, EDXS elemental spectrum) and soil suction which have long since been investigated, recent study developments on expansive soil/clay benefited from latest advances in equipment technologies dealing with soil structure. Among those techniques, mercury intrusion porosimetry (MIP) and environmental scanning electron microscopy (ESEM) have been given special attention in the structure studies focused on the investigation of soil structure at particle/aggregate scale less than 100 μm (Romero and Simms 2008).

MIP is used to quantitatively describe the microporosity structure by measuring the relationship between cumulative pore volumes and pore radius, based on the Washburn equation applied for cylindrical pores and parallel infinite plates (Juang and Holtz 1986, Webb and Orr 1997) that the entrance pore radius is inversely proportional to the pressure applied to mercury to enter the pore. A typical MIP result includes a graph presenting the logarithmic differential of intrusion function (or pore size distribution function, PSD) versus entrance pore size (Romero and Simms 2008). The major contribution of the research efforts applying MIP on natural or compacted clayey soils is confirmation of the existence of their dual-structure (***macrostructure*** and ***microstructure***) characterized by two standing PSD peaks at around 0.02~0.3 μm and 7~10 μm (depending on soil type), respectively (Romero and Simms 2008). The first peak highlights the volumetric accumulation of intra-aggregate micropores that are determined by interactions between clay platelets (described as "microstructure"). The second describes the inter-aggregate macropore volume that is controlled by aggregate/cluster shapes, alignment, orientation and contact style (depicted as "macrostructure"). The inter-aggregate volume decreases with densification, suction

and the number of weathering cycles, whereas the intra-aggregate space well sustains these effects (Simms and Yanful 2002, Li and Zhang 2009). Extended efforts were carried out on the PSD for correlation with the hydraulic behavior of clayey soils like SWCC and water permeability (Romero et al. 1999, Simms and Yanful 2002&2005) or for quantified characterization of structure (Romero et al. 1999, Nowamooz and Masrouri 2008&2009, Li and Zhang 2009, Koliji et al. 2010). The feasibility of the technique in the development of correlations with engineering level properties is quite restrained.

It is desirable to acquire immediate observation of intact soil structure. This was made possible by the application of ESEM in such a way as to maintain specific environmental conditions varied through a range of vapor pressures or temperatures (Baker et al. 1995, Komine and Ogata 1999, Komine and Ogata 2004, Zhang et al. 2004, Maison et al. 2010). No sample desiccation and coating are required; as a result, the micrographs are more reflective of what the soil is like in reality in comparison with those done by conventional SEMs. The main drawback of ESEM is associated with the image quality in terms of contrast and brightness which strongly depends on the chamber humidity (Maison et al. 2010). The observed images could be dimmed by interference of water to various degrees and some associated particle alignment information may be lost. The compromised resolution makes ESEM compare unfavorably with conventional SEM that is able to produce micrographs of high resolution (Romero and Simms 2008).

Another promising but still under-development technique in structure studies is neutron computed tomography (CT). Application of the technique was reported by

Koliji et al. (2010) in assessment of three-dimensional structure evolution of an aggregated soil in response to various vertical stress and matric suction conditions. Still, the evolution was analyzed in a rather qualitative than quantitative way, and largely in a conceptual rather than practical stage.

1.4 Microscale Properties and Macroscopic Behavior Investigated

1.4.1 Microscale Properties Chosen for Investigation

In order to physically describe the macroscopic expansive soil properties and responses from a microscopic point of view, two aspects were addressed: 1. advancing the understanding of microscale properties; 2. deriving various relationships, preferably in a quantitative way, of these properties with the macroscopic behavior. To achieve these goals, the types of microscale parameters were carefully chosen, and some representative macroscopic behaviors were required to be qualitatively described or quantitatively characterized. The microscale properties chosen in this research program are introduced and justified here.

S_a, CEC, pH and surface conductance λ_{ddl} were chosen as microscale physicochemical properties. These items are regarded as the inherent soil properties that depend only on composition, regardless of water content, pore fluid chemistry, and time, etc.; and therefore are fundamental in describing the fine-grained soil behavior. CEC, a function of S_a and surface charge density, should be used in conjunction with S_a to help predict expansive soil behavior by using pore fluid chemistry constituents (i.e., pH, temperature and cation concentrations), which have been shown to be extremely important in microscopic soil behavior (Hillel 1998, Mitchell and Soga 2005). It is not

surprising that geotechnical engineers have by and large overlooked this area of work because much of the literature related to these properties of clays appeared in journals associated with the disciplines of geology, soil science, ceramics and chemistry. From the S_a and CEC data, a more comprehensive property, surface conductance λ_{ddl}, can be estimated as the product of surface charge density and cation mobility (Santamarina et al. 2001), which is written in the following form (Lin and Cerato 2012a):

$$\lambda_{ddl} = \frac{\sum u_i P_i \cdot CEC}{S_a} \qquad \textbf{(1.1)}$$

Where u_i is cation mobility; P_i, is percentage of each exchangeable cation (in quantity). The mobility for cations such as K, Mg, Ca, Na and H is 7.6, 5.5, 6.2, 5.2, 36.2 ($\times 10^{-8}$ $m^2V^{-1}s^{-1}$), respectively; according to the mobility chart of cations provided by Santamarina et al (2001). Cation mobility is an ion property determining the drift velocity of electrons it can mobilize under an applied electrical field. Further discussion on the assumptions and limitations of Equation 1.1 will be presented in section 2.2. In this study, the calculated surface conductance of each soil sample accounts for the soil portion passing the No. 40 U.S. sieve. Since more than 95 % of particles passed the No.40 U.S. sieve for all the samples studied, it can be well assumed that the conductance is representative of the entire soil sample.

The engineering features of expansive soils are influenced by their geological and geochemical features which embrace a variety of information from the studies of XRD pattern, SEM micrograph and EDXS spectrum. In this regard, these techniques are of significant importance in this research for the expansive soils concerned, as they were selected for microscale investigations within the geology discipline regime. It

must be noted here that except for SEM micrograph, which was in some degree associated with sample compaction, the other aforementioned microscale characteristics (S_a, CEC, pH, and λ_{ddl}, XRD pattern, EDXS spectrum) are reflective of the intrinsic nature of the particles of a soil irrespective of its hygroscopic status; neither are they informative of or related to stress history and sampling condition of the soil. Although these properties are important for understanding the microscopic mechanisms, others that are capable of reflecting the sample states (moisture content, density and disturbance) are also desired for detailed investigation, which are diffuse double layer thickness, real relative permittivity, effective electrical conductivity and suction. These four important microscale properties will be discussed in detail later.

The volume change of clay particles in response to adsorbate sorption (or desorption) largely include two parts. The first part known as ***crystalline swelling*** is controlled by interlayer forces that cause hydration of crystalline surfaces (e.g., hydrogen bonding) (Yong 1999, Likos and Lu 2002, Likos and Lu 2006, Laird 2006). Crystalline swelling is confined to the first several water layers (2~4 layers, depending on the particle composition and the aqueous chemistry) in the external surface of the tetrahedral sheet (limited by outer Helmholtz plane, or stern layer; Yong 1999). Therefore, it describes the water holding capacity of clays at very low water contents (i.e., crystalline swelling takes place as a result from the hydration process upon first exposure to water or water vapor), and therefore has been explored mostly in the clay sciences regime. The second part, described as ***double-layer swelling*** (Yong 1999, Laird 2006) or ***osmotic swelling*** (Mitchell and Soga 2005, Likos and Lu 2006), originates from the chemical ionic gradient in between the phyllosilicate surface and the

external environment (i.e., liquid phase in macropores). This volume change is manifested by expansion (or contraction) of the diffuse layer (interlayer or interlamellar swelling or shrinkage beyond the stern layer) and governed by the interplay between surface forces like capillary force, Coulombian electrostatic attraction, van der Waals force and double layer repulsion (Mitchell and Soga 2005, Amarasinghe and Anandarajah 2011). In consequence, osmotic swelling controls the macroscopic behavior of expansive soils, from an engineering point of view, and will be the focus of this study.

As a result, the macroscopic behavior of expansive soils, at an engineering scale, comes from their microscopic behavior, which is further dependent on the surface forces within the soil matrix. These surface forces are electro-physico-chemical forces created by three independent variables: mineralogy, structure and pore fluid. Here the term "structure" is referred to "fabric" insofar as to describe the information of soil particle geometry, alignment, aggregation and packing in this research. The variables exclusively determine the overall effects of various surface forces on the macroscopic behavior. It must be noted that the term "independent" points to their individual physical role though these variables are bound to interact with each other in multiphase porous media. For instance, part of the pore fluid transforms to adsorbed water film on clay particles described as bound water. In this context, the interparticle interactions are governed by surface forces through the medium of bound water of which the properties are dependent on both soil mineralogy and pore fluid. Likewise, electro-kinetic flows and forces take place in between pore fluid and bound water.

Identification and quantification of the aforementioned surface forces can be extremely challenging. Instead, this study attempts to explore eleven microscale properties that can reflect the interplay of the three independent variables, including specific surface area (S_a), cation exchange capacity (CEC), surface conductance (λ_{ddl}), pH, mineralogy (XRD), structure (SEM), elemental composition (EDXS), diffuse double layer thickness (t), real relative permittivity (κ'), effective electrical conductivity (σ), and suction (s). The capability of the eleven microscale properties in describing the three variables can be demonstrated by Table 1.1 below.

Table 1.1 Capability of the microscale properties in studying the three variables

Micro-scale properties	**Mineralogy**	**Structure**	**Pore fluid**
Specific surface area, S_a	**x**		
Cation exchange capacity, CEC	**x**		
Surface conductance, λ_{ddl}	**x**		
Soil acidity, pH	**x**		
Mineralogy (XRD)	**x**		
Structure (SEM)	**x**	**x**	
Elemental composition (EDXS)	**x**		
Diffuse double layer thickness, t	**x**	**x**	**x**
Real relative permittivity, κ'	**x**	**x**	**x**
Effective electrical conductivity, σ	**x**	**x**	**x**
Suction, s	**x**	**x**	**x**

Table 1.1 implies that the diffuse double layer thickness (t), real relative permittivity (κ'), effective electrical conductivity (σ) and suction (s) have the capacity of

revealing the effects from all the three independent variables that control the surface forces, and in turn, govern the macroscopic behavior of expansive soil. In consequence, these four properties are not only dependent on, but also reflective of, the sample states, as mentioned earlier.

1.4.2 Macroscopic Behavior Investigated

The macroscopic behavior is investigated to envelop most of the scenarios in real life where the nature of expansive soil controls engineering designs or poses potential hazards. At this point, the behavior can be categorized into two primary fields of study: change in volume and evolution in shear strength.

The topics of volume changes covered in this research encompass settlement due to compression or shrinkage, rebounding caused by unloading, heave attributed to expansion and deformation induced by shear stresses. The aspects of shear strength include sample stiffness, sample strength at optimum states and under confined conditions, stress paths and stress-strain relationships of saturated and unsaturated samples under varying confining stresses. The constitutive modeling efforts are beyond the scope of this research.

Concerning the laboratory testing conditions, the environmental factors are simplified such that de-ionized water was adopted for soil mixing and wetting while the room temperature was kept approximately constant at 25 ± 0.5 °C. Other factors like chemical and bacterial attacks were not taken into account in this study.

1.5 Objectives and Scope of Research

The research goal is to advance the understanding of macroscopic unsaturated expansive soil behavior using microscopic surface phenomena. The objectives of the

research are to 1. Investigate the selected microscale properties of expansive soils; 2. Determine how each property alone or in combination, affects macroscopic soil behavior of expansive soils in terms of volume change and shear strength. It is believed that the outcome of this research will bring an insightful view to the field of study on expansive soil and assist in physical modeling for future research.

Investigating the influence of microscale properties on macroscopic expansive soil behavior is an important and broad research topic, and therefore, it is necessary to carefully define the scope of the work to ensure impactful results in a finite timeframe. To meet the objectives of this study, the scope of this research encompasses:

1. Perform laboratory experiments to disclose the common geotechnical and physicochemical characteristics of four naturally collected expansive soils and two stabilized soils using class-C fly ash (CFA). Compare these characteristics and evaluate the impact of fly ash stabilization on the alteration of these characteristics.

2. Conduct XRD, SEM and EDXS to reveal the mineralogy, structure, and mineral distribution of the compacted samples and the changes of these features ascribed to chemical stabilization.

3. Design, construct and calibrate a new laboratory testing system that allows the dielectric measurement of expansive soils in a 1-D oedometer cell. Attain dispersion curves of both the compacted and stabilized samples at the stages of initial compaction, full expansion, compression, rebounding and recompression.

4. Quantify the macroscopic behavior of the six soil samples in terms of shear strength and volume change including unconfined compressive strength, swell pressure, percent of free swell and linear shrinkage. Investigate the effect of chemical

stabilization with CFA on the microscale properties and the corresponding change of macroscopic behavior. Assess the roles of the microscale properties in the evolution of macroscopic behavior to better understand the fundamental behavior of expansive soils.

5. Analyze, quantitatively, the roles of suction along varying capillary paths on the hydraulic and mechanical behavior of the Carnisaw and Eagle Ford soils including 3-D volumetric expansion and shrinkage, saturated and unsaturated shear strength (through a specifically designed unsaturated triaxial test program). The roles of other microscale properties in influencing the aforementioned macroscopic characteristics will be evaluated in a qualitative manner.

1.6 Dissertation Outline

Chapter 2 provides detailed information about the common geotechnical and physicochemical properties of the four untreated and two stabilized soils. Chapters 3 and 4 present the analysis of soil composition and structure using various parts of the electromagnetic spectrum for XRD, SEM, EDXS studies and for radio-wave range dielectric measurements. Chapter 5 narrates the attainment of soil suction and hysteretic soil water characteristic curves (HSWCCs), as well as cyclic swell-shrink volume evolution. An examination of shear strength and shear-induced volume change of Carnisaw and Eagle Ford will be elaborated in Chapter 6. In Chapter 7 summary and conclusions are proposed.

Chapter 2: Common Geotechnical and Physicochemical Properties

2.1 General Geotechnical Features

Four naturally collected and reconstituted expansive soils named Carnisaw, Hollywood, Heiden and Eagle Ford were studied, with the first three sampled from Oklahoma and the last from north Texas. Additional samples of stabilized Hollywood and Heiden soils prepared using class-C fly ash (CFA), named red rock fly ash, were investigated. The physical and chemical properties of the CFA used in this study are listed in Table 2.1. Chemical stabilization has been widely applied to expansive soils for improving their engineering workability by reducing swell potential, decreasing soil plasticity and increasing bearing capacity. Some stabilization materials commonly used are lime, cement kiln dust (CKD) and calcium fly ash (CFA). Lime tends to be much more expensive for a large stabilization project (e.g., roadway subgrade stabilization), while CKD and CFA are industrial byproducts and are commonly available and environmentally and economically attractive (Cokca 2001, Phani Kumar and Sharma 2004). CFA is an extracted material from the flue gases of coal combustion. It is recognized as a heterogeneous silt with mineral composition varying from particle to particle, which is highly dependent on the source and the combustion conditions.

Table 2.1 Chemical composition and physical characteristics of red rock fly ash[a]

Chemical composition		**Physical properties**	
Name of chemical	**Percentage**	**Property**	**Value**
Silicon dioxide (SiO_2)	36.7	% passing No.325	83.1
Aluminum oxide (Al_2O_3)	18.6	Density (Mg/m^3)	2.69
Iron oxide (Fe_2O_3)	7.0	Strength activity index with Portland cement[b]	95
Calcium oxide (CaO)	25.0		
Magnesium oxide (MgO)	5.5		
Sulfur trioxide (SO_3)	1.5	Water requirement[b]	94
Sodium oxide (Na_2O)	1.8	Soundness, autoclave expansion or contraction, %	0.06
Potassium oxide (K_2O)	0.5		

[a] Information was provided by the supplier
[b] % of cement control

Among the four natural soils, Carnisaw is red brown residual silt with high plasticity weathered from shale of Pennsylvania age. Eagle Ford soil can be described as yellowish/tan highly plastic clay weathered from fossiliferous clayey shale with sandy shale lenses. Hollywood is yellowish olive fat clay with traces of grey limestone from clayey colluvial sediments over limestone of cretaceous age, and Heiden is depicted as olive grey fat clay weathered from clayey shale and with trace of organic root. The soils were processed through a No.10 U.S. sieve prior to laboratory experiments in order to remove occasional coarse sands or gravels (grain size definitions in accord with the Unified Soil Classification System (USCS)) from field

sampling. Common geotechnical lab tests were performed following ASTM standards (ASTM 2011) and the attained soil information is given in Table 2.2.

Specifically, the optimum moisture content (w_{opt}) and maximum dry unit weight (γ_{dmax}) were determined from the Harvard miniature compaction instead of standard compaction proctor test in order to save soil. Each soil was compacted in a Harvard miniature compaction mold using a 30.48 cm (12 in) drop and 392.3 g (0.863 lb) hammer in five equal layers with six blows performed on each layer. This compaction process was designed and calibrated by Khoury and Khoury (2005) on two CH soils, one CL and one ML soil with the results closely matching the compaction characteristics of a standard proctor test. Additional standard proctor compaction tests were conducted on the Carnisaw and Eagle Ford soils according to ASTM-D698 (2011) with the findings closely matching those from the calibrated Harvard miniature compaction test (both types of compaction generate similar compaction energy (Khoury and Khoury 2005)). For all the specimen preparation in this project, the soil was initially compacted in five equal lifts to w_{opt} and γ_{dmax} (the optimum state) using volume-based (impact) compaction. Notice that in common engineering practices, the compaction state of (w_{opt} - 2 %) is frequently encountered in roadway construction or slope stabilization due to moisture loss, while the state of (w_{opt} + 2 %) is more likely desired in landfill clay liner for permeability concerns.

The swell potential was assessed by following method A of the one-dimensional swell test of cohesive soils (ASTM-D4546 1999). Each soil specimen was compacted at the optimum state directly in an oedometer ring of 63.5 mm in diameter and 10 mm in height. The specimen was then submerged in de-ionized water in an oedometer cell and

allowed to swell under a seating load of 1 kPa. After complete expansion, the samples were consolidated to their original height so that the swell pressure could be retrieved. The unconfined compressive strength (q_u) was determined on the specimens compacted to the optimum state form a Harvard miniature mold.

To produce the stabilized samples, the soil particles mixed with various percentages (proportion per dry weight of soil) of the CFA were compacted at the according optimum state in a Harvard miniature mold, and cured for 14 days after which the strength was determined from unconfined compression tests according to ASTM-D2166 (2011a). As ASTM-D4609 specified, the minimum strength gain for a soil to be considered effectively stabilized is 345 kPa above the untreated soil strength. Lab tests found that both samples stabilized adequately when 9 % or more CFA was used. Therefore, the Hollywood and Heiden specimens stabilized with 9 % CFA were selected for further study herein. The geotechnical properties of the two stabilized soils can be characterized as shown in Table 2.2.

Table 2.2 Some common geotechnical properties of the studied soils*

Test sample	w_{opt} (%)	γ_{dmax} (kN/m^3)	G_s (-)	LL (%)	PL (%)	PI (%)	CF (%)	q_u (kPa)	δh (%)	p_s (kPa)	USCS
Carnisaw	26.2	16.2	2.68	59	32	27	51	578	2.3	75	MH
Eagle Ford	27.1	14.2	2.71	92	35	57	66	304	12.7	263	CH
Hollywood	20.6	16.7	2.78	54	20	34	62	365	5.6	141	CH
Stabilized Hollywood	19.6	16.3	2.77	47	21	26	34	727	0.0	0	CH
Heiden	24.2	15.5	2.77	67	23	44	50	313	9.3	230	CH
Stabilized Heiden	21.5	15.8	2.76	53	26	27	25	763	0.0	0	CH

*G_s, specific gravity; LL, liquid limit; PL, plastic limit; PI, plasticity index; CF, clay size fraction (< 2μm); q_u, unconfined compressive strength (at w_{opt} and γ_{dmax}); δh, Percent of swell (under a vertical stress of 1 kPa); p_s, swell pressure; USCS, unified soil classification system

2.2 Some Physicochemical Properties

Some physicochemical properties are obtained or derived from experimental data as shown in Table 2.3. The total S_a was obtained following the EGME (Ethylene Glycol Monoethyl Ether) surface area determination method proposed by Cerato and Lutenegger (2002). The external S_a was determined with the BET (Brunauer-Emmett-Teller) method developed by Brunauer et al. (1938). The CEC and the pH of each soil were measured by Harris Laboratory, Inc., Lincoln, Nebraska using a 1 N ammonium acetate (CH_3COONH_4) extraction method (Rhoades 1982). The surface conductance was determined by Equation 1.1 provided the S_a, CEC data and the percentages of the exchangeable cations obtained from the CEC tests (also given in Table 2.3).

Table 2.3 Some physicochemical properties of the studied soils[a]

Test sample	Total S_a (m^2/g)	External S_a (m^2/g)	Internal S_a (m^2/g)	CEC (meq/100g)	pH (%)	K^b (%)	Mg^b (%)	Ca^b (%)	Na^b (%)	H^b (%)	λ_{ddl} ($\times 10^{-8}$ S)
Carnisaw	107.5	47.5	60.0	27.3	4.4	0.9	9.1	1.8	0.2	88.0	7.97*/0.17†
Eagle Ford	213.5	60.6	152.9	49.6	7.7	1.5	13.2	77.8	7.5	0.0	1.36
Hollywood	145.5	40.3	105.2	26.4	7.2	1.3	4.6	93.2	1.0	0.0	1.08
Stabilized Hollywood	101.0	35.9	65.1	38.8	8.6	0.7	6.1	91.6	1.5	0.0	2.28
Heiden	229.0	51.5	177.5	50.7	8.7	0.8	11	82.2	6	0.0	1.30
Stabilized Heiden	176.5	32.6	143.9	59.6	9.1	0.6	3.4	90.4	5.6	0.0	2.00

[a]S_a, specific surface area; CEC, cation exchange capacity; and λ_{ddl}, estimated surface conductance; [b]percentage of exchangeable cation
*taking into account the contribution of hydrogen; †excluding the effect of hydrogen

In Table 2.3, the much higher mobility of hydrogen (36.2×10^{-8} $m^2V^{-1}s^{-1}$) than the other cations and the significant hydrogen concentration produce a large λ_{ddl} (7.97×10^{-8}) of Carnisaw, which falls sharply to a magnitude of 1.7×10^{-9} if excluding the effect of hydrogen. The validity of the contribution of hydrogen to λ_{ddl} will be challenged in the discussion later. Equation 1.1 also assumes that the anionic deficit in the diffuse double layer is zero whereas in reality λ_{ddl} is dependent on both the concentration of excess cations and the deficit of anions, in which the latter is much smaller than the former and can be neglected in estimation (Klein and Santamarina 2003). A correction factor was introduced for justifying this deficit for a single chemical solute (Lyklema 1995, Klein and Santamarina 2003), which was derived as a monotonical function of zeta potential on the basis of theoretical models of electrokinetic phenomena. In the soil cases of this study such modeling efforts can be challenging in respect of the complex solutes in the bulk fluid. Moreover, the ionic mobility of the cations in the double layer was assumed to be the same as in a diluted solution, which in fact is prone to be restrained by negatively charged surface.

2.3 Summary

Several comments can be made on the information of geotechnical characterization (Table 2.2). In general, soil with a higher plasticity index shows greater percent of swell and swell pressure, however, a smaller unconfined compressive strength. Chemical stabilization by CFA altered the mechanical behavior of the untreated soils resulting in reduced plasticity index, significantly enhanced unconfined compressive strength (99 % for Hollywood and 144 % for Heiden), and substantially

decreased swell potential (non-expansive soils). The underlying microscopic mechanisms for these modifications will be discussed later.

The physicochemical properties given in Table 2.3 exhibit general trends of the four natural soils as increases of both S_a (regardless of type) and CEC with plasticity index. Chemical stabilization with CFA markedly reduces the magnitudes of S_a and CEC of Hollywood and Heiden, and in other aspects, increases the pH and the surface conductance. Special attention must be paid to the case of Carnisaw. The strong acidity of the soil (pH = 4.4 and H^+ % = 88 %) is observed concurrently with a particularly high surface conductance (Table 2.3). The physicochemical performances of the studied soils as well as their impact on the macroscopic behavior will be covered in more details later.

Chapter 3: Investigations on Mineralogy and Structure

3.1 X-ray Diffraction (XRD) Investigation

In order to understand the mineralogical composition of the untreated soils and changes associated with CFA stabilization, XRD tests were performed on both untreated and stabilized samples. For each of the four untreated soils, 10 grams of air-dried soil particles passing the U.S. No. 200 sieve (0.075 mm) were thoroughly mixed with 1 liter of 10^{-3} M (suggested molarity by Moore and Reynolds 1997) sodium hexametaphosphate solution. For the stabilized soils, soil cylinders were air-dried and thoroughly crushed to collect 10 grams of particles, which were then processed in much the same way as were the untreated soils. Soil suspensions were then centrifuged to separate out particles of clay size fraction (< 2 μm) for the following XRD analysis on clay minerals.

For Carnisaw and Eagle Ford, air-dried, glycolated and heated samples were prepared on glass slides as oriented mounts and tested according to USGS laboratory manual for X-ray powder diffraction (USGS 2001). The oriented mounts aid in discriminating individual clay minerals by maximizing signal from (00*l*) reflections. The Rigaku D/Max XRD unit was operated with a Cu X-ray tube and graphite monochromator. Data were collected from 4° to 34° 2θ at a rate of 0.05° 2θ/sec and presented as diffraction patterns (Figures 3.1-3.2) in terms of counts per second (CPS) versus phase angle 2θ (2-Theta). For the untreated and stabilized Hollywood and Heiden samples, the collected clay particles were divided into two identical sample groups for different test purposes in order to identify the possible byproduct generated

from chemical stabilization. The first was prepared as an oriented mount on glass slides and tested in exactly the same manner as for Carnisaw and Eagle Ford. Figures 3.3-3.4 and Figures 3.5-3.6 present the X-ray diffraction patterns of both untreated and stabilized Hollywood and Heiden samples prepared as oriented mounts, respectively. In order to further distinguish the dioctahedral from trioctahedral phyllosilicates, the second group of samples were prepared as random mounts to observe the (060) phyllosilicate reflections. Data were collected with a Rigaku Ultima IV XRD with a Cu tube and graphite monochromator. Scans collected over a 2θ range of 58°-64° are presented for untreated and stabilized Hollywood (Figure 3.7) and Heiden (Figure 3.8). Also in Figure 3.7 and Figure 3.8, the solid vertical lines mark the d-spacing values (in unit of Å) of the untreated soil and the dashed lines represent those of the stabilized soil. The mineral symbols in Figures 3.1-3.8 are representative of: M, montmorillonite; V, vermiculite; K, kaolinite; I, illite; GO, Goethite; Q, quartz.

In Figures 3.4 and 3.6, the kaolinite identification was based upon the positions of several diagnostic peaks. Additionally, the peak at ~7.2 Å was expected to disappear after heating to 550 °C, as was observed in the untreated Hollywood and Heiden samples (Figures 3.3 and 3.5). However, the ~7.2 Å peak remained with reduced intensity after heating in the stabilized Hollywood and Heiden samples (Figures 3.4 and 3.6). One possible explanation is that the trioctahedral equivalents to kaolinite, the serpentine group minerals, were produced by chemical reactions between the soil and the fly ash. However, neither Figure 3.7 nor Figure 3.8 shows any significant change in (060) reflections caused by stabilization and the serpentine peak of the stabilized soils within the d spacing range of 1.531-1.538 Å (60.47-60.16° 2θ). The values of d-spacing

for the (060) reflections and 2θ for clay minerals are from the data table given in Moore and Reynolds (1997). These measurements confirm the presence of kaolinite. The peak around 1.54 Å is most likely a result of quartz rather than trioctahedral phyllosilicates, inferred by the presence of a 1.82 Å quartz peak (Moore and Reynolds, 1997). Regardless, there is no significant change between the treated and untreated soils except a small reduction in total intensity for both random mount patterns (Figures 3.7-3.8). As a result, the aforementioned kaolinite/serpentine peaks tend to imply the existence of kaolinite. The reason why the kaolinite peaks weaken instead of disappearing may be attributed to the following two possibilities: 1. the CFA shell residing on the kaolinite particle surface thermally protected the kaolinite; 2. the irregular fixation of metal hydroxyls from the fly ash in the interlayer space restrained collapse.

Table 3.1 summarizes the XRD together with other geological and geotechnical descriptions. The brief notations of the minerals and cations in Table 3.1 indicate: M, montmorillonite; K, kaolinite; I, illite. It must be noted that the percentage values shown in parentheses in Table 3.1 were calculated from multiplying the proportion of each mineral in the clay size material determined from semi-quantitative mineralogical description using USGS (2001) with the clay size fraction (CF in Table 2.2). Therefore, the percentage values represent the proportions of clay minerals of the entire soil sample, not the clay size portion only.

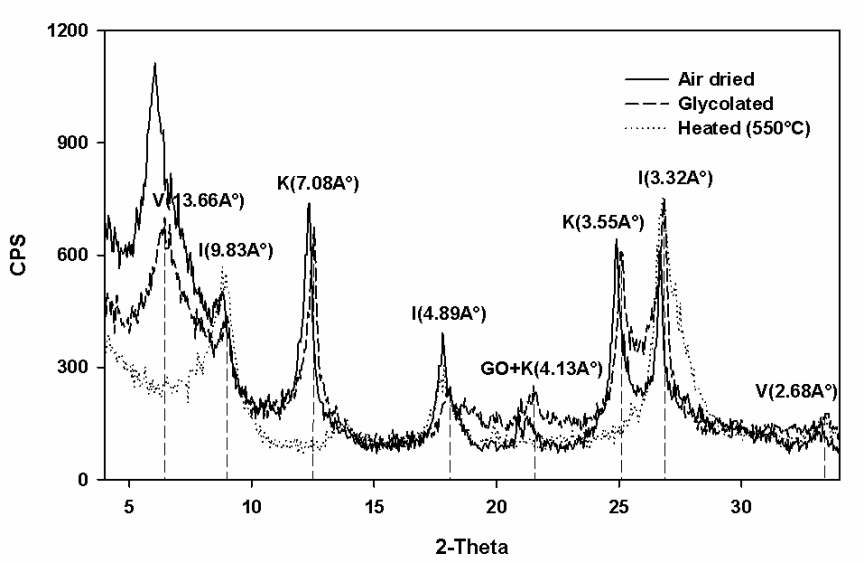

Figure 3.1 X-ray diffraction pattern of Carnisaw (oriented mount)

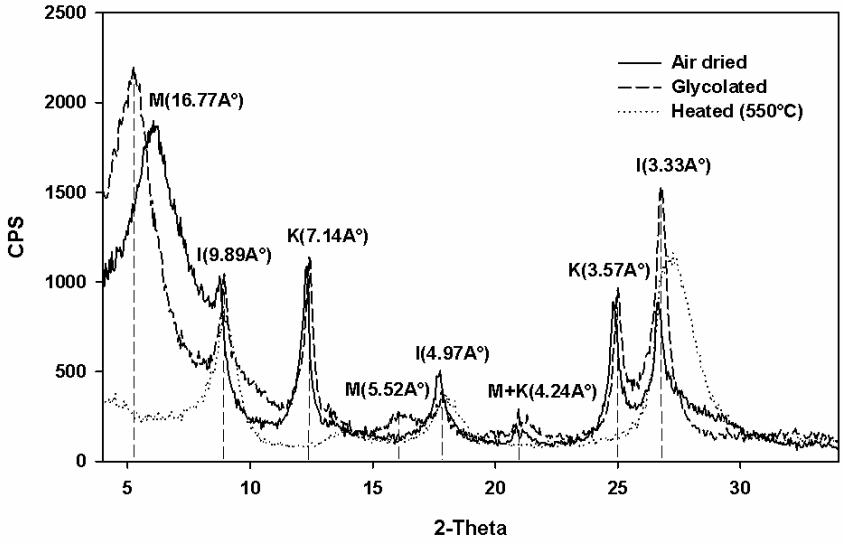

Figure 3.2 X-ray diffraction pattern of Eagle Ford soil (oriented mount)

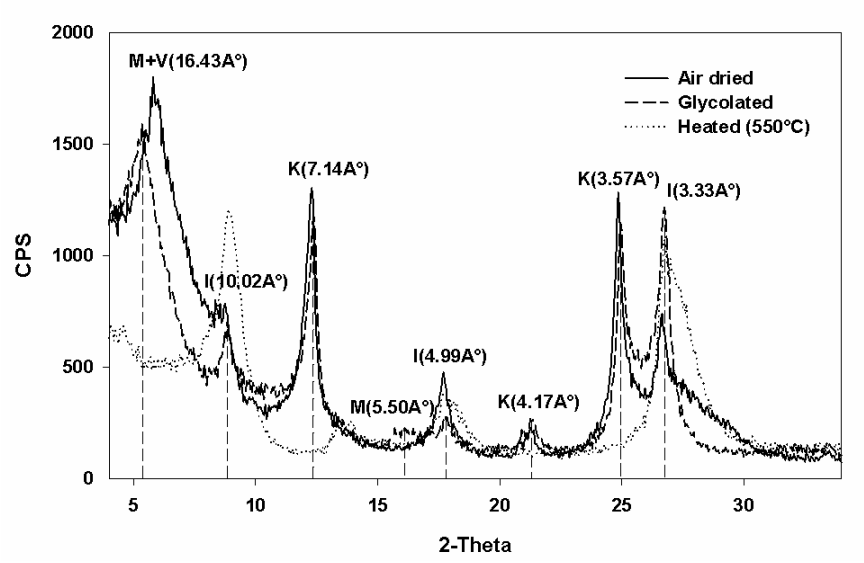

Figure 3.3 X-ray diffraction pattern of untreated Hollywood (oriented mount)

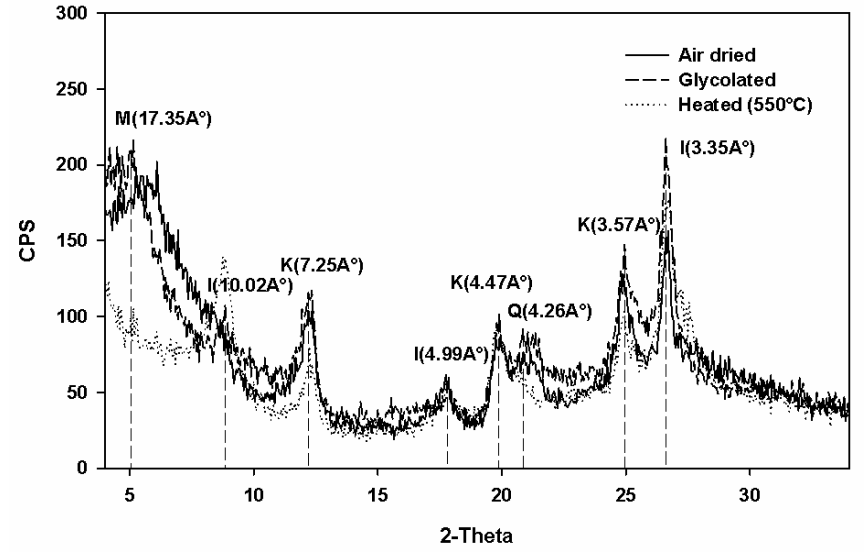

Figure 3.4 X-ray diffraction pattern of stabilized Hollywood (oriented mount)

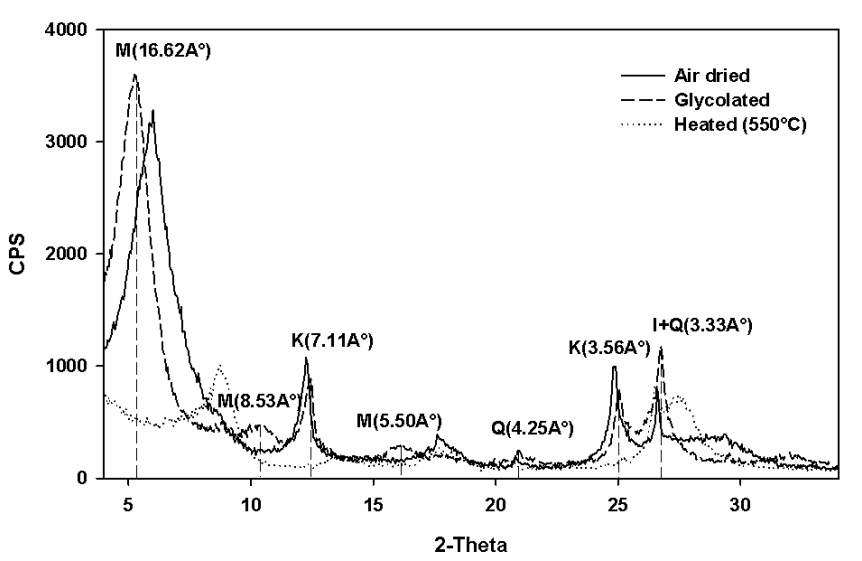

Figure 3.5 X-ray diffraction pattern of untreated Heiden (oriented mount)

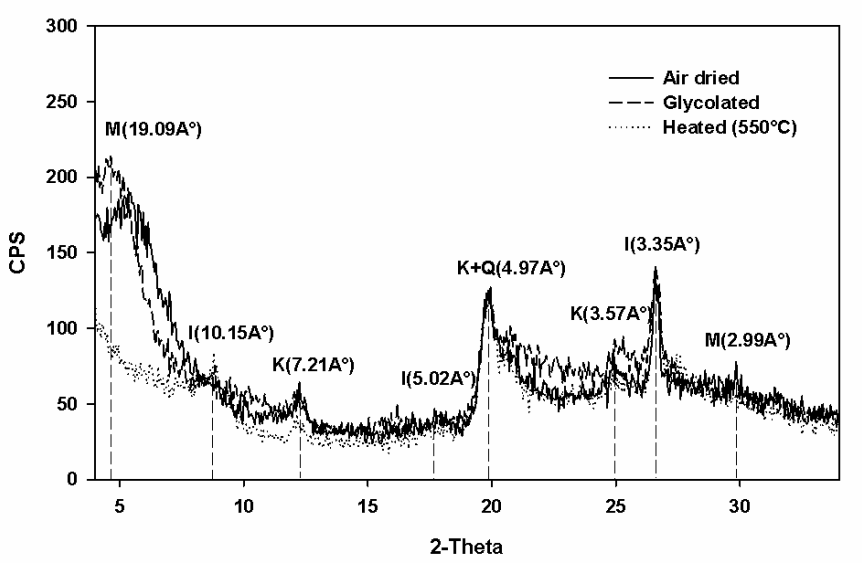

Figure 3.6 X-ray diffraction pattern of stabilized Heiden (oriented mount)

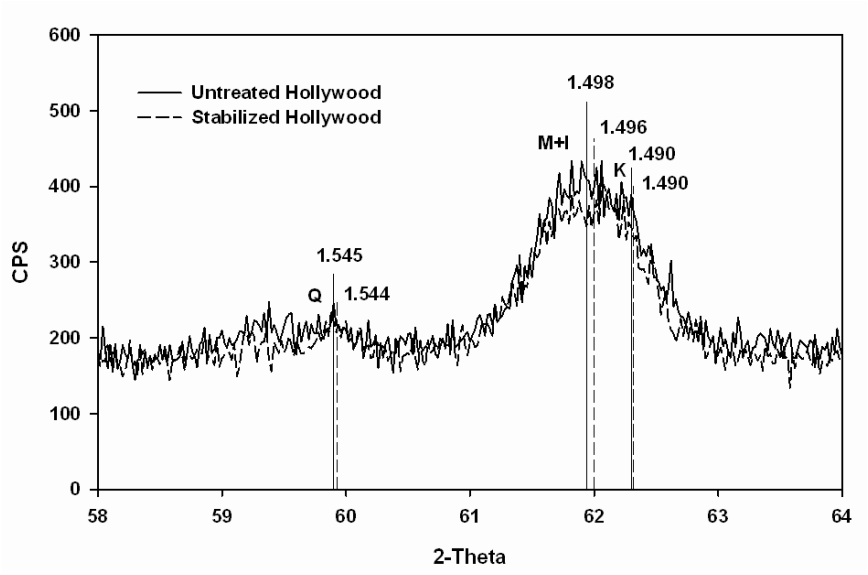

Figure 3.7 X-ray diffraction pattern of Hollywood (random mount)

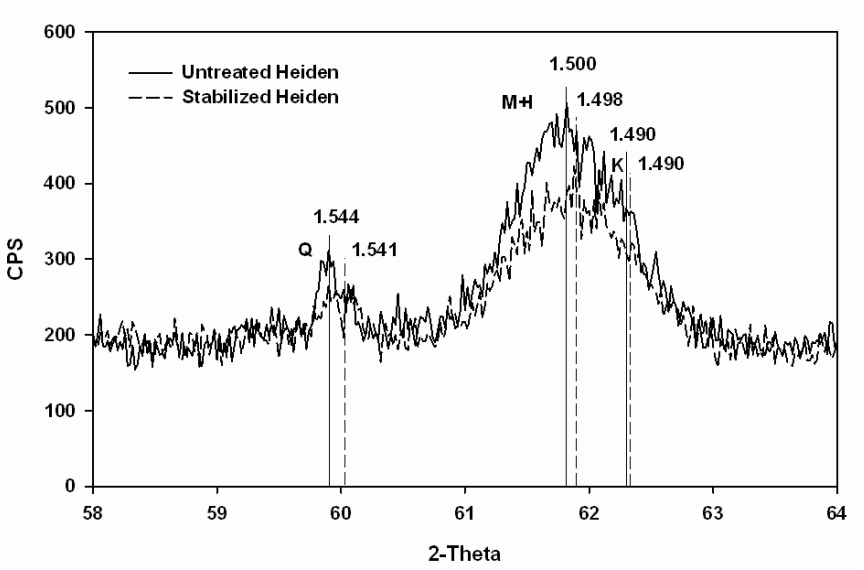

Figure 3.8 X-ray diffraction pattern of Heiden (random mount)

Table 3.1 Summary of the geological and geotechnical descriptions

Test sample	Geological classification	Geotechnical description	Clay size minerals (%)*
Carnisaw	Residuum weathered from shale of Pennsylvanian age	Red brown silty clay or elastic silt	V (12), I (25), K (14)
Eagle Ford	Fossiliferous clayey shale with sandy shale lenses	Yellowish tan highly plastic pure clay	M (28), I (27), K (11)
Hollywood	Clayey colluvial sediments over limestone of Cretacious age	Yellowish olive fat clay with trace of light grey limestone	M (23), I (21), K (18)
Stabilized Hollywood	Hollywood soil stabilized by 9 % red rock fly ash	Yellowish tan highly plastic fat clay	M (16), I (7), K (11)
Heiden	Clayey shale of Cretacious age	Olive gray highly plastic fat clay with trace of organic root	M (37), I (5), K (8)
Stabilized Heiden	Heiden soil stabilized by 9 % red rock fly ash	Gray highly plastic fat clay	M (15), I (3), K (7)

*M, montmorillonite; K, kaolinite; I, illite; V, vermiculite

3.2 Scanning Electron Microscopy (SEM) Observation

Given the resource limitations (e.g., inaccessibility to ESEM facilities) but the necessity to understand the particle information, conventional SEM research was performed on the as-compacted specimens at revealing the initial structure. The author acknowledges the advantages of ESEM. The SEM research was performed on the as-compacted and stabilized specimens to both understanding the influences of structure on soil behavior and revealing the structure change attributed to chemical stabilization.

In conventional SEM studies, there exists no single sample preparation technique that is considered most appropriate (Al-Rawas and McGown 1999), since air-drying, freeze-drying and critical point-drying all have their associated problems

concerning sample disturbance (Tovey 1970, Barden and Sides 1971, Collins 1978, Smart and Tovey 1982): (i) air drying induces linear and volumetric shrinkage in wet clayey soils; (ii) freeze drying introduces overall swelling at the macrostructure (and presumably microstructural level); (iii) critical drying can cause particle breakup.

The air drying method was implemented in this study on the compacted samples. The process of soil specimen preparation was slightly modified from the methods of Collins (1978) and Al-Rawas and McGown (1999). Each soil sample was first compacted in a one-dimensional compaction mold to be a cylinder with a dimension of 32 mm in diameter and 71 mm in length. A prismatic specimen approximately $1 \times 1 \times 1$ cm in dimension was trimmed from each cylinder using a sharp knife and a hacksaw and air dried in a desiccator with a relative humidity of 20 % over a period of 4 weeks. Preferred orientation of particles as a result of drying is negligible since differential linear shrinkage is minimal (Collins 1978), especially when isotropic shrinkage of the specimens occurred only slightly from their optimum state. The dried specimen was then fractured by cutting a V-shaped groove at the middle and applying combined bending and pulling action as suggested by Smart (1967), in order to expose a fresh and undisturbed section which is parallel to the direction of compaction. The surface for study was then cleaned with adhesive tape to remove particles damaged from fracturing as proposed by Barden and Sides (1971). The base of the specimen was trimmed flat and cemented to an aluminum stub. The specimen was then sputtered with gold–palladium alloy, and the SEM micrographs were taken at a magnification ratio of 2500 X representative of the clay arrangement fabric level (Al-Rawas and McGown 1999). CFA was also investigated at a condition dried from its hydrated state.

Figure 3.9 shows that the morphology of the CFA is mainly formed of varying size (0-20 μm) glassy, smooth surface spheres and attached elongated crystals, presumably gehlenite ($Ca_2Al[AlSiO_7]$) based on morphology with the long axis approximately parallel to the sphere surface. The formation of the needle-like gehlenite crystals was reported in the works of Bosbach and Enders (1998) and Tishmack and Burns (2004).

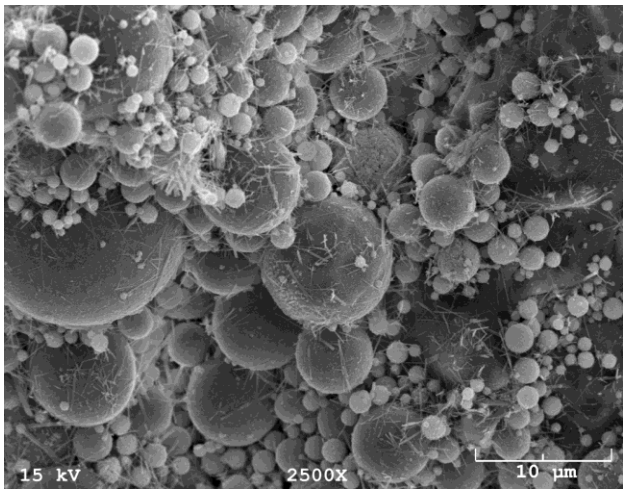

Figure 3.9 SEM micrograph of the CFA used (red rock fly ash)

Figure 3.10 (a~f) presents the SEM micrographs of the structure of the six studied soil samples, respectively, after dried from their original optimum state.

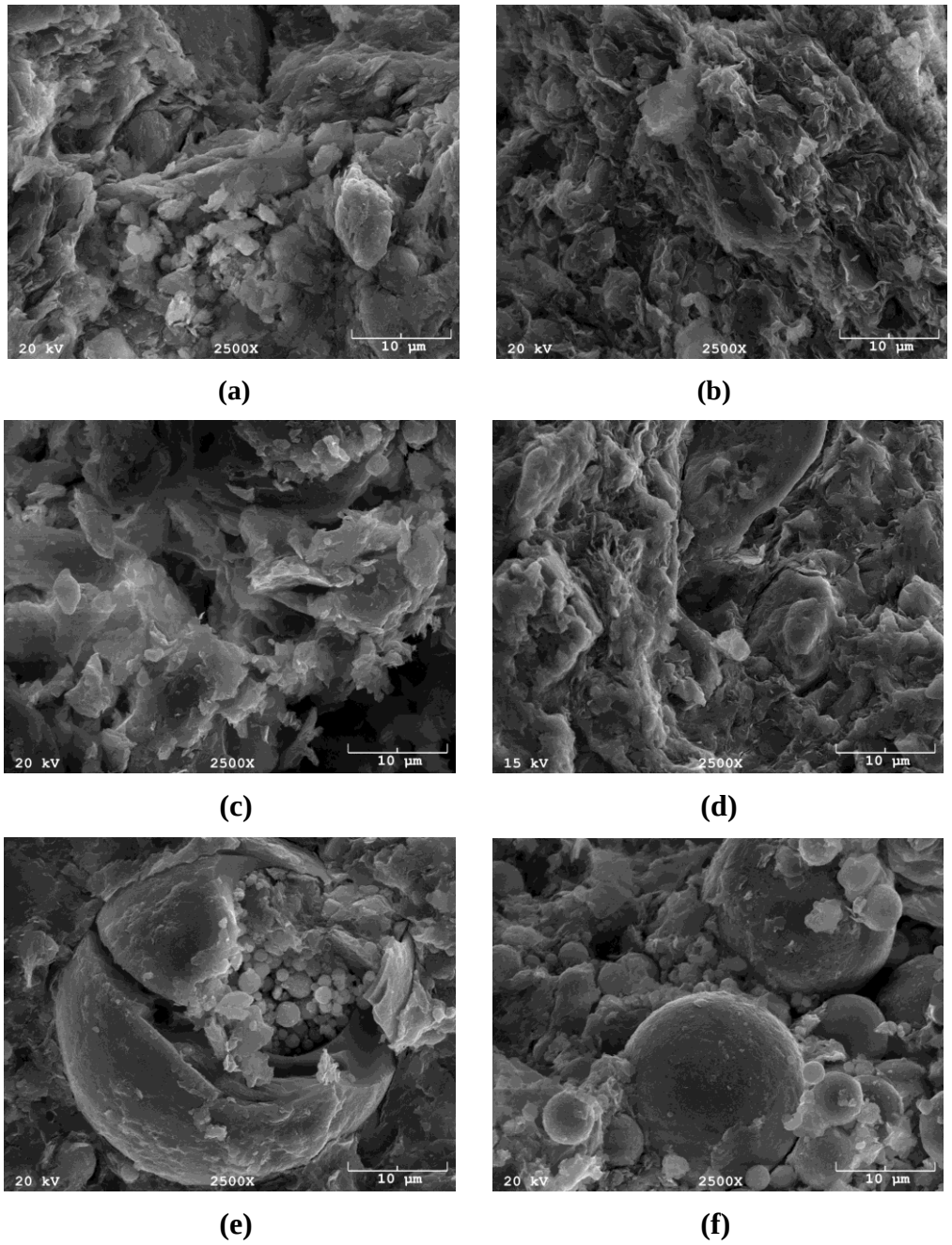

Figure 3.10 Micrographs of the six studied samples*

*(a) Carnisaw, (b) Eagle Ford, (c) Hollywood, (d) Heiden, (e) stabilized Hollywood, (f) stabilized Heiden

Carnisaw develops a flocculated structure dominated by the edge to edge and edge to face associations of clay aggregates (Figure 3.10 (a)). The more plastic Eagle Ford shows a laminar structure with dispersive larger, thinner clay platelets or aggregates mostly associated in the face to face style (Figure 3.10 (b)), suggesting a higher swell potential than Carnisaw. The untreated Hollywood sample features a loosely packed texture with edge to face and face to face clay particle alignment (Figure 3.10 (c)). Some inter-aggregate pores exist resulting from inadvertent removal of silt or sand grains. The untreated Heiden develops a slightly aggregated structure with intermediate face to face in contact clay platelets (Figure 3.10 (d)). After stabilization, the morphology is dominated by the presence of spheres; a well-known component of fly ash that forms as the calcium-aluminosilicate residual melt cools while influenced by frothing gas bubbles (Figure 3.10 (e) and (f)). Specially, Figure 3.10 (e) shows a plerosphere, which is multi-wall hollow sphere packed with smaller spheres (Tishmack and Burns 2004, Glasser 2004). An interesting phenomenon occurs as some clay particles invade into the internal space of the plerosphere through the exposure by the broken part of the wall, as shown on the upper right area of Figure 3.10 (e). Other micrograph areas of the stabilized Hollywood exhibit similar configuration as illustrated in Figure 3.10 (f).

It is necessary to emphasize the difficulties encountered in applications of SEM micrographs when interpreting expansive soil behavior. First of all, investigation of the effect of hydraulic history (drying-wetting paths) on soil structure is feasible only through ESEM, with only a few preliminary efforts (Montes-H et al. 2003a&b, Montes-H et al. 2004, Viola et al. 2005, Agus and Schanz 2005) successfully conducted on bentonite or sand-bentonite mixtures. The corresponding digital image analyses were

unavoidably constricted by poor image quality (as previously discussed in section 1.3) and extreme sensitivity to working conditions such as scan rate, chamber gas pressure and working distance (Romero and Simms 2008). The scarcity and expense of ESEM equipment made it inaccessible for this research project. The author is continuingly seeking efforts for possibly a future ESEM project on the hydraulic hysteresis of natural expansive soils. Secondly, to date, no solution has been available to disclose the actual structure of a saturated sample under consolidation or an unsaturated sample when confined (without pressure release). Last but not least, some surface forces (e.g., electrostatic attractive force) that were binding the particles/aggregates together are inevitably weakened during specimen drying. The structure change of expansive soil/clay has been therefore indirectly inferred from volumetric evolutions (e.g., Alonso et al. 1995, Alonso et al. 1999), changes of physicochemical characteristics such as pH and salt concentration (e.g., Wang and Siu 2006a&b), and also electromagnetic properties in this study (next chapter). These methodologies, on the basis of the preliminary micrograph information provided in Figure 3.10, will be adopted by this research project for analysis in the following chapters.

3.3 Energy Dispersive X-ray Spectrometer (EDXS) Analysis

EDXS spectra were obtained simultaneously with the SEM observations. Qualitative elemental analysis by EDXS was performed on certain selected areas of a lower magnification (330 X) in order to reveal a more comprehensive elemental distribution. The settings included electron energy at 20 kV, takeoff angle at 40 °C and elapsed live time for 50 sec. The EDXS spectra of the untreated and stabilized specimens are presented in Figure 3.11 for Carnisaw and Eagle Ford, and in Figure 3.12

for both untreated and stabilized Hollywood and Heiden. All of the six samples show outstanding peaks of silicon, aluminum, and oxygen, which are typical chemical elements forming aluminosilicate minerals.

It is shown in Figure 3.12 that the Ca and Fe peaks strengthen in response to CFA stabilization, with the phenomenon more apparently recognized in Figure 3.12 (b) than in Figure 3.12 (a). This indicates the pozzolanic reactions that generate calcium silicate hydrate (CSH) and calcium aluminum hydrate (CAH) type bonds (Ca peak) and the potential Fe oxides coating (Fe peak) as an isolation film on clay aggregate surfaces, and will be further addressed in the discussion section below. A Mn peak is observed in the spectrum of stabilized Hollywood (Figure 3.12 (a)). Bosbach and Enders (1998) reported a trace amount (0.13 %) of MnO in the chemical composition of a high calcium fly ash (CaO comprises 21.5 % weight) similar to the CFA used in this research. One possibility may be that the slight amount of MnO was not detected by the manufacturer while being locally concentrated in CFA particles (as mentioned above, the CFA is a heterogeneous material).

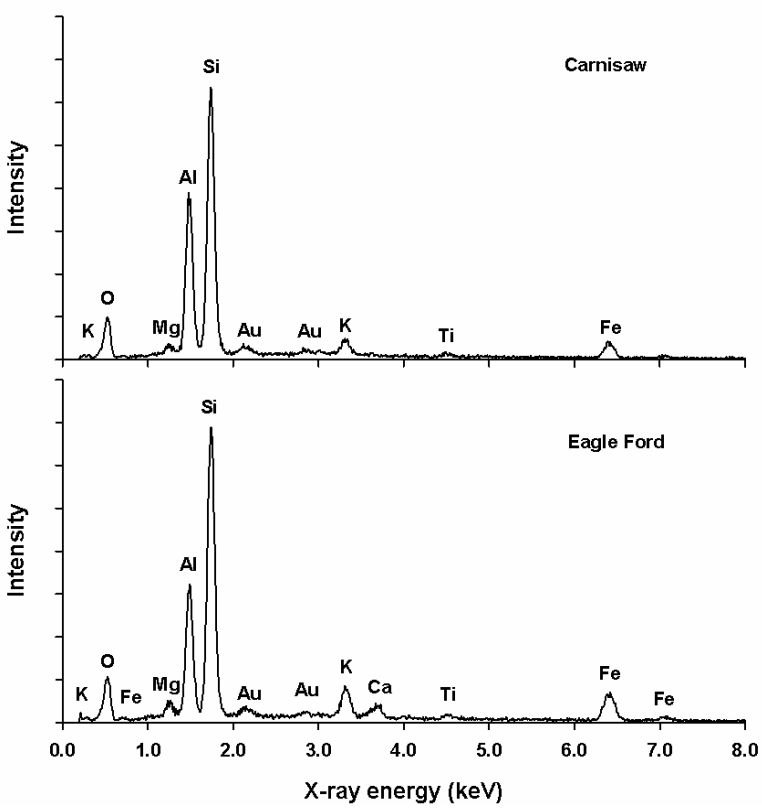

Figure 3.11 Elemental spectra of Carnisaw and Eagle Ford

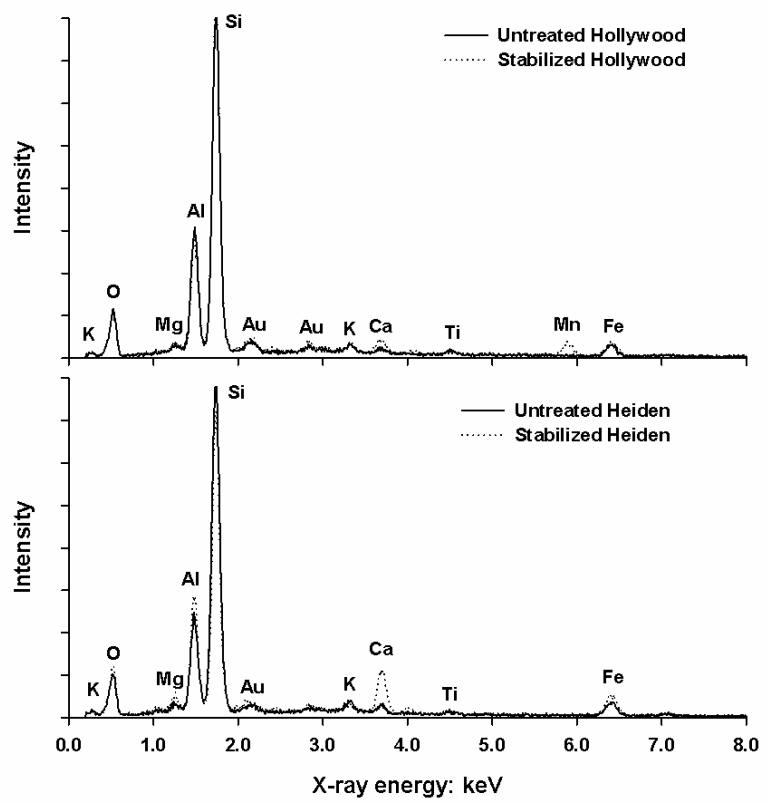

Figure 3.12 Elemental spectra of untreated and stabilized Hollywood and Heiden

3.4 Discussion on Mineralogical and Structure Studies

3.4.1 Discoveries in Untreated Samples

The presence of montmorillonite has been recognized as the major cause of soil expansion. Other expansive components can be vermiculite and expansive chloride. Even though montmorillonite is regarded as the most expansive clay mineral provided its very weak interlayer bonding, definitive comparison of the expansiveness with that of the other two potential expansive minerals is not yet available, owing to natural occurrence of various polytypes of a given species. Moreover, the type of exchangeable cation has a significant influence on the swelling potential of a clay mineral. In the

samples of Hollywood, Heiden and Eagle Ford montmorillonite was found to be the major clay mineral with the percentage following an order of Heiden (37 %) > Eagle Ford (28 %) > Hollywood (23 %). However, the compacted samples indicate an order of both swell percent and swell pressure in a sequence of Eagle Ford > Heiden > Hollywood (Table 2.2). Carnisaw contains 12 % vermiculite (Table 2.3) and exhibits the least amount of swelling (Table 2.2) in comparison to the other untreated samples. In Table 2.3, Ca^{2+} is the predominant type of cation for the four untreated soils except Carnisaw in which H^{+} is detected as the primary cation. Nevertheless, divalent cations as Ca^{2+} and Mg^{2+} prevail as interlayer hydrated cations in the mineralogical unit of Carnisaw compared to the percentages of Na^{+} and K^{+} in Table 2.3. Apparently, initial water content and structure are the other two basic factors that also control the expansion behavior.

Clay particle contact, alignment and aggregation play important roles in determining the swelling capacity of expansive soils. During the swelling of expansive soils, the major part of the surface forces is double layer repulsion caused by interaction of double layers of like charge. As a result, the overall effect of surface forces is taking clay particles away from each other during soil expansion. As seen in Figure 3.10 ((a) and (c)), Carnisaw and Hollywood have a structure featuring aggregated matrices comprised mostly of clay platelets/aggregates at edge to face contact with slight parallelism but strong perturbation. The corresponding alignment mode can be described as “turbulent”. At the same time, the degree of aggregation can be seen stronger in Carnisaw than Hollywood. The platelets of Eagle Ford soil are parallel aligned with their long axis normal to the direction of compaction. Such a parallelism is

also implied in the fabric of Heiden, though in a lesser extent. The more dispersive the structure, the more effective surface area is available for the contact between particles and water molecules resulting in greater expansion. As a result, part of the volume increase during swelling of Carnisaw and Hollywood is compensated by readjustment of clay particles for the tendency of reaching the parallel and dispersive state. On the other hand, both Heiden and Eagle Ford exhibit stronger face to face contact and "laminar" alignment which means the volume increase is able to be fully developed during the swelling process.

Clay particle morphology can also impact the swell potential of a soil, given that physicochemical effects and interactions are more significant with wide, flat and parallel aligned clay particles (Cui et al. 2002). A comprehensive summary of the structure observations is given as Table 3.2 which also shows an order of swell potential equal to that of percent of swell or swell pressure implied in Table 2.2.

Table 3.2 Summary of the observations made from SEM micrographs

Test sample	**SEM Observation**				**Swell potential**
	Particle size	**Particle contact**	**Alignment**	**Aggregation**	
Carnisaw	Medium	Edge to edge and edge to face	Turbulent	Intense	Low
Eagle Ford	Medium-Large	Primarily face to face	Laminar	Weak	Very high
Hollywood	Small	Edge to face	Turbulent	Medium	Low-Medium
Heiden	Large	Face to face and face to edge	Laminar	Weak-Medium	Medium-High

The EDXS spectra (Figures 3.11 and 3.12) give little geological or morphological information about the four untreated natural soils. Nevertheless, a careful examination of the figures implies Fe oxides coating that occur in natural soils. This type of coating is capable of acting in a way similar to cementing agent that enhances soil stiffness. A more detailed discussion will be provided in section 3.4.2.

3.4.2 Effects of Chemical Stabilization by CFA

The predominant alteration in mineralogy related to chemical stabilization was a decrease of the amount in each mineral component (Table 3.1). If no mineralogical change occurred, the percentages of clay minerals of the stabilized Hollywood and Heiden soils, adjusted for the proportion of CFA would be: stabilized Hollywood—M (21), I (19) and K (16); stabilized Heiden—M (34), I (5) and K (7). These percentage values are higher in comparison with the actual values given in Table 3.1, which implies that the chemical stabilization with CFA reduced the amount of clay minerals. However, no new clay-size mineral was found following chemical stabilization except for scarce amount of silica introduced by CFA (Table 2.1, Figures 3.4 and 3.6). Calcium silicate hydrate (CSH) and calcium aluminum hydrate (CAH) gels may form with interaction between the water and fly ash. For example, Zevenbergen et al. (1999) observed poorly crystalline aluminosilicate gels and iron oxide nanoparticles were rapidly produced during reaction of coal fly ash particles with water. These poorly crystalline reaction products are not likely to be observed with XRD, which requires long-range crystalline ordering as a basis for phase detection. However, these poorly crystalline nanoscale reaction products likely interact with clay particles or aggregates through chemical bonding. In this regard, the decreased proportions of the clay mineral

may turn into chemically-stable aggregates that cannot be dispersed by the sodium hexametaphosphate solution (dismissed from sampling) and therefore not able to be represented in the XRD tests.

Because it is montmorillonite that mostly accounts for the swelling behavior of untreated soils, the greater montmorillonite percentage in Heiden soil (Table 3.1) explains the greater free swell and higher swell pressure than Hollywood soil. However, no swelling behavior was found in either stabilized soils (Table 2.2), although each soil still possessed a certain amount of Montmorillonite (Table 3.1). This is mainly because of flocculation from cation exchange and cementation as a consequence of chemical reactions of the soil particles/aggregates with CFA, which can be readily observed in Figure 3.10 (e) and (f). Figure 3.12 shows slightly enhanced peaks of calcium, which is indicative of chemical stabilization (Table 2.1 also shows that CFA comprises 25 % of anhydrite lime). These peaks are a result of the cation exchange reaction introduced by divalent cations, such as Ca^{2+}, and the pozzolanic reactions forming hydrated calcium silicates and hydrated calcium aluminates acting as cementing agents that result in soil structure flocculation. This type of flocculation created chemical bonds in between clay particles forming hydrophobic aggregates that cannot experience intra-aggregate expansion during wetting of the specimen. In short, flocculation is one of the mechanisms causing the increase of soil strength and decrease of swelling (Table 2.2) for expansive soils (Mitchell and Soga 2005), turning "fat" clays into "lean" clays; moreover, this chemical flocculation is not simple aggregation of clay particles but formation of special soil-chemical assemblages. In other words, the CFA stabilization introduced chemical inter-reactions between soil and CFA transforming the formerly

"edge to face" (Figure 3.10 (c)) or "face to face" (Figure 3.10 (c) and (d)) fabric into an "interweaved aggregate-cementing agent-fly ash" structure (Figure 3.10 (e) and (f)). This is also indicated by the reduction of S_a following CFA stabilization (Table 2.3).

Flocculation/aggregation alone, however, is not adequate in explaining the losses of clay minerals caused by CFA stabilization as mentioned above. There must be chemically stable aggregates that were able to sustain the attack of sodium hexametaphosphate solution, which acted as a de-flocculating agent. Consequently, there exists a second mechanism that modified the soil structure during CFA stabilization. As shown in Figure 3.12, some amount of iron was present in the untreated samples as isomorphous substitution of Fe^{3+} cations in the phyllosilicates and perhaps nanoscale iron (hydr)oxide minerals not detected by XRD (< 5 wt %). The Fe peaks strengthened slightly following stabilization (although not obvious, the phenomenon is also implied by the 7 % Fe_2O_3 in the added CFA as shown in Table 2.1) indicative of Fe oxides forming (e.g., ferrihydrite, hematite, goethite) from the hydration process. Zhang et al. (2004) discovered the phenomenon of Fe oxides coating on clay platelets in a natural alluvium soil. This type of coating is indicated by the Fe peaks on the elemental spectra of the natural and untreated soils (Figures 3.11 and 3.12). The additional Fe oxides from CFA tend to form a regional coating on the surfaces of clay aggregates preventing the de-flocculating agent from direct interaction with the clay minerals. This strengthened Fe oxides coating also forms as a stiff and brittle shell that bolsters the shear strength of the soil (Zhang et al. 2004). The mechanism of Fe oxides coating explains the loss of clay minerals during the XRD sample preparation process of the stabilized samples. It is hypothesized that, when

crushed and mixed with sodium hexametaphosphate solution in order to separate out the clay-size particles, some Fe oxides coated aggregates were isolated from the dispersing solution and thus dismissed during the centrifuge process; while the CSH and CAH cemented but not coated aggregates were de-flocculated and the impounded clay content was retrieved.

Zhang et al. (2004) found that the presence of Fe oxides coating on the clay surfaces of natural soils reduces the measured CEC of clay minerals. In their soil, the Fe oxides are naturally associated with the particles and not from chemical stabilization. However, this research observed a slight increase of CEC in both CFA stabilized Hollywood and Heiden soils (Table 2.3). This is because adding high-Ca fly ash (CFA is originated from sub-bituminous or lignite coal) leads to a more basic environment, as proven by the higher pH values in Table 2.3 for the stabilized soils. It is well known from soil science that silica-and alumina-rich gels in stabilized soils have a greater CEC at higher pH (McBride 1994). At higher pH there are fewer protons in the pore fluid causing protons on the surface of the gel to migrate into the fluid, leaving a residual net negative charge that attracts cations. Similar behavior should also exist for CSH and CAH gels. This effect overcame the decrease of the quantity of exchangeable cations attributed to coating or cementation. The work of Hong and Glasser (2002) also suggested that CSH and CAH gels have a higher CEC. Nalbantoglu and Tuncer (2001) stabilized an expansive soil using class C Soma fly ash. They revealed, contrary to Hong and Glasser (2002) and the work presented in this study, that there was a decrease of CEC of the stabilized soil with the increase of percent of fly ash, as a result of formation of new mineral phases. However, as their samples were cured for 100 days, it

is suggested that over a long time, the gel recrystallized into newly formed minerals with a lower CEC that also blocked pores, preventing access of cations to preexisting clay minerals. The curing time used in this study was only 14 days and no new clay minerals were found to emerge. A comparison of the relationships between CEC and fly ash percentage between this study and the result of Nalbantoglu and Tuncer (2001) is given in Figure 3.13.

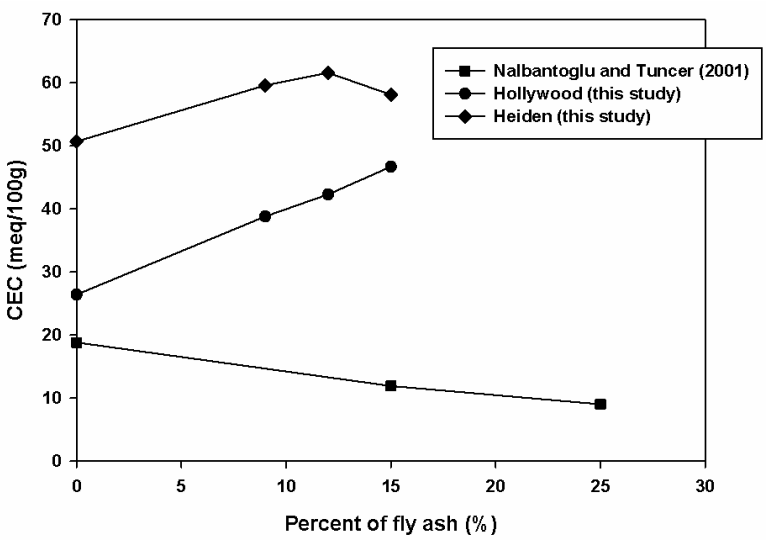

Figure 3.13 Variation of CEC with percent of fly ash

3.5 Conclusions and Summary

The findings of this study lead to several conclusions:

1. A combination of the analysis based on mineralogy, structure and elemental spectra aids in qualitative assessment of swell potential of natural expansive soils. The expansive mineral (mostly montmorillonite) can be considered an intrinsic determinative factor on soil expansion which is dependent on composition only. The exchangeable cations, structure and water content also govern the actual expansion.

2. Structure analysis has shown that a soil sample comprised of thin and large clay flakes contacting in face to face style, “laminar” alignment with weak aggregation tends to have a high swell potential. Inversely, a sample having a “turbulent” structure formed by relatively thick and narrow clay platelets with edge to edge/edge to face interaction and aggregated intensely is more likely to exhibit small capacity of swelling.

3. CFA stabilization decreased the clay size portion in expansive soils but retained a certain amount of the expansive montmorillonite. However, even with the remaining montmorillonite, the stabilized soils did not exhibit any swelling behavior because the combined effects of the cementation of clay particles and the formation of hydrophobic aggregates resulted in reduced expansion and enhanced strength. Therefore, it can be concluded that while mineralogical change is minimal, it seems as though the structural changes dominate.

4. Cementation from the reaction between soil and CFA is not only a result of chemical flocculation creating CSH and CAH cementing agents in between clay particles, but also Fe oxides coating on the surfaces of some flocculated aggregates. The Fe oxides coating was observed in the four natural and untreated soils with the effects enhanced in the two stabilized samples.

5. The S_a of both soils decreased through particle flocculation while the CEC increased because the higher pH values of the stabilized soils promote negative charge accumulation on CSH and CAH gels, which are more capable of attracting cations from the solution. An increase of stabilization time from 14 to 100 days may result in the formation of new mineral phases, which may have lower CEC and block the transport paths of cations.

Chapter 4: Electromagnetic Studies on Expansive Soils

4.1 Introduction

4.1.1 Dielectric Nature of Soil

A naturally collected or lab-compacted soil sample can be viewed as a dielectric with electromagnetic properties of magnetic permeability and dielectric permittivity. In nature, most of the soil types are non-ferromagnetic. For non-ferromagnetic soils, polarization of bound charges and dipoles occurs in response to an electric field and the response is out of phase with excitation (Santamarina et al. 2001). In this regard, the polarization can be described with a frequency dependent complex quantity, named dielectric permittivity, which is expressed as

$$\varepsilon^* = \varepsilon' - i\varepsilon'' \quad \textbf{(4.1)}$$

Where $i = \sqrt{-1}$, ε' and ε'' are representative of soil polarization and polarization loss, respectively. The dielectric permittivity ε^* is usually normalized by the dielectric permittivity of vacuum ε_0 (8.85×10^{-12} F/m) and expressed as

$$\kappa^* = \kappa' - i\kappa'' \quad \textbf{(4.2)}$$

In which the real part is described as real (relative) permittivity (also called "dielectric constant") and the imaginary part is usually studied in terms of effective (electrical) conductivity which is expressed as

$$\sigma = \omega\varepsilon_0\kappa'' + \sigma_{dc} \quad \textbf{(4.3)}$$

In which σ_{dc} is direct current (dc) conductivity that also contributes to the polarization loss. Since the polarization effect is produced by forces and torques imposed by the electric field, and these forces and torques are opposed by inertial and

viscous forces within the dielectric medium (Santamarina et al. 2001), the electromagnetic properties (real permittivity and effective conductivity) are directly related to the physical nature of the soil. In practice, these two properties have been used to monitor soil moisture (Selig and Mansukhani 1975), predict porosity (Arulanandan 1991), and determine the presence of contaminants (Thevanayagam 1993) and sulfates (Bredenkamp and Lytton 1994). It has also been shown that in clay minerals, electromagnetic properties vary as a function of frequency, the phenomenon of which is called dielectric dispersion or relaxation (Arulanandan and Yogachandran 2000) as a result of certain polarization mechanisms, with the corresponding curves described as dielectric spectra (Arulanandan 2003, Liu 2007). The magnitude of dielectric dispersion in a given frequency range is defined as the difference in magnitude at highest and lowest frequencies at which the real permittivity or effective conductivity curve levels off. This value has been shown to be a function of the mineralogy and mineral solution interface characteristics, e.g., minerals of higher specific surface area usually exhibit higher dispersion magnitudes than those of lower surface area (Arulanandan 2003).

4.1.2 Dielectric Measurement Instruments and Approaches

One type of dielectric measurement of a compacted soil sample invokes the usage of a two-terminal electrode system within the radio frequency range from several Hz to less than 100 MHz (Liu 2007). For expansive soils, it is desirable to investigate electromagnetic properties during swelling or compression, for which the two-terminal electrode system is considered the most suitable option because the test configuration is able to accommodate one dimensional deformation of the sample. The two-terminal

electrode system employs an impedance measurement device along with a pair of parallel electrodes seated on the top and bottom of a cylindrical or prismatic sample holder aimed at performing dielectric measurement in the vertical direction of a compacted or consolidated soil sample (Arulanandan and Smith 1973, Arulanandan 1991, Arulanandan 2003, Rinaldi and Francisca 1999, Klein and Santamarina 1997, Klein and Santamarina 2003). Additionally, Varghese (1996) introduced a two-terminal system composed of two slightly curved electrodes embedded at the inner wall of an annular Plexiglas cylinder. The two electrodes faced each other with their surface normal to the longitudinal direction of the cylinder so that measurement in the horizontal direction of a compacted sample was practicable.

In several research efforts (Arulanandan and Smith 1973, Arulanandan 1991, Arulanandan 2003), the cylindrical cell that holds soil samples had a fixed inner diameter of 15 mm and an adjustable length at a maximum of 44 mm. Rinaldi and Francisca (1999) studied the dielectric dispersion of clay slurries using a HP4191A impedance meter and a HP16091 termination fixture that allowed for a sample being measured between two electrodes. The maximum sample dimension allowed is 10 mm in diameter and 20 mm in length. The cell used by Klein and Santamarina (1997&2003) had an inner diameter of 89 mm (cylindrical section) and 68 mm (prismatic section), respectively. The Plexiglas annular cylinder adopted by Varghese (1996), with an inner diameter of 70 mm and a length of 178 mm, allowed for measurement of soil samples at compacted states only. All of these cells did not allow the properties or the geometry of the soil sample to be changed during the test. In many cases, these changes may be desired (e.g., vertical swelling of expansive soils or compression during consolidation);

therefore, this study proposes a test method that accommodates both the vertical deformation of the sample and the change of fluid chemistry.

A major problem associated with the two-terminal measurement system lies in the phenomenon of electrode polarization, which originates from charge accumulation at the electrode-sample interface that artificially increases the measured real permittivity or decreases the obtained effective conductivity at low frequencies up to several MHz (Bordi et al. 2001). The measured effective conductivity is minimally affected by electrode polarization at kHz frequencies and higher while the polarization can strongly affect the measurements of relative permittivity at the same frequencies (Parkhomenko 1967, Santamarina et al. 2001, Klein and Santamarina 2003). Additionally, as the salt concentration in the liquid phase increases, the frequency at which electrode polarization manifests in the measurement of real permittivity can increase significantly, while effective conductivity observations show negligible changes (Bordi et al. 2001, Klein 2004). Klein and Santamarina (1997) introduced a four-terminal electrode system to avoid the effects of electrode polarization by using separate current injection and potential monitoring electrodes. However, the test setup involves inserting a pair of needle-shaped electrodes into the middle of the soil sample, which may create disturbance to the sample, especially during its deformation.

Other commonly used dielectric measurement systems include a network analyzer with reflection probe (also named coaxial termination probe, used over a frequency range of 20 MHz-1.3 GHz) (Klein and Santamarina 1997, Liu 2007), network analyzer with cylindrical chamber probe (several MHz-3 GHz) (Shang et al. 1999) and time domain reflectometry (TDR, for the frequency range of 20 MHz-1.5

GHz) (Lin 2003a&b, Liu 2007). These systems involve different types of probes and sample holders excluding the 1-D hydromechanical circumstances, and therefore were not taken into consideration in this study.

4.1.3 Polarization Mechanisms

Over the frequency range of 1 MHz-1 GHz, interfacial polarization has been identified as the predominant mechanism contributing to the dielectric dispersion behavior of fine-grained soils, illustrated as increased measurement of real permittivity and a decreased measurement of effective conductivity of a soil-electrolyte mixture than the measurement of its liquid phase alone (Santamarina et al. 2001, Liu 2007). Interfacial polarization originates from the accumulation of charges at interfaces between constituents of different electrical properties in response to an electrical field (Santamarina 2001, Klein 2004). It increases with a larger difference between the conductivity of particle surfaces and conductivity of the pore fluid (Arulanandan 2003, Liu 2007). For clayey soils with relatively high S_a, a second mechanism of double layer polarization arises following the relative displacement of the diffuse layer counterion clouds with respect to the charged particle; however, its effect decreased sharply with increased electrolyte or particle concentration (Santamarina et al. 2001). Another mechanism named bound water polarization that stems from directional alignment of adsorbed water on soil particle surfaces (Santamarina et al. 2001) is negligible in the range of 1 MHz-100 MHz and only slightly affects the dielectric spectra at frequencies higher than 100 MHz (Liu 2007).

4.1.4 Initiative of the Study on Electromagnetic Properties

The goal of this study is to investigate the dielectric responses of expansive soils when compacted as well as during 1-D hydromechanical deformation, and consistently and effectively relate the electromagnetic properties to macroscopic behavior.

Liu and Mitchell (2009a) developed a physically-based model to predict dielectric spectra for sand, silt, pure clay and mixtures of sand and pure clay based on a series of predetermined and optimized physicochemical parameters. The three optimized parameters include the direct current (dc) conductivity of pore fluid, surface conductance and shape factor. While the former two can be experimentally determined or approximated, the last one, which was taken as the average length ratio of the longest over the shortest axis of individual particles, must be assumed or optimized. This parameter is especially complicated to determine in natural clayey soils because a variety of clay minerals coexist. Furthermore, the physicochemical interaction between clay and sand or silt or between various clay minerals was not taken into account in the model. The results of the dielectric spectra of expansive soils in this research provide a database for future validation and improvement of the model, especially on clayey soils. Additionally, the correlations analyzed in this study between the electromagnetic properties and the hydromechanical characteristics will help bridge the gap between the current geophysical models (e.g., Liu and Mitchell 2009a) and mechanical constitutive models (e.g., Barcelona Expansive Model (BEM) by Alonso et al. 1999&2005).

4.2 Test Setup and Procedure

In deducing the test data of a two-terminal electrode system, the expressions for real (relative) permittivity and effective (electrical) conductivity are:

$$\kappa' = \frac{\mathrm{Im}(1/Z)}{\omega \varepsilon_0 \alpha A/d} \quad \textbf{(4.4)}$$

$$\sigma = \frac{\mathrm{Re}(1/Z)}{\beta A/d} \quad \textbf{(4.5)}$$

Where ω is circular frequency; Z is impedance of the sample; A is area of each of the two identical electrodes and d is spacing between the two electrodes; α and β are calibration factors for a specific electrode pair (Cerato and Lin 2012).

A HP 4193A vector impedance meter with 400 kHz-110 MHz frequency range powered the two-terminal electrode system. Open circuit, short circuit and standard circuit measurements were performed for the initial calibration of the equivalent circuit according to the HP 4193A operation manual. The calibration factors α and β were introduced by Cerato and Lin (2012) for a given pair of electrodes. Usually, a calibration needs to be conducted by testing a standard liquid or electrolyte with a constant value of κ' or σ (invariant within the radio frequency range) in order to obtain the actual values of κ' and σ of the sample under test. In the interest of measuring electromagnetic properties during soil deformation, the electrode spacing, d, should be able to change during the test. The ratio A/d is variable; therefore, calibration factors should then be deduced with dependence on the electrode size and spacing. Parallel electrode pairs of various size and spacing were used to determine calibration factors with a detailed process discussed in Cerato and Lin (2012). The relationships between α and β and R_{eq}/d (R_{eq} = sqrt(A/π)) were found to follow trends described by the following two equations:

$$\alpha = k_1 + m_1 (R_{eq}/d)^{-n_1} \quad \textbf{(4.6)}$$

$$\beta = k_2 + m_2(R_{eq}/d)^{-n_2} \quad \textbf{(4.7)}$$

In which k_i, m_i and n_i (i = 1,2) change with frequency. Their values were attained corresponding to each of the 43 sweeping frequencies (ranging from 400 kHz-110 MHz) of the HP4193A in the automatic sweep mode. The R^2 value varies between 0.92~0.99 for the frequencies applied. As a result, the factors α and β not only change with R_{eq}/d but also vary with frequency. It must be noted that R_{eq}/d is used instead of A/d so that both sides of Equations (4.6) and (4.7) are dimensionless. The values of k_i, m_i and n_i and R^2 corresponding to each tested frequency are given in Appendix A.

The two-terminal electrode system used in this study includes two setups for which the calibration was performed within a Faraday cage(s). The dielectric measurement normal to the direction of sample compaction (described as horizontal) was undertaken in the first setup (Figure 4.1). In the sample preparation and test procedures, the ambient temperature was maintained to be 25.0 ± 0.5 °C. Each soil sample was initially compacted (at the optimum state) in a Plexiglas ring with a pair of slightly curved electrodes embedded in the inner wall. In this case, the calibration factors α and β only evolve with frequency because the electrodes shown in Figure 4.1 are integrated in the ring such that the R_{eq}/d value is constant. It is worth noting that each sample must be compacted directly inside the ring in order to ensure a decent contact with the lateral electrodes. After compaction, the sample in the ring was sealed for moisture equalization in a humidity room for two weeks. During the test in the first setup (Figure 4.1), the top and bottom surfaces of the sample were covered by cling wrap and Plexiglas plates to prevent loss of moisture. The copper wires were connected from the electrodes to the component adapter while both the ring and the adapter were

enclosed in a Faraday cage. The reason for using a Faraday cage for both the calibration and test processes will be discussed later.

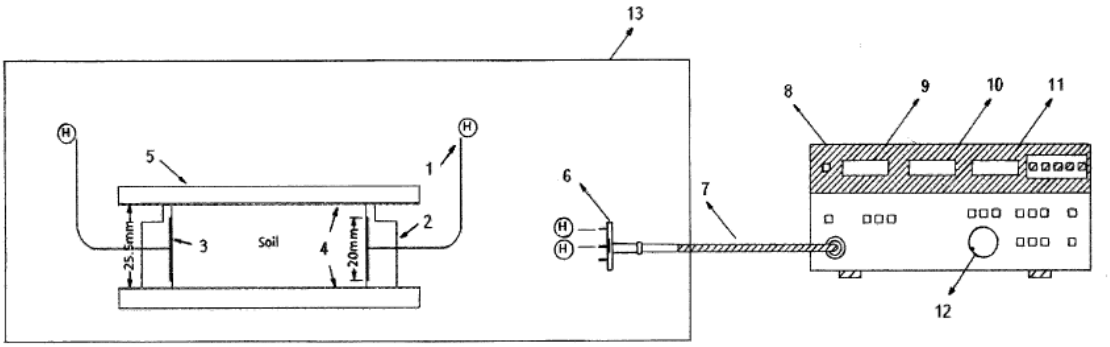

Figure 4.1 Dielectric measurement setup 1*

*H-Horizontal measurement (1- Coated copper wire, 2- Plexiglas ring, 3- Copper electrode, 4- Cling wrap sheet, 5- Plexiglas plate, 6- Component adapter, 7- Probe, 8- HP 4193A vector impedance meter, 9- Magnitude of impedance, 10- Phase angle, 11- Frequency, 12- Frequency control dial, 13- Faraday cage)

After the horizontal dielectric measurement was completed with the setup shown in Figure 4.1, the soil sample was uncovered and carefully extruded with a hydraulic jack into another Plexiglas ring of the same size and dimension but with no electrodes and wires attached. The second ring was then installed in a modified oedometer cell as shown in Figure 4.2, with the bottom and top stones containing flat electrodes for the dielectric measurement in the direction of compaction (marked as vertical). It must be noted that in Figure 4.2 the value of R_{eq}/d varies with soil deformation. Therefore, the magnitudes of α and β vary with both frequency and R_{eq}/d in this setup and should be calculated from Equations (4.6) and (4.7) according to each test frequency. An initial seating load of 1 kPa was applied on the sample and the measurement was taken. Afterwards, de-ionized water was introduced to inundate the sample to let it experience free swelling under the seating load, and then the applied load was varied so that the

sample underwent a series of deformation stages including consolidation to the original height, rebounding under the seating load (1 kPa), and recompression to the initial height. Dielectric measurements were performed at the end of each stage.

For the two stabilized samples (stabilized Hollywood and stabilized Heiden), where no meaningful swelling was observed ($\delta h < 0.1$ %), the dielectric measurements were performed at their initial compacted states and approximately 24, 48, 72 and 144 hours after inundation of the sample in de-ionized water.

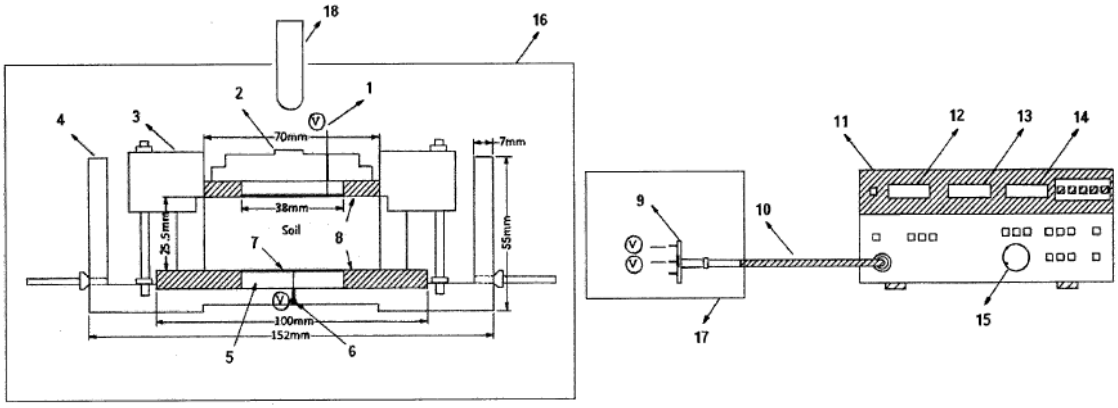

Figure 4.2 Dielectric measurement setup 2*

*V-vertical measurement (1- Coated copper wire, 2- Plexiglas cap, 3- Plexiglas frame, 4- Plexiglas cell, 5- Indented Plexiglas plate, 6-Notch for outreach of the bottom copper wire, 7- Copper electrode, 8- Porous stone, 9- Component adapter, 10- Probe, 11- HP 4193A vector impedance meter, 12- Magnitude of impedance, 13- Phase angle, 14- Frequency, 15- Frequency control dial, 16- Faraday cage 1, 17-Faraday cage 2, 18- Loading piston)

Initially it was thought that the dielectric measurements could be taken in both directions concurrently (i.e., the curved electrode pair embedded in the ring wall and the pair of flat electrodes in the bottom and top stones implemented simultaneously for both horizontal and vertical measurements), as was illustrated in the work of Cerato and Lin (2012). However, it was found that the two pairs of electrodes created interference for each other, as will be presented later. Therefore, the use of each pair must be isolated.

In order to gather both horizontal and vertical measurements on an identical sample, the sample had to be extruded from the ring with the embedded curved electrodes into one without embedded electrodes after finishing the horizontal measurement. The order in which the setup in Figure 4.1 was used first and the one in Figure 4.2 second cannot be reversed. Extruding the sample into the ring with the embedded curved lateral electrodes cannot assure a decent contact between the sample and the lateral electrode and may cause contamination of the lateral pair of electrodes with lubricant grease, which is commonly applied to minimize the soil-ring friction.

4.3 Issues Associated with the Test Approach

4.3.1 Enclosure of the DUT in a Faraday Cage

A Faraday cage is recommended to enclose the device under test (DUT) in order to block out potential external electromagnetic interferences. It is practically an ideal hollow conductor which is able to rearrange charges produced by any externally applied electric fields leading to the cancellation of the applied field inside so that the internal atmosphere becomes neutral. The Faraday cages used in this research were made of copper mesh with a maximum opening of 6 mm, which is much less than the wavelengths of radio radiation of this study (≈ 5 m~500 m).

In order to evaluate the impact of a Faraday cage on the test results, horizontal measurements (with the setup shown in Figure 4.1) were undertaken on Carnisaw and Eagle Ford samples with and without using a Faraday cage and the comparisons are presented in Figure 4.3. In addition, a Minco silt (LL = 20, PI = 4) sample of 15 % moisture content and 19.2 kN/m^3 wet unit weight was tested for its real permittivity

curves for comparison with the findings of Varghese (1996), who tested an identical compacted sample within a Faraday cage (Figure 4.3). It must be noted that Varghese (1996) failed to report effective conductivity data that would otherwise be useful for comparison with the effective conductivity data of this study.

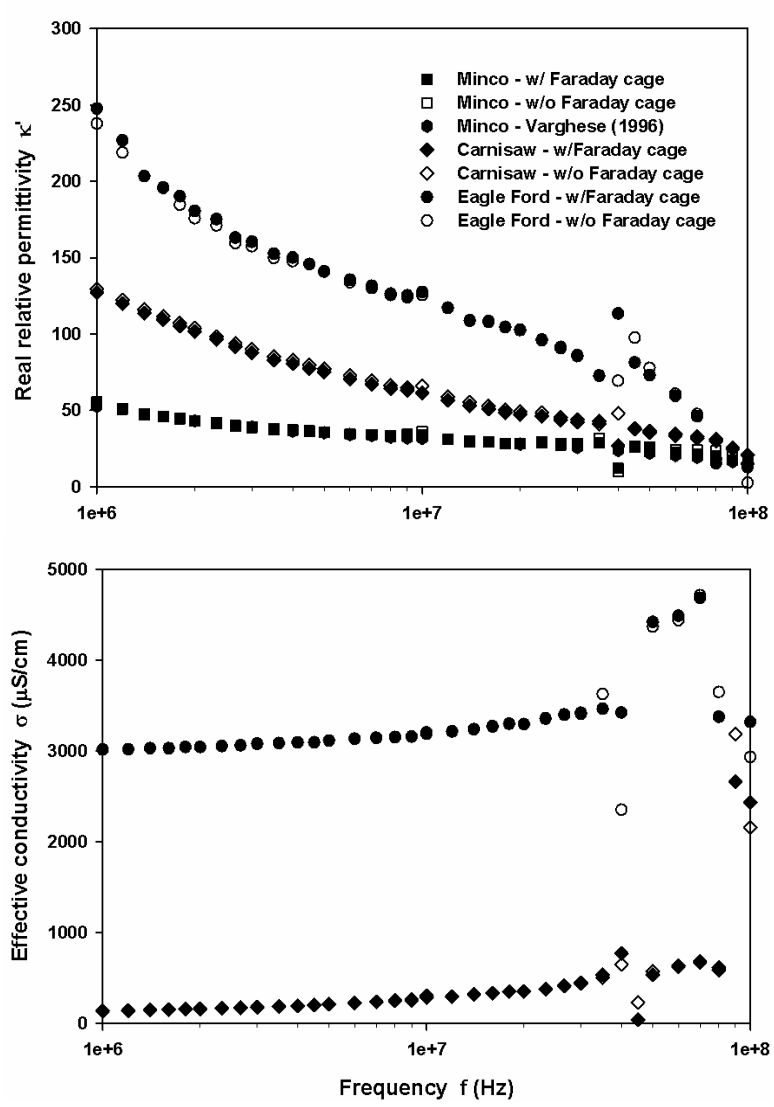

Figure 4.3 Effect of Faraday cage on dielectric measurements

As seen from Figure 4.3, the Faraday cage is insignificant in affecting real permittivity within the frequency range concerned (1 MHz-100 MHz), except at 40

MHz where a peak takes place because of electronic resonance. In terms of effective conductivity, σ, the most significance of the Faraday cage was again seen at the peaks around 40 MHz. Beyond this frequency, the external electrical interference results in slight deviation with respect to the measured effective conductivity. The close correspondence between the test data with and without Faraday cage implies that the test environment in this research (a basement room) had little external electromagnetic interferences. Nevertheless, to ensure consistency and repeatability of the test results, the Faraday cage was used in all dielectric measurements.

4.3.2 Separated Applications of Two Electrodes Pairs

As discussed briefly before, simultaneous application of the two pair of electrodes is not recommended because electronic interactions increase the measurement of both real permittivity and effective conductivity. This phenomenon is highlighted in Figure 4.4 for the results of a compacted Carnisaw sample.

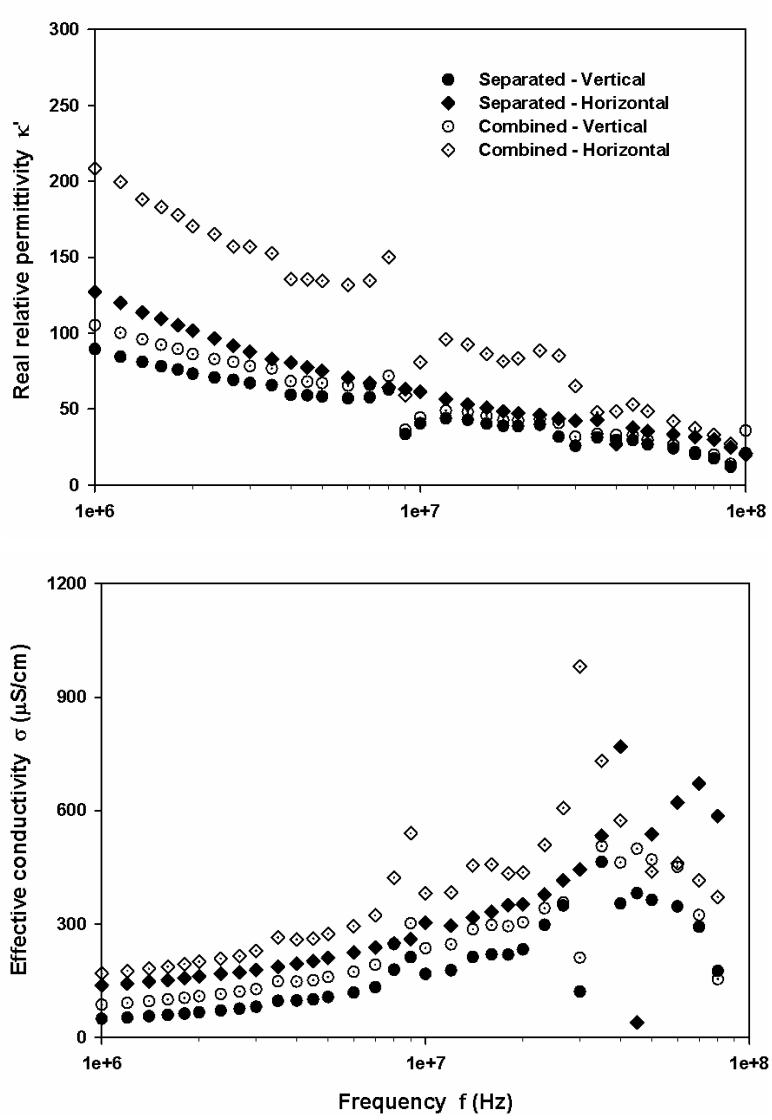

Figure 4.4 Separated vs. combined applications of the two pairs of electrodes

Such an interaction affects the real permittivity when using the horizontal electrode pair (the one performing the horizontal measurement) more significantly than the vertical (the pair taking the vertical measurement). This may be due to the relative geometric alignment of the two pairs when they are used in combination which promotes charge movement that strengthens interfacial polarization. The influence of electrode interaction on the measurement of effective conductivity influences each pair

to a similar extent (Figure 4.4). The existence of the second pair of electrodes shortens the peripheral electrical paths for the test electrodes providing overestimation of the electrical conductivity.

4.3.3 Measurement Accuracy

As mentioned, the major problem associated with the two-terminal electrode system in the radio-frequency range is electrode polarization caused by charge accumulation on the surface of electrodes. This charge accumulation results in the formation of an electrical double layer that modifies the ion distribution within the sample under investigation. Electrode polarization has been revealed (Klein and Santamarina 1996&1997, Bordi et al. 2001) based on testing various electrolyte solutions. For a specific soil-electrolyte mixture, however, the lower frequency boundary at which electrode polarization becomes negligible is still uncertain and can only be approximated using the method developed by Klein and Santamarina (1997). The lower frequency boundary of the soils investigated in this study was estimated to vary within 50 kHz-2 MHz. Please note that the frequency boundary at which effective conductivity is affected by electrode polarization is much lower than that of real permittivity as discussed earlier.

The measured real permittivity curves exhibit satisfactory continuity (Figure 4.3 and 4.4), whereas the effective conductivity measurement produces highly scattered data at frequencies greater than 20 MHz. This phenomenon may be attributed to the limitations of the two-terminal system in measuring effective conductivity at the frequency range beyond 20 MHz. A network analyzer in conjunction with a coaxial probe test configuration was shown to provide continuous measurement of soil

conductivity (from 20 MHz-1.3 GHz) Klein (2004). The measurement of real permittivity using the two-terminal system, however, is highly repeatable as shown by the comparison of the data of this study versus those of Varghese (1996) (Figure 4.3). To further ensure repeatability using the two-terminal system, additional tests were conducted on Hollywood and Heiden soils providing corroboration of the real permittivity (1 MHz-100 MHz) and effective conductivity (1 MHz-20 MHz) data.

4.4 Quantification of Diffuse Double Layer

It is necessary to quantify the diffuse double layer (DDL) and pore fluid conductivity that will be held responsible for a possible explanation of the dielectric responses of each soil presented later. However, the thickness of the DDL remains, in many respects, a theoretical concept (Mojid and Cho 2006). The equation proposed by Mojid and Cho (2006), described as the thickness of DDL equal to the "critical state water content" normalized by S_a and density of water, was constrained by the absence of dissolved solutes. It predicted DDL thicknesses for sand-bentonite mixtures in distilled water within a range of 5-107 % difference in comparison with the method of Schofield (1947), but showed 507-9834 % larger DDL thicknesses for mixtures with salt existence in the suspension (Mojid and Cho 2006). The method of Mojid and Cho (2006), therefore, was not considered in this study due to the possibility of salt presence in natural expansive soils.

Schofield (1947) described the thickness of a fully developed DDL as:

$$t_1 = \frac{q}{\sqrt{\nu\beta n}} - \frac{4}{\nu\beta\Gamma} \qquad \textbf{(4.8)}$$

The DDL thickness can also be evaluated as the Debye-Hückel length (Santamarina et al. 2001) and expressed as:

$$t_2 = \sqrt{\frac{\varepsilon_0 R \kappa' T}{2F^2 n \nu^2}} \qquad \textbf{(4.9)}$$

Within Equations (4.8) and (4.9), q is a factor dependent on cation versus anion ratio (e.g., 2 for NaCl and 1.46 for Na_2SO_4), ν is cation valence, β stands for $8\pi F^2/(\varepsilon_0 \kappa' RT)$, $\varepsilon_0 = 8.85 \times 10^{-12}$ F/m is permittivity of vacuum, κ' is real relative permittivity, $F = 9.6485 \times 10^4$ C/mol is Faraday's constant, R = 8.314 J/(K·mol) is gas constant, T is absolute temperature (= 298.15 K) here, n is salt concentration (mol/m^3), Γ is surface charge density (meq/m^2).

In order to deduce salt concentration, n, a convenient and universal approach is to create 1:5 soil water mixtures from which the dc conductivity of the bulk fluid (extracted liquid after filtering), σ_{bl_1} is obtained (Munns 2004, Pansu and Gautheyrou 2006). It is worth mentioning that "bulk fluid" refers to the fluid phase of a soil suspension while "pore fluid" represents the fluid phase of a compacted or consolidated soil sample. The magnitude of σ_{bl_1} was measured in this study using a calibrated conductivity benchtop manufactured by Thermo electron corp. A value of 1 mS/cm approximately equals 640 mg/L of soluble salts (Silva and Uchida 2000, Munns 2004). Additional sulfate tests following OHD L-49 (2005) were carried out and sulfate was detected in Eagle Ford, stabilized Hollywood and stabilized Heiden with a recorded value of 354, 92 and 122 ppm. Provided SO_4^{2-} and Cl^- are the most frequently existing anions in soil salts (Pansu and Gautheyrou 2006), for simplicity purposes Na_2SO_4 was assumed as the salt in extract liquid of the samples detected with sulfate and NaCl was

assumed for the other three soils; therefore, the salt concentration, n, can be transformed from mass per volume to molarity per volume. The bulk fluid (extracted liquid) was then measured for κ'_{bl} and σ_{bl_2} using the dielectric measurement setup shown in Figure 4.1. For electrolytes only (without soil inclusion), effective conductivity does not vary with frequency (within radio frequency range) and is approximately equal to the dc conductivity. The estimated parameters used to calculate the DDL thicknesses using two theories (t_1 and t_2) are listed in Table 4.1. The magnitudes of σ_{bl_1} measured using a dc conductivity probe, and σ_{bl_2} of the extracted liquid measured in the dielectric setup, are relatively close. The favorable comparison between σ_{bl_1} and σ_{bl_2} further verifies the dielectric measurement methods of this study. The dielectric measurements were conducted on the bulk fluid not only for verification purposes but also to obtain the value of κ'_{bl} which is used to calculate the DDL thickness.

Table 4.1 Estimated thickness of fully developed DDL

Soil sample	σ_{bl_1} (μS/cm)	σ_{bl_2}[a] (μS/cm)	κ'_{bl}[a]	n (mol/m^3)	Γ^* (meq/m^2)	t_1 (μm)	t_2 (μm)	Variation[†] (%)
Carnisaw	21	23	86	0.23	2.54×10^{-3}	0.012	0.021	44
Eagle Ford	1344	1292	84	6.06	2.32×10^{-3}	0.002	0.004	59
Hollywood	105	105	83	1.15	1.81×10^{-3}	0.005	0.009	44
Stabilized Hollywood	617	592	85	2.78	3.84×10^{-3}	0.002	0.006	59
Heiden	149	156	87	1.63	2.21×10^{-3}	0.004	0.008	44
Stabilized Heiden	713	701	87	3.21	3.38×10^{-3}	0.002	0.006	59

[a]do not vary with frequency for electrolytes within the radio frequency range
[*]$\Gamma \approx CEC/S_a$ (Santamarina et al. 2001) [†]Variation = $(t_2-t_1)/t_2$

The fully developed DDL thickness in each soil, t_1 and t_2, as calculated from Equations (4.8) and (4.9), respectively, compare well. In both equations, the DDL

thickness is largely governed by the bulk fluid concentration, n, which is revealed by the bulk fluid conductivity, σ_{dc}, regardless of the physicochemical nature of the clay particle itself. The n governs the DDL thickness calculations in part because κ' of an electrolyte remains nearly constant with varying salt concentrations (Bordi et al. 2001). In addition, assumption of other salt types has little impact on the thickness and will not change the sequence of the four untreated samples rendering the bulk fluid conductivity (σ_{bl_1} or σ_{bl_2}) the determining factor in evaluating the DDL thickness. Therefore, it is not surprising that Carnisaw shows a significantly thicker DDL than that of the much more plastic Eagle Ford concerning the markedly greater conductivity of the extract liquid of Eagle Ford. Meanwhile, chemical reaction with CFA brings in additional salts to the bulk fluid and leads to a decrease of the DDL thickness (Table 4.1). It must be noted that even though there is parameter Γ (controlled by S_a and CEC) on the right side of Equation (4.8), the magnitude of the second term is much smaller than the first and can be ignored (Mojid and Cho 2006).

The thickness data (t_1 and t_2) deduced in Table 4.1 are representative of the fully developed state of the DDL when the clay particles are hydrated in 1:5 soil water suspensions. The electromagnetic properties of the pore fluid phase of a compacted or consolidated oedometer soil sample are not currently measureable and thus the corresponding DDL thickness cannot be quantified. Instead, the DDL thickness can be qualitatively analyzed for an oedometer soil sample. First of all, its soil-water ratio is much higher than when in suspension, meaning a relative increase in concentration, n and a consequent reduction of DDL thickness. Second, the interaction of adjacent particles is enhanced, resulting in DDL contraction. Last but not least, the development

of DDL is suppressed as the sample becomes unsaturated. On the other hand, the bulk fluid conductivity (measured on extracted liquid of a soil suspension) is used to qualitatively represent the pore fluid conductivity (conductivity of the pore fluid phase of an oedometer soil sample) because the latter is not, at present, experimentally achievable (the dielectric measurements on an oedometer soil sample obtain effective conductivity of the entire sample).

Another quantitative description of DDL is surface conductance λ_{ddl} (Table 4.2), which when normalized by the DDL thickness produces surface conductivity (conductivity of the DDL) (Santamarina et al. 2001), σ_{ddl}. The degree of interfacial polarization of clayey soils is determined by the difference in magnitude between surface conductivity σ_{ddl} and that of pore fluid (Santamarina et al. 2001, Liu and Mitchell 2009b). Since σ_{el} (also a constant) is not directly measurable, its magnitude was qualitatively evaluated by σ_{bl} instead. The comparison of σ_{ddl} with the bulk fluid (electrolyte) conductivity, σ_{bl}, is illustrated in Table 4.2.

Table 4.2 Surface conductivity versus bulk fluid conductivity

Soil sample	λ_{ddl} (μS)	t_{avg}[a] (μm)	σ_{ddl} (μS/cm)	σ_{bl}[b] (μS/cm)	$\sigma_{ddl} - \sigma_{bl}$ (μS/cm)
Carnisaw[*]	0.080[*]	0.016	48597[*]	24	48574[*]
Carnisaw[†]	0.002[†]	0.016	1032[†]	24	1008[†]
Eagle Ford	0.014	0.003	47659	1292	46367
Hollywood	0.011	0.007	15024	105	14918
Stabilized Hollywood	0.023	0.004	53815	592	53223
Heiden	0.013	0.006	20957	156	20801
Stabilized Heiden	0.020	0.004	50133	701	49432

[a]average of t_1 and t_2 given in Table 4.1; [b]the values of σ_{bl_2} (Table 4.1) are used;
[*]taking into account the contribution of hydrogen; [†]excluding the effect of hydrogen

Table 4.2 shows that if the contribution of hydrogen to λ_{ddl} is not accounted for then the sequence of the magnitude of (σ_{ddl} - σ_{bl}) accurately corresponds with the ranking of the extent of interfacial polarization phenomenon indicated in Figure 4.5. The smaller magnitude of (σ_{ddl} - σ_{bl}) of Carnisaw is more reasonable, owing to the fact that the hydrogen ion diffuses much more rapidly than the other types of cations in the free liquid phase so that the associated conductivity may not contribute to the conduction of the diffuse ion swarm constrained around clay surfaces. Another profound feature of Table 4.2 is the overwhelming magnitude of σ_{ddl} relative to that of σ_{bl}. This may arise from the underestimation of diffuse double layer thickness (t_{avg}) due to its predominant dependence on bulk fluid concentration (as discussed earlier) that leads to over-prediction of σ_{ddl}; on the other hand, the usage of σ_{bl} instead of σ_{el} may result in underestimated conductivity of the pore fluid phase in a soil sample.

4.5 Results and Discussion

4.5.1 Dielectric Responses of the Compacted Samples

The test method proposed in this study introduces a convenient approach to study the microscopic electromagnetic behavior of soil samples that are suitable for conventional oedometer testing. Even though the dielectric measurements were performed in the device frequency range of 400 kHz-110 MHz, the permittivity and conductivity data were presented for the frequency range of 1 MHz-100 MHz only, within which the effects of electrode polarization were minimized and electronic resonance (at 110 MHz) avoided. The dielectric spectra of the four untreated samples are presented in Figure 4.5.

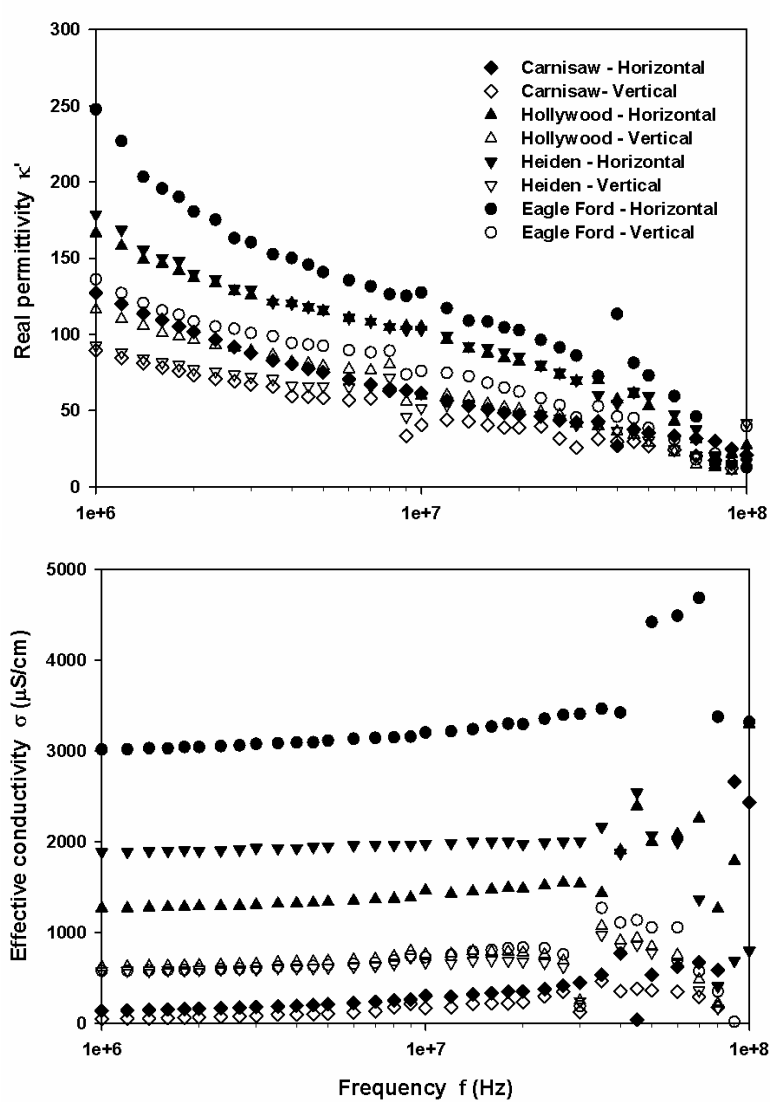

Figure 4.5 Dielectric spectra of the four untreated samples

For the untreated samples, both κ', σ and the dispersion of κ' increase in magnitude in the order of Carnisaw < Hollywood < Heiden < Eagle Ford. This sequence coincides with the order of the magnitude difference of (σ_{ddl} - σ_{bl}) (Table 4.2), which determines the degree of interfacial polarization, regardless of the measurement direction. Surface conduction (the act of surface conductance λ_{ddl}) has been shown as the dominant mechanism in determining the polarization and conduction and an

important contributor to global soil conductivity in pure clay saturated with low ionic concentration pore fluid (Santamarina et al. 2001, Klein and Santamarina 2003). It is therefore proven here that the degree of interfacial polarization across the radio-wave frequency range can be qualitatively predicted by the quantities of (σ_{ddl} - σ_{bl}). Meanwhile, a comparison of Table 4.1 and Figure 4.5 indicates that the both the bulk fluid conductivity σ_{bl} and the conductivity of the compacted sample σ follow the same order of Carnisaw < Hollywood < Heiden < Eagle Ford and are significantly higher in Eagle Ford than in Carnisaw. This suggests that the pore fluid conduction can contribute substantially to the effective conductivity of a compacted natural expansive soil. It must be noted that surface conduction plays the predominant role in determining the overall conductivity of clay suspension washed with de-ionized water (the reason why the clay-water mixture conductivity is greater than that of water). As the bulk fluid concentration increases the bulk fluid conductivity σ_{bl} begins to take on a more important role in controlling the suspension conductivity (Raythatha and Sen 1986, Liu and Mitchell 2009b). Nevertheless, the contribution of pore fluid conductivity σ_{el} relative to surface conductivity σ_{ddl} of a compacted sample is not well understood yet due to the fact that the pore fluid conductivity σ_{el} of a compacted or consolidated sample is not experimentally achievable. At the same time, all of the samples exhibit various degrees of electrical anisotropy as implied by the higher measurement of κ' and σ in the horizontal, rather than the vertical direction. These findings support the geophysical model (Liu and Mitchell 2009a) in the predictions of electrical anisotropy of clay-water mixtures.

4.5.2 Dielectric Responses of the Stabilized Samples

The dielectric spectra of the untreated and stabilized Hollywood and Heiden are depicted in Figures 4.6 and 4.7, respectively. Some interesting findings are discussed in the following paragraphs.

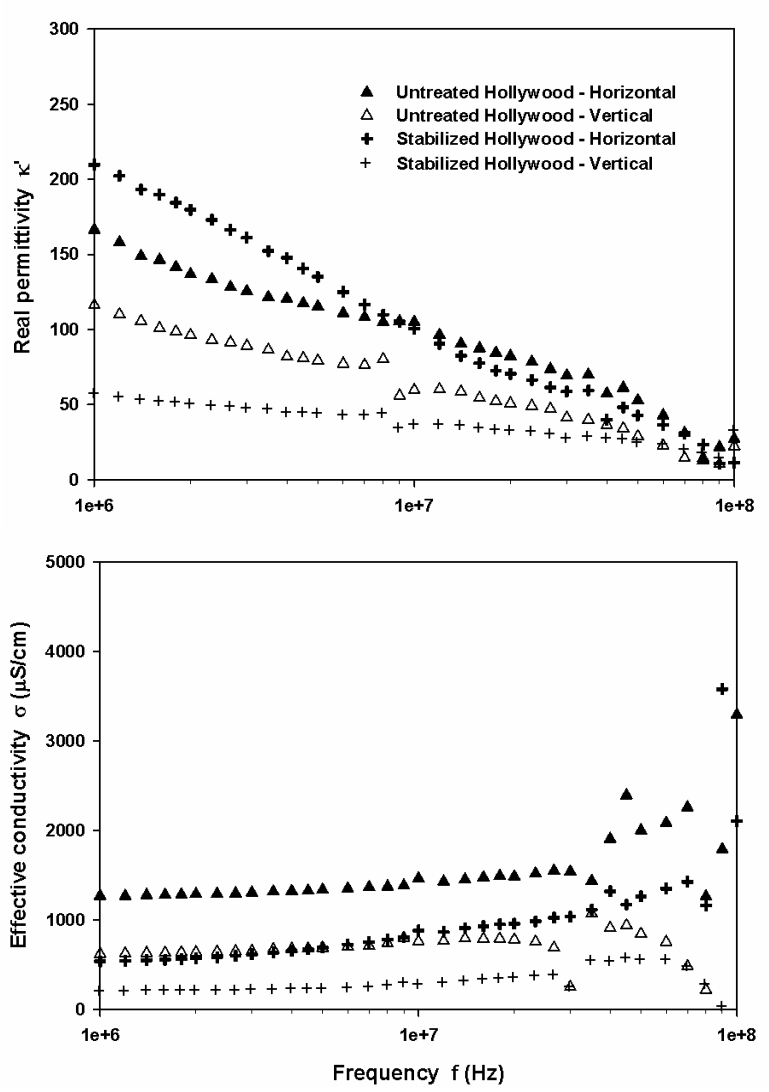

Figure 4.6 Dielectric spectra of untreated and stabilized Hollywood

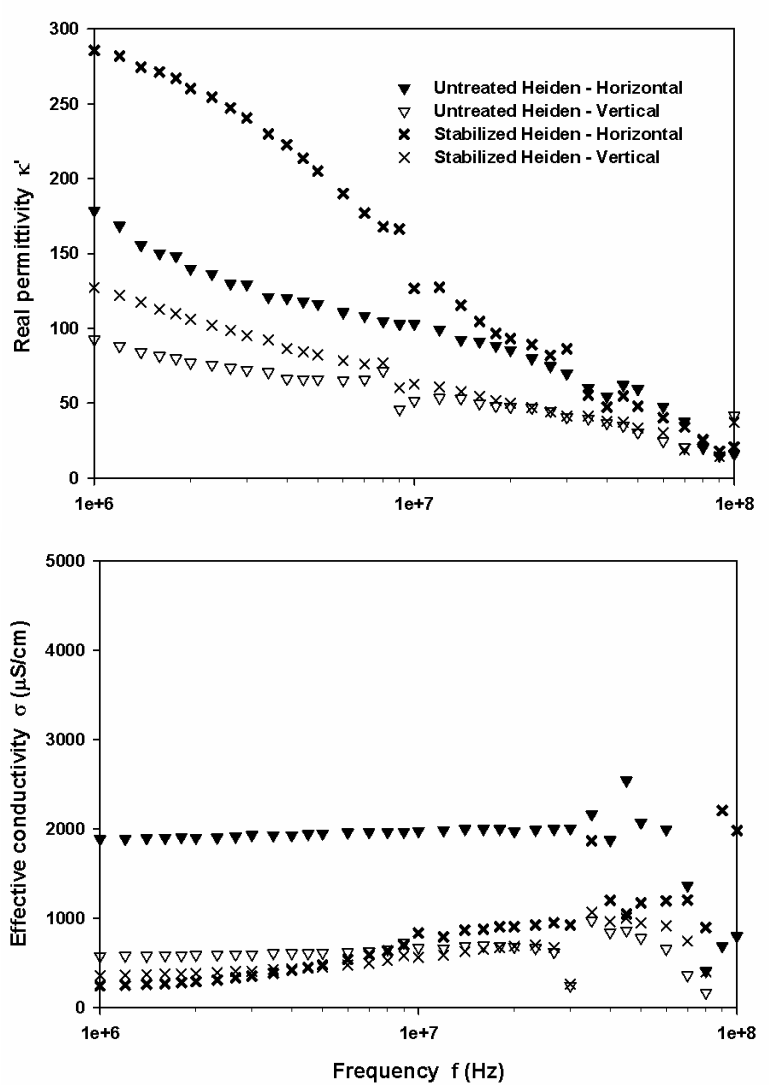

Figure 4.7 Dielectric spectra of untreated and stabilized Heiden

Chemical stabilization of expansive soils with CFA created significant changes of physicochemical characteristics of the soil highlighted by the increases of CEC and decrease of S_a (Table 2.3), as well as the decrease of t_{avg} (Table 4.2) the overall effects of which produced higher surface conductance λ_{ddl} (Table 2.3 and 4.2) and surface conductivity σ_{ddl} (Table 4.2). In the meantime, the magnitudes of σ_{ddl} overwhelm σ_{bl} (Table 4.2) though the latter also increase following stabilization. This is verified by the

comparison of dielectric responses between untreated and stabilized samples (Figures 4.6 and 4.7); implying chemical stabilization by CFA generally strengthened polarization and dispersion except for the vertical measurement of real permittivity of stabilized Hollywood. A special performance of the stabilized samples is highlighted by the reduced effective conductivity in both vertical and horizontal measurements compared to their untreated counterparts (Figure 4.7); whereas, both the significant contribution of σ_{ddl} and σ_{bl} (Table 4.1) and intensified polarization (Table 4.2) would supposedly be expected to strengthen the effective conductivity of the stabilized samples similar to the case of Eagle Ford compared to Carnisaw. Notice that such an anomaly cannot simply be explained by the drastic change in structure, as it had been seen in both vertical and horizontal measured results.

Difficulties were encountered when attempting to explain the abnormal responses of the stabilized soils, not only because their structure became complicated and ambiguous, but also due to insufficient understanding of the roles of the fly ash gel surfaces and the cementing agent in the polarization. It is worth mentioning here that no research on the dielectric spectra of CFA stabilized soils was found in the literature that could be otherwise used for comparison and reference. Further research on underlying electromagnetic mechanisms of the chemically stabilized soils is recommended.

4.5.3 Definitions of κ'_{inf} and σ_{dc} of Soil Samples

The electromagnetic properties of a compacted sample are dependent on water content, mineralogy, structure and σ_{dc} of the liquid phase (pore fluid). Interfacial polarization functions as the major polarization mechanism occurring within the radio frequency range, however, the κ' becomes nearly constant and independent of frequency

when the frequency reaches a certain value where there is not enough time for charge accumulation at the interfaces (Arulanandan 2003). The κ' at this point, which was defined as κ'_{inf} (Santamarina et al. 2001, Arulanandan 2003), is also independent of pore fluid conductivity σ_{el}, which only affects the electromagnetic properties during relaxation. In short, for a specific soil (with fixed mineralogy), κ'_{inf} reveals the intrinsic particle/aggregate shape and alignment and the state of saturation in macro and micro pores. In the works of several researchers (Fernando et al. 1977, Campbell 1990, Arulanandan 1991, Varghese 1996, Arulanandan and Yogachandran 2000), κ'_{inf} was taken to be the magnitude of permittivity at 50 MHz and shown to be mainly a function of saturation ratio, structure and mineralogy while independent of pore fluid chemistry. The analysis of real permittivity dispersion, however, is complicated by the ionic conductivity of the pore fluid (σ_{el}). Moreover, the magnitude of dispersion may suffer from electrode polarization at low MHz frequencies as discussed earlier; the effect of which can hardly be quantified. In this regard, this study qualitatively evaluated the dielectric dispersion behavior and quantitatively analyzed the κ'_{inf} magnitude during various stages of deformation.

The effective conductivity, σ, is a product of the interaction between DDL and pore fluid and varies with frequency. The σ below 1 MHz has been used to evaluate soil anisotropy (Meegoda et al. 1989, Klein and Santamarina 2003) and estimate stiffness and liquefaction of granular soils (Arulmoli et al. 1985, Arulanandan and Muraleetharan 1988). As has been illustrated (Figures 4.4-4.7), the measurement of σ with the test system in this study is satisfactory up to 20 MHz, while electrode polarization has little influence on the conductivity measurement at the frequency range concerned (1 MHz-

100 MHz). Moreover, since the contribution of the polarization loss to σ becomes trivial at frequencies less than 1 MHz, the σ value at these frequencies can be used to approximate the dc conductivity of a soil-electrolyte mixture (Liu and Mitchell 2009a&b), marked here by σ_{dc}. As a result, for the oedometer soil samples concerned, σ at 1 MHz is taken as the approximate magnitude of σ_{dc}. It must be noted that this σ_{dc} represents the dc conductivity of the entire soil sample, which combines the effects of both pore fluid conduction and surface conduction.

4.5.4 Evaluation of Anisotropy

In this context, the electrical anisotropy of the samples at the compacted or stabilized state can be evaluated as the ratio of κ'_{inf} and σ_{dc} measured at two directions, as illustrated in Table 4.3.

Table 4.3 Evaluation of sample anisotropy based on κ'_{inf} and σ_{dc}*

Soil sample	$(\kappa'_{inf})_h$	$(\kappa'_{inf})_v$	$(\sigma_{dc})_h$	$(\sigma_{dc})_v$	$(\kappa'_{inf})_h/(\kappa'_{inf})_v$	$(\sigma_{dc})_h/(\sigma_{dc})_v$
Carnisaw	35.6	26.8	138	49	1.33	2.82
Eagle Ford	73.1	38.6	3018	578	1.89	5.22
Hollywood	52.8	29.0	1269	621	1.82	2.04
Stabilized Hollywood	42.9	24.7	536	199	1.74	**2.69**
Heiden	59.4	30.4	1888	576	1.96	3.28
Stabilized Heiden	48.1	33.3	244	356	1.44	**0.69**

*Note: subscripts "h" and "v" represent the horizontal and vertical directions, respectively

For the untreated samples (compacted), the tendency for the platy clay particle or elongated aggregates to have their long axis oriented in the horizontal plane favors the contribution of surface conduction to the sample conductivity when exposed to the horizontal electrical field, while the tortuosity of the pore fluid path is substantially decreased in the horizontal direction. The larger $(\kappa'_{inf})_h$ than $(\kappa'_{inf})_v$ implies that the

strengthened effect of surface conduction overcompensates for the enhanced contribution from pore fluid conduction, whereas such an alignment strengthens the contributions of both pore fluid conduction and surface conduction to the overall $(\sigma_{dc})_h$ relative to $(\sigma_{dc})_v$. Therefore, the electrical anisotropy acts as a direct reflection of structural anisotropy. Such anisotropy is revealed more substantially in the case of Eagle Ford (Table 4.3), regarding its greater S_a and larger, thinner clay platelets in a more laminar structure in comparison to the case of Carnisaw (Figure 3.10 (a) and (b)).

Meanwhile, the stabilization dramatically altered the structure from formerly face-to-face or face-to-edge clusters to interweaved aggregate-cementing agent-fly ash gel complex, as proven by the SEM research on the studied soils (Figure 3.10 (e) and (f)). This should result in a decrease of anisotropy and is indeed verified by the reduced $(\kappa'_{inf})_h/(\kappa'_{inf})_v$ (Table 4.3). However, the ratio of $(\sigma_{dc})_h/(\sigma_{dc})_v$ shows either a slight increase (Hollywood) or a radical reduction (Heiden) in magnitude (Table 4.3). Such an abnormality can be related to the conductive nature of the fly ash gels, as discussed earlier; with the mechanisms remaining unclear.

4.5.5 Relationships of κ'_{inf}, σ_{dc} with Deformation or Time

Each untreated sample followed a procedure of free expansion-compression-rebounding-recompression using the setup shown in Figure 4.2. κ'_{inf} and σ_{dc} were obtained at the end of each stage, measured at 50 MHz and 1 MHz, respectively, and their relationships with deformation are plotted in Figure 4.8. The stabilized samples were tested with the same setup; however, since they did not exhibit any swelling behavior under the 1 kPa seating load the correlations of κ'_{inf} and σ_{dc} with the inundation time are depicted instead in Figure 4.9.

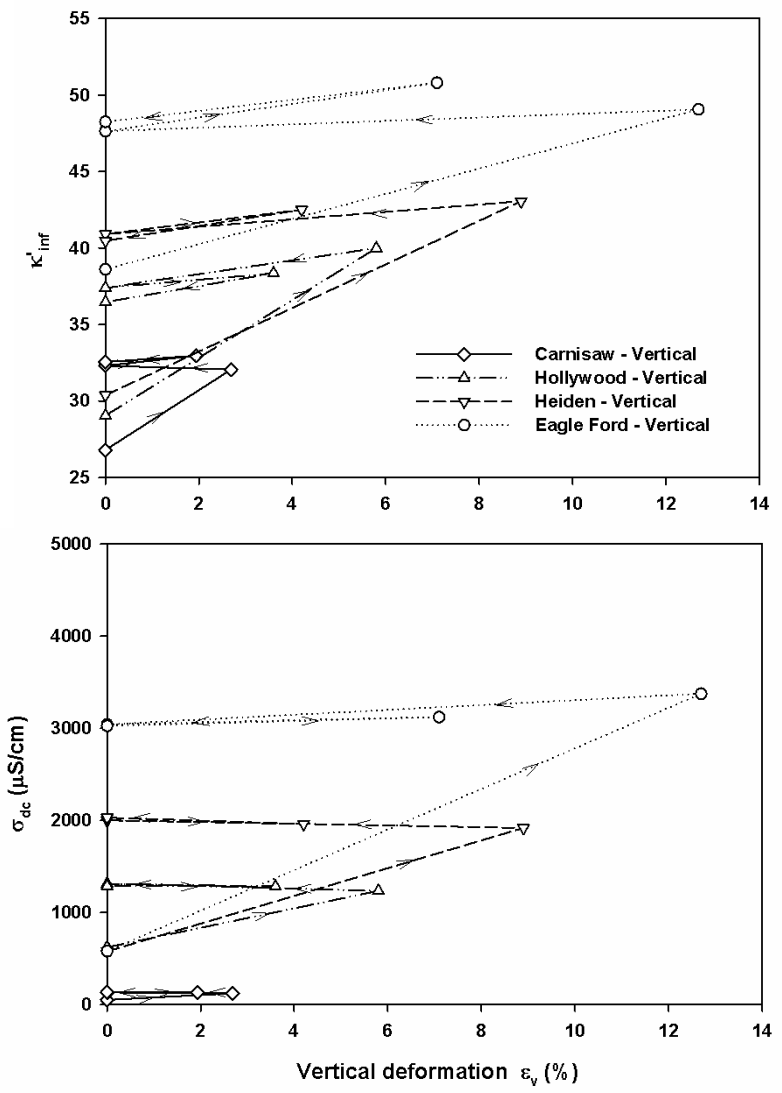

Figure 4.8 κ'_{inf} and σ_{dc} vs. deformation of the untreated samples

Both κ'_{inf} and σ_{dc} increase monotonically with the vertical expansion during the first stage of deformation (free swelling). Beyond this stage, the magnitudes become relatively insensitive to soil deformation. This phenomenon implies that the parameters κ'_{inf} and σ_{dc} of a single soil sample are primarily dependent on the saturation ratio, since the free swelling also acts as a hydration process whereas the following stages are merely compression-rebounding-recompression of saturated samples. The hydration

process interconnects previously isolated clay aggregates by gradually filling macropores, resulting in well-developed continuous flow paths favoring electrical conduction. Further widening or collapsing of macropores during the following deformation stages only slightly affect the pore fluid conduction. This also implies that the increase of σ_{dc} throughout the swelling process resulted mostly from the increase of continuous electrically conductive pathways in the pore fluid phase.

The evolutions of κ'_{inf} and σ_{dc} in response to the hydration process are also evident in the cases of the two stabilized samples as illustrated in Figure 4.9, which features increments of both κ'_{inf} and σ_{dc} with the inundation time.

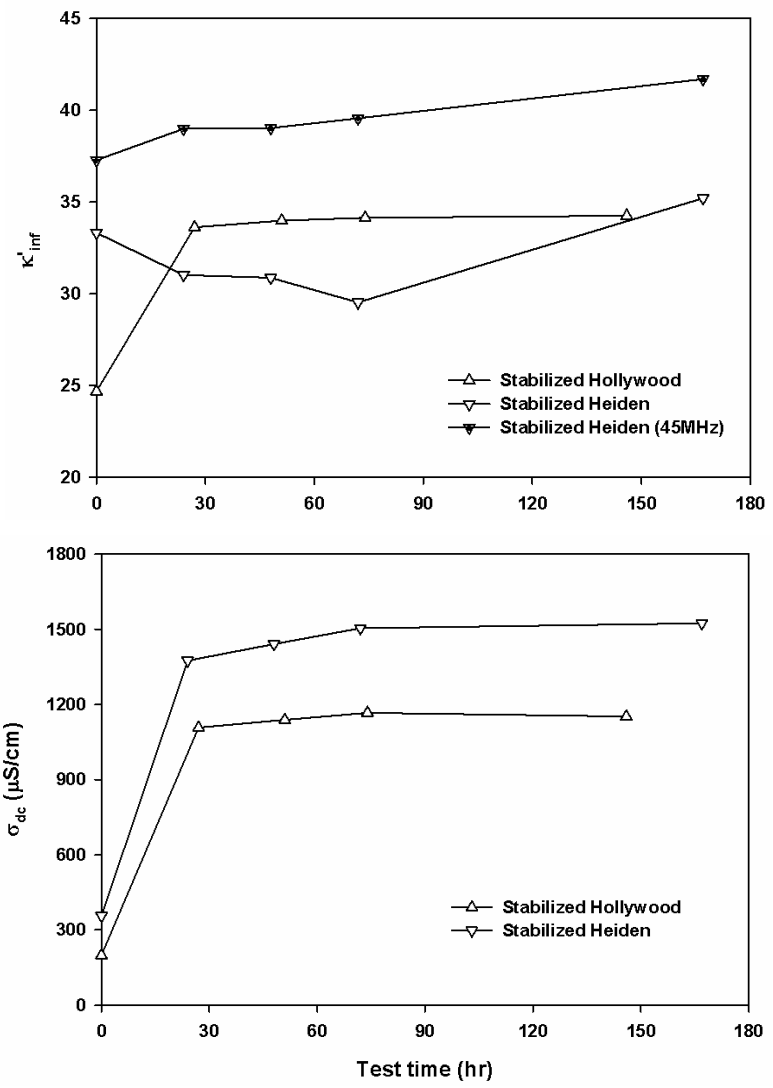

Figure 4.9 κ'_{inf} and σ_{dc} vs. test time of the stabilized samples

The κ'_{inf} curve of stabilized Heiden shows a little offset from the trend, but the curve at the former adjacent frequency (45 MHz in the automatic sweeping mode) clearly confirms this trend. The increase of κ'_{inf} and σ_{dc} with the hydration process seems to fall within the same mechanism as for the untreated samples: the effect of surface conduction is enhanced due to expansion of the DDL thickness, while pore fluid

conduction is strengthened by the filling of macropores and expelling of occluded air in the sample.

4.5.6 Discussion of the Roles of DDL and σ_{dc} on Dielectric Responses

Provided the much greater PI (Table 2.2) and higher montmorillonite content (Table 3.1) of Eagle Ford than those parameters of Carnisaw, a thicker DDL (when fully developed) of Eagle Ford tends to be expected. However, the thickness of DDL in the case of Carnisaw turned out to higher. In this regard, it may be necessary to re-evaluate the current Gouy-Chapman theory to take into account the impact of soil mineralogy and structure. The strong chemical reactions taking place in soil stabilization also blunts the theory since the development of DDL around a "clay platelet-fly ash gel complex" is suspicious.

For clay-water mixtures where the pore fluid concentration is relatively low (e.g., up to the level in this study), surface conduction plays the major role in controlling the extent of interfacial polarization and the effective conductivity of the mixture, revealed as enhanced dielectric dispersion, real permittivity and effective conductivity of a clay-water mixture relative to the electrolyte only. Meanwhile, the contribution of surface conduction is revealed to be affected by mineralogy, pore fluid chemistry, structure and water content (Santamarina et al. 2001, Liu and Mitchell 2009b). On the other hand, the development of pore fluid conduction is influenced by structure and water content as indicated by the anisotropy (Table 4.3) and the increase of σ_{dc} with the hydration process (Figures 4.8 and 4.9). Nevertheless, the magnitude of pore fluid conductivity σ_{el} is not yet measurable in a soil sample under hydromechanical

conditions and therefore may only be evaluated from the bulk fluid (liquid extract) conductivity σ_{bl} of a soil.

4.6 Conclusions and Summary

In this chapter, the real permittivity and effective conductivity of four untreated and two stabilized expansive soils were obtained from dielectric measurements using specifically designed setups of a two-terminal electrode system and a modified oedometer cell. Several comments and conclusions follow.

1. A special dielectric test procedure was developed by adopting the ideology of a two-terminal electrode system. This test can measure the initial electromagnetic properties of an undisturbed or compacted soil sample in directions normal to or parallel with that of consolidation/compaction, with the use of different pre-calibrated test setups. Moreover, integration of dielectric measurements with a modified oedometer cell accommodates the monitoring of dielectric responses of soil samples under various hydromechanical conditions.

2. Efforts were directed towards quantification of the DDL (in its fully developed state) in terms of thickness and surface conductance/conductivity. Two approaches in estimating the DDL thickness achieved close results with a variation less than 59 %. The thickness was largely influenced by the salt concentration, n, in the bulk fluid of the studied soil samples implied by its decrease with increasing concentration, regardless of soil type. However, neither mineralogy nor structure was accounted for in the underlying theory. The development of DDL in a soil sample is restrained by the interaction from adjacent particles as well as intrusion of air if the sample becomes unsaturated.

3. Interfacial polarization serves as the predominant polarization mechanism in the radio frequency range of 1 MHz-100 MHz not only for pure clay-water mixtures but also for naturally collected expansive soils. The measure of the polarization is well evaluated by the difference between the surface conductivity σ_{ddl} and the pore fluid conductivity σ_{el} but quantified as (σ_{ddl} - σ_{bl}) because of the challenge in obtaining σ_{el}. Electrical anisotropy was seen with higher real permittivity and effective conductivity measurements in the horizontal rather than the vertical direction, as a result of structural anisotropy, and can be quantified by $(\kappa'_{inf})_h/(\kappa'_{inf})_v$ or $(\sigma_{dc})_h/(\sigma_{dc})_v$. Meanwhile, the electrical anisotropy is more significant for the untreated samples with higher S_a; and less pronounced for the stabilized samples in comparison with their untreated counterparts, except for the case of $(\sigma_{dc})_h/(\sigma_{dc})_v$ of the stabilized samples.

4. Based on the experimental information provided by this study, the investigation of κ'_{inf} and σ_{dc} introduced a way to assess the hydraulic state and structural anisotropy of expansive soils. Increases of κ'_{inf} and σ_{dc} were observed with the hydration process in terms of vertical strain or time. Further research is aimed at determining a quantitative relationship of κ'_{inf} and σ_{dc} with suction for individual expansive soils through the integration of a suction-controlled system. Combined assessments of geophysical and mechanical models are necessary for prospective physical modeling of hydromechanical behavior of clayey soils. Improvement on quantifying DDL thickness and conductivity, measurement of pore fluid conductivity and evaluation of the role of surface conductivity relative to pore fluid conductivity in contribution to effective conductivity of a consolidated/compacted sample will also be topics of interest.

Chapter 5: Water Retention and Volume Change Behavior of Expansive Soils

5.1 Introduction

Engineering problems associated with expansive soils commonly occur in arid and semiarid regions. Seasonal precipitation and drought cause severe damage or failure of engineering facilities such as bridges, roads, slopes and light structures due to substantial volume expansion or shrinkage of expansive soils. These situations are examples of expansive soil behavior subject to seasonal moisture fluctuation and under zero or relatively low overcharge circumstances. Figure 5.1 shows a landslide failure in a roadway cut-slope consisting of highly plastic, expansive soil, beside US Highway 70 in Southeastern Oklahoma, U.S.A. This landslide occurred after an abnormally wet summer, when water absorption decreased the soil strength and stiffness. The slide mass blocks the drainage channel and encroaches on the pavement surface causing maintenance issues and potential danger to transportation flow. In this regard, a detailed understanding of the hydraulic and mechanical behavior of expansive soils, in terms of soil water characteristics and volumetric evolution, is of vital importance to evaluate the stability of engineering structures or natural geologic features subjected to soil swelling or shrinkage under zero/low overburden pressures.

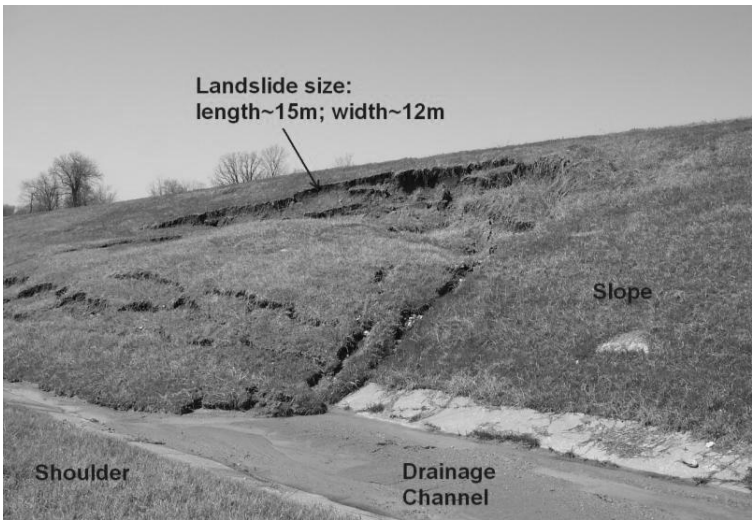

Figure 5.1 A landslide beside US State Highway 70

In most cases, in-situ or as-compacted expansive soils remain unsaturated, and therefore, their behavior is highly affected by surface tension forces at the air-water interface (Nelson and Miller 1992, Fredlund and Rahardjo 1993). In turn, the mechanical behavior is highly dependent on their soil water characteristic curves (SWCCs). Common laboratory methods of measuring SWCCs (the primary drying curves) of highly clayey soils (clay size fraction > 50 %) include the axis-translation technique (Tinjum et al. 1997, Miller et al. 2002, Leong et al. 2003, Wang and Benson 2004, Agus and Schanz 2006, Puppala et al. 2006b) with a matric suction measuring range of 0-1.5 MPa and the chilled mirror hygrometer technique (Leong et al. 2003, Wang and Benson 2004, Thakur et al. 2005, Agus and Schanz 2006, Thakur et al. 2006, Birle et al. 2008, Agus et al. 2010), with a total suction range of 0~300 MPa. While some researchers have obtained hysteretic soil water characteristic curves (HSWCCs) using the axis-translation technique for sandy and silty soils (Han et al. 1995, Konyai et al. 2006, Chen et al. 2007, Miller et al. 2008, Muraleetharan et al. 2009), reports on the

HSWCCs of highly clayey soils are scarce, due to extremely long moisture equilibrium periods required during the wetting process in the axis-translation technique. In addition, wetting data from the chilled mirror hygrometer technique have not yet been reported.

Romero et al. (1999) achieved the HSWCCs (wetting-drying paths) of Boom clay (50 % particles < 2μm) compacted at two densities. The HSWCCs data were attained using the axis-translation technique at low suction values (under 0.5 MPa for both wetting and drying), transistor and thermocouple psychrometers (2-15 MPa on the drying path), and vapor equilibrium technique (relative humidity imposed through vapor transfer by saline solutions, shortened for VET) for the suction range of 15-300 MPa on the subsequent wetting-drying paths. This same approach was adopted by Fleureau et al. (1993&2002) in acquiring the drying-wetting paths of several clayey soils, with different suction ranges. A major concern with this approach (Romero et al. 1999, Fleureau et al. 1993&2002) lies in the inconsistency of the initial sample states along either drying or wetting path (which imply different sample structure) in using these different test methods. Delage et al. (1998) made the combined use of the osmotic technique (over the suction range of 0.3-10 MPa) and the VET (10-262 MPa) for attainment of both drying and wetting curves of a densely compacted clay (80 % clay size particles). Again, the initial sample structures were not consistent between the two test methods. The osmotic technique can be reasonably applied in the suction range of 0-10 MPa. The major drawback is the weakness of the semi-permeable membrane that is susceptible to bacteria attack (Blatz et al. 2008). On the other hand, the VET method shows limitation at suction measurement below 10 MPa because if assessed by Kelvin

law, a 1 % relative uncertainty on the relative humidity will introduce 1.38 MPa variance of the suction magnitude (Delage et al. 1998). Moreover, the VET technique suffers from extremely long sample equalization periods (1-3 months to take one data point) and strict requirements of precise temperature control (Delage et al. 1998, Blatz et al. 2008).

Previous studies on cyclic swell-shrink behavior of expansive soils were usually carried out in a temperature or suction controlled oedometer by which vertical (1D) deformation was used to approximate volume change, whereas in the current research, three dimensional (3D) deformations was directly measured. These studies can be grouped into two categories: 1. water content versus volumetric deformation; 2. suction versus volumetric deformation. A representative work on the first category was conducted by Tripathy et al. (2002) on two highly clayey expansive soils in which the water content-void ratio or percent of volumetric deformation paths were presented. The second was illustrated as the cyclic controlled-suction drying and wetting paths acquired either by VET (Alonso et al. 1995, Alonso et al. 1999, Romero et al. 1999, Alonso et al. 2005, Agus and Schanz 2006), or osmotic technique (Nowamooz and Masrouri 2008). The combination of both categories was seen in the research efforts of Fleureau et al. (1993&2002) and Tripathy and Subba Rao (2009). The former (Fleureau et al. 1993&2002), however, failed to report the swell-shrink behavior of the soils under study; whereas the latter (Tripathy and Subba Rao 2009) deduced the suction values during the swell-shrink cycles based on one monotonic drying path of the SWCC from filter paper tests. None of these research efforts provided a comprehensive study of a

coupled cyclic water content change-suction variation-volumetric deformation behavior on the basis of the HSWCCs. This study attempted to fill this gap.

In this study, research efforts were invested in obtaining the primary drying path of all six soil samples in the suction range of 0.001-1 MPa through the use of the pressure plate test (with axis-translation technique). Particularly, the primary drying, primary wetting and secondary drying paths of Carnisaw and Eagle Ford within the 1-150 MPa suction range were attained using the chilled mirror hygrometer technique. For Carnisaw and Eagle Ford soils, the specimens for the two types of tests were identically compacted and saturated at the onset of each test to ensure identical capillary history and structure. In addition, measurements of three-dimensional volume change were conducted on Carnisaw and Eagle Ford based on which the cyclic swell-shrink paths were deduced in terms of volumetric strain versus either water content or suction. There are two reasons for selecting Carnisaw and Eagle Ford for detailed investigation of the HSWCCs and cyclic shrink-swell behavior. First, such an investigative effort is extremely time-consuming and expensive regarding soil resource and equipment availability. Secondly, Carnisaw and Eagle Ford represent two extreme cases in respect of plasticity (Table 2.2) and structure (Figure 3.10), and therefore provide a wide range of possible comparisons in macroscopic performance.

5.2 SWCC Studies on the Six Studied Soils

Compacted or stabilized specimens of each of the six samples were investigated in the pressure plate (also called porous stone or ceramic disk) tests using a procedure detailed in Lin and Cerato (2012b). Each soil sample was compacted (volume-based and at w_{opt} and γ_{dmax}, as defined earlier) in a 63 mm diameter by 132 mm length steel

mold, using a 24.4 N (5.5 lb) steel hammer. The compacted sample was then trimmed into four rubber rings with each specimen of measuring 51.3 mm in diameter and 10.2 mm in thickness. The contained specimens were then wrapped with clear plastic wrap and stored in the 100 % humidity room. The stabilized Hollywood and Heiden specimens were cured for 14 days while all the other types of specimens were only cured for 2 hours before being saturated. After curing, each specimen was sandwiched in between two porous stones and placed in an ice container filled with de-ionized water where it was allowed to imbibe water under a surcharge pressure of 1 kPa for a period of 72 hours. At the end, the degree of saturation for all the specimens used in the study was estimated to be more than 96 % by volume-mass calculations.

Figure 5.2 shows the pressure plate apparatus for measuring SWCC. Pressure porous disks (plates) with air entry values (AEV) of 0.1 MPa (100 kPa), 0.3 MPa (300 kPa), 0.5 MPa (500 kPa) and 1.5 MPa (1500 kPa) were used with the specimens seated directly on top of them. The flow of water from the specimens into burettes was monitored in intervals of 24 hours until stabilized after suction was imposed. The SWCC was determined in a 15-bar (1500 kPa) pressure plate extractor manufactured by Soilmoisture Equipment, Corp, following the drying path approach according to ASTM-D6836-02(2008)e2 (2011).

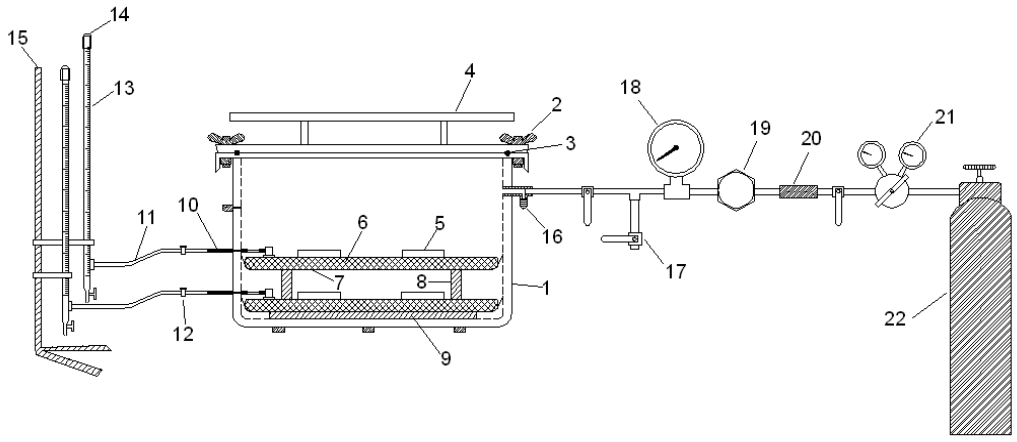

Figure 5.2 Pressure plate test apparatus for the SWCC studies*

*1- Extractor chamber, 2- Clamping bolt, 3- "O" ring, 4- Lid handle, 5- Soil sample, 6- Porous disk, 7- Disk membrane, 8- Plexiglas spacer, 9- Triangular supporter, 10- Outlet port, 11- Outflow tube, 12- Plastic clipper, 13- Burette, 14- Plastic cap, 15- Steel stand, 16- Safety valve, 17- Venting valve, 18- Pressure dial gauge, 19- Pressure adjuster, 20- Air filter, 21- Pressure regulator, 22- Nitrogen bottle

There are two important issues associated with the pressure plate test that need to be clarified. First of all, the axis-translation technique applied to a pressure plate extractor usually allows desorption of the water from specimens at the initially saturated state through an incremental increase of air pressure. If any sorption test is practiced afterwards, air that diffused through the ceramic disk will block the flow back into the test specimen and result in anomalous water contents (Tinjum et al. 1997). Efforts to obtain the wetting path of SWCC in this project also failed. Other researchers (Tinjum et al. 1997, Puppala et al. 2006b, Thakur et al. 2006) only attempted the drying path using a similar extractor in testing expansive/highly plastic clays. After personal discussion with Dr. Anand J. Puppala at the University of Texas at Arlington, a conclusion was reached that the wetting path is unavailable from a pressure extractor chamber as shown in Figure 5.2. The water retention hysteresis using the axis-translation technique can only be investigated through a process of both pore air

pressure control (on top of the sample) and pore water pressure control (applied to the pressure plate beneath the sample), during which the sample was placed insofar as to cover the entire exposed portion of the plate. This is advantageous in controlling the matric suction of silt or sand with works seen in Gallage and Uchimura (2006), Miller et al. (2008) and Khoury (2010); but requires extremely long durations for homogeneous moisture distribution throughout a clay sample and also requires an advanced flushing system to remove the diffused air in the pressure plate (Ho and Fredlund 1982, Houston et al. 2008). Moreover, the hysteresis setup for clay testing using the axis-translation technique forbids replacement of pressure plates (the detailed setup can be found in Tinjum et al. (1997)). This renders the measurement at low suction application (e.g., 0~100 kPa) using a plate of high AEV (e.g., 15 bar, or 1500 kPa) suspicious, while switching to lower AEV porous stones will interrupt the progress of the wetting path. The second issue lies in the form of SWCCs presented in terms of volumetric water content. The volume change monitoring is feasible in Tempe pressure cells or volumetric pressure plate extractors that are often used for low range matric suction applications allowing for a maximum suction of 200 kPa (Fredlund and Rahardjo 1993). In the literature presenting the pressure plate results on clays (Tinjum 1995, Tinjum et al. 1997, Ebadi and Elektorowicz 1999, Miller et al. 2002, Puppala et al. 2006b), the volume changes of the specimens were neglected (with maximum matric suction applied at around 1000 kPa). Tinjum (1995) argued that the attempts to make corrections for volume changes were found to have little effect on the data. In this research project, only the Eagle Ford specimen showed observable shrinkage at the end of the test with approximately 0.7 mm decrease in diameter. This was found to be

negligible in affecting the SWCC data. For this reason, and because volume change was difficult to monitor due to irregularity of sample shrinkage and the configuration of the 15 bar extractor used, the sample volumes were taken to be constant in the calculation process.

5.3 HSWCCs and Cyclic Swell-Shrink Paths of Carnisaw and Eagle Ford

5.3.1 Measurement Using a Dew-point Potentiameter (WP4)

The WP4 tests were carried out on Carnisaw and Eagle Ford for measuring their HSWCCs. Each soil sample was first thoroughly mixed with de-ionized water. After mixing, the material was placed in a sealed container and allowed to equilibrate for 48 hours. Afterwards, the soil was compacted in a stainless steel tube with a dimension of 100 mm in length, 36.5 mm in inner diameter and 1 mm in thickness. The compacted soil sample with the tube was cured in a humidity room for two weeks, after which it was carefully extruded from the tube using a solid wooden cylinder with a length of 100 mm and a diameter of 36 mm, carefully cut into five stainless steel cups of 10 mm in depth, 36.5 mm in inner diameter and 1.5 mm in thickness, with the aid of a sharp knife and a wire hacksaw. A thin spatula was used to trim and smooth the surface of the soil specimen inside the cup so that the final specimen thickness reached approximately 5 mm. As required by the WP4-T manual, the contained specimen should fill the cup to less than half of the depth in order to avoid contamination of the chamber. Special attention was paid to ensure that both the top and bottom of the extruded sample were smooth and consistent.

The half-filled cups were first saturated by being immersed in water contained in a desiccator placed in a humidity room for 72 hours. Filter paper and a porous stone

were placed on top of the soil specimen in each cup to prevent soil loss to water. The degree of saturation was found to be more than 98 % after the inundation period. For the drying processes, the specimens were air dried for approximately 20~35 minutes before each measurement. For the wetting procedure, the specimens were placed in an ice chamber and wetted by water vapor generated from a humidifier for about 15~30 minutes. After each drying/wetting effort, each specimen was sealed for 3-4 hours for moisture homogenization, and then placed in the sample equilibration area on the top surface of the WP4-T for an additional two hours for further temperature and moisture equilibrium. After this process the temperature of the specimen was within 0.2 °C difference from the WP4-T chamber temperature preset at 25 °C. This procedure permits acquisition of two data points per day, and was found adequate for moisture equalization throughout the soil specimen, as the suction measured following this procedure matched well the magnitude obtained after the 24 hour sealing period suggested by Agus and Schanz (2006), with the difference of magnitude falling within the device accuracy. The equalized specimen was then tested in the WP4-T chamber for water potential (the negative form of suction), after which the specimen weight was immediately recorded. The test time for each suction measurement was around 5~10 minutes for the studied soils. The above process was repeated for the next suction measurement at the subsequent water content. At the end of the secondary drying process, the specimens were oven dried from which the gravimetric water content corresponding to each measured suction value were back-calculated.

It is worth noting that when testing the drying paths (in terms of gravimetric water content) of clayey soils using the WP4 technique the influence of initial

compaction dry density is negligible at the suction values greater than 1 MPa (Thakur et al. 2005, Thakur et al. 2006, Birle et al. 2008). Below 1 MPa, suction increases with compaction effort as determined in the pressure plate apparatus (Miller et al. 2002). In order to combine results from the two different types of tests, soil specimens of both the pressure plate and WP4 tests were initially compacted in the same manner (at w_{opt} and γ_{dmax}). Osmotic suction was neglected when presenting the HSWCCs measured by the WP4 in the suction range of 1-150 MPa. Also, the HSWCCs from the WP4 tests were originally gravimetric; in order to convert them to be volumetric, additional volumetric deformation measurements are necessary.

5.3.2 Cyclic Volume Change Measurements

Volumetric measurements were conducted on Carnisaw and Eagle Ford soils in order to obtain their HSWCCs in terms of volumetric water content. Because volumetric measurements could not be performed directly on the WP4 specimens, additional triaxial specimens were prepared instead for this purpose, not only providing accurate and convenient determination of three-dimensional deformation, but also supplying information for a planned triaxial testing program (narrated in Chapter 6) on unsaturated expansive soils. For each soil sample, two specimens were tested to ensure reproducibility of the test results in terms of volumetric deformation measurements. The soil was compacted to the optimum state in a stainless steel mold to form a cylinder of 35.6 mm (1.4 in) in diameter and 71.1 mm (2.8 in) in length covered by a rubber membrane. The compacted specimen was then sandwiched by porous stones and stored in a 100 % humidity room. De-ionized water was introduced at the top and the bottom

allowing for free specimen expansion until saturation was reached. The saturated specimens were then sealed for an additional two weeks for moisture equalization.

Efforts were first attempted on wrapping filter paper drain or geotextile strip vertically along the specimen to provide a pathway for water liquid or vapor movement along the exterior of specimen. However, filter paper was stuck to and became part of the specimen when saturated while soil infiltrated the openings of geotextile during expansion, not to mention the restraint they created on soil expansion. It appears that either method when applied on expansive soils renders the potential use of such an auxiliary moisture transport channel inefficient. Hence, neither paper nor geotextile cage was implemented. For drying purposes, the membrane-contained and porous stone-sandwiched specimens were air-dried slowly in a desiccator with calcium chloride placed at the bottom and a fan applied at the top, in a room with constant relative humidity of 20 % and temperature of 25 °C. The specimens were dried at a markedly slow rate at around 2 %/day water content decrease from the initial state to less than 0.2 %/day when the specimens reached their residual state. For wetting purposes, the membrane-wrapped cylindrical specimens had their top and bottom exposed to water vapor in a 100 % relative humidity room in a similar wetting manner for the WP4 specimens. However, water absorption proceeded at an extremely slow rate (less than 0.2 %/day) even at the driest condition of the specimens. According to Vanapalli et al. (1999), suction represents the energy deficiency in the soil water phase so water retention equilibrium by liquid flow or with vapor phase is not of concern for the definition of soil water characteristics. Therefore, in order to aid moisture absorption while introducing as little sample disturbance as possible, water dripping by pipette was

implemented with special attention paid to the rate of water content increase, maintaining approximately 2 %/day when the specimen showed greatest affinity for water absorption (at the driest condition).

After dried or wetted for 1-2.5 days, each specimen was sealed with cling wrap and plastic tape, then placed in a humidity and temperature-controlled room for two weeks to obtain moisture equalization throughout the specimen before each weight and volumetric measurement was attempted. This curing time is considered adequate as there was no further observable dimensional evolution beyond two weeks. At each measurement attempt, the membrane contained specimen was uncovered from cling wrap and the weight was recorded using a digital balance with accuracy of 0.01 g. Immediately afterwards, the strains were obtained by means of measuring specimen dimensions using a digital caliper (accuracy of 0.01 mm). Three radial measurements at the quarter points of the specimen height and three height records were conducted for each specimen and the averaged magnitude (adjusted for the membrane thickness) was recorded. The process was repeated for each drying/wetting effort until the change of water content reached a rate of less than 0.2 %/day. At the end of the secondary drying path, the membrane was removed and the soil specimen was oven-dried for 24 hours from which the moisture content, according to each volume measurement attempt, was back-calculated.

5.4 Results and Discussion

5.4.1 SWCCs of the Studied Soils

Figures 5.3 and 5.4 summarize the SWCCs of the four untreated and the two stabilized soils from the pressure plate tests. The Fredlund and Xing (1994) model was

used in fitting the result data with the fitted parameters listed in Table 5.1. The mathematical description of the model is expressed as:

$$\theta = \theta_s \left[1 - \frac{\ln(1 + s / s_r)}{\ln(1 + 10^6 / s_r)} \right] \left[\frac{1}{\{\ln[e + (s/\alpha)^n]\}^m} \right] \qquad \textbf{(5.1)}$$

Where "θ" is volumetric water content; θ_s is volumetric water content at saturation; s represents suction (kPa); s_r is suction (kPa) at residual water content; α (kPa) is optimized parameter related to air-entry suction; "e" is base of natural logarithm; and "n", "m" are model parameters reflecting pore size distribution and shape of the SWCC at high suction. The estimated air entry value air entry values (AEV), which are determined as matric suction values at the intersection point of the horizontal line through the point of saturated volumetric water content and the tangent line of the desorption curve (Fredlund and Xing 1994, Vanapalli et al. 1996), are also summarized in Table 5.1. Here osmotic suction is neglected so that the suction s is equal to matric suction s_m.

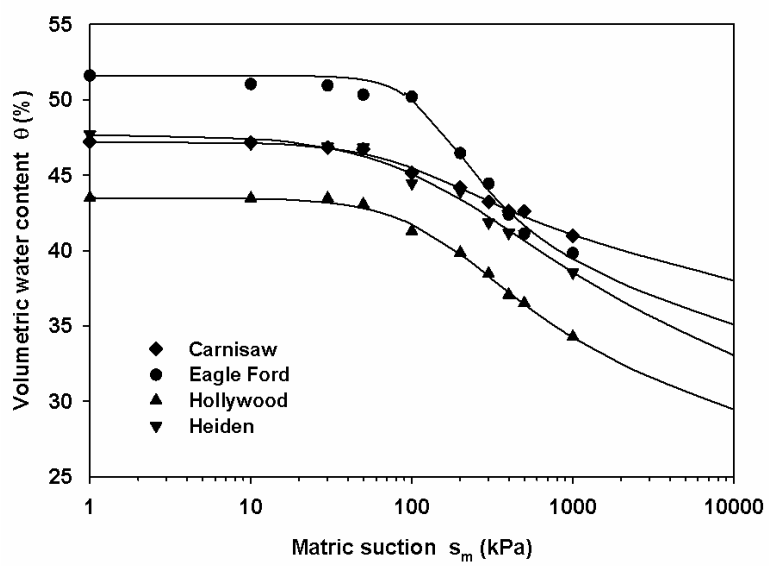

Figure 5.3 SWCCs of four natural expansive soils

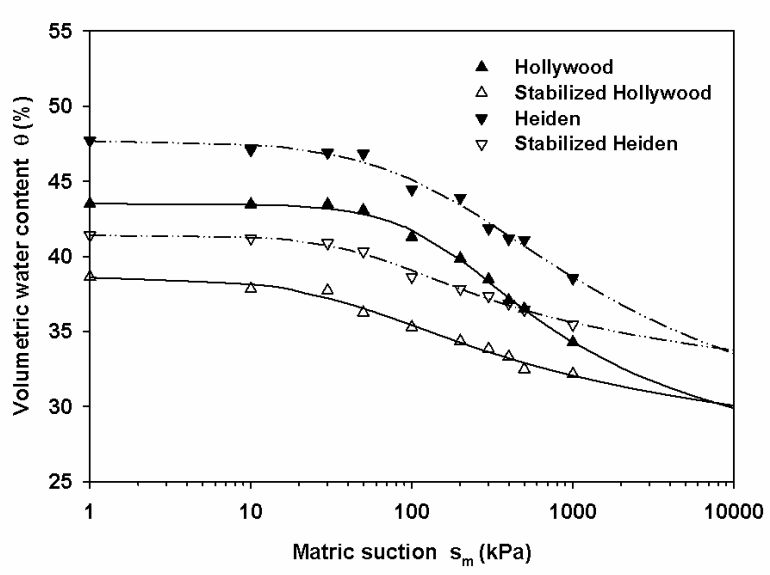

Figure 5.4 SWCCs of untreated and stabilized Hollywood and Heiden

Table 5.1 SWCC parameters of the six studied soil samples

Test sample	AEV* (kPa)	α (kPa)	n	m	s_r (kPa)	R^2	s_{opt}† (kPa)	PI
Carnisaw	43	77	1.48	0.10	10^6	0.99	469	27
Eagle Ford	74	111	2.85	0.15	10^6	0.99	1126	57
Hollywood	70	121	1.59	0.19	10^6	0.99	758	34
Stabilized Hollywood	17	29	1.16	0.13	10^6	0.99	637	26
Heiden	55	112	1.06	0.23	10^6	0.99	1120	44
Stabilized Heiden	23	44	1.51	0.10	10^6	0.99	1476	27

*As defined in Fredlund and Xing (1994)
†Matric suction at the optimum state

In Figure 5.3, Eagle Ford maintains the greatest volumetric water contents at the matric suction range below 100 kPa as a result of significant DDL expansion that stores a large amount of water at low suctions. Being the least plastic of the four natural samples (Table 5.1), however, Carnisaw (classified as MH) shows greater volumetric

water contents at this range than Hollywood which is a more plastic soil (CH). This exception suggests that the soil affinity for water not only depends on the formation of a DDL but also on soil structure, as Carnisaw shows a structure that has larger inter-aggregate macropores than does Hollywood (Figure 3.10).

The soil with higher PI exhibits higher AEV and greater matric suction values at the optimum (w_{opt} and γ_{dmax}) state (s_{opt} in Table 5.1). An exception lies in the comparison between Hollywood and Heiden, among which the former is less plastic than Heiden but has a higher AEV. This indicates that the AEV can also be affected by other factors than plasticity, such as the shrinkage of DDL. For highly plastic soils, the volumetric water content decrease starting from their AEV is more likely from the contracted double layer thickness rather than the extrusion of pore water in pore spaces. In other words, for Heiden and Eagle Ford soils, the "AEV" reported in Table 5.1 does not represent the matric suction at which air begins to enter the largest pores, but the magnitude where the DDL begins to contract, while the specimens can still retain the saturated states even with the decrease of water content (Lin and Cerato 2012b). This is because for fine-grained soils, a higher suction component comes from adsorption forces occurring in intra-aggregate pores (at contacts between clay particles), while a lower component is from capillary forces in inter-aggregate pores (Ferber et al. 2006). Therefore, the reason that Hollywood has a greater AEV than Heiden may originate from its specific clay minerals' capacity of retaining water in intra-aggregate pores.

As shown in Figure 5.4, for both Hollywood and Heiden, soil stabilization with 9 % fly ash decreases the volumetric water contents by approximately 2-7 % when matric suction is below 1000 kPa. As matric suction increases, the reduction in

volumetric water content decreases. These trends are consistent with those of Puppala et.al (2006b) and originate from a change in particle and pore-size distribution, and the binding of fine clay platelets (Puppala et.al 2006b). The flocculation and coating decrease the ability of clay aggregates in holding adsorbed water. At the same time, the flocculation and coating produce more open particle arrangements that increase the permeability of the soils, as indicated by the reduced AEV of the SWCCs (Table 5.1). The rising matric suction close to 10,000 kPa suggests convergence of the SWCCs of the untreated and stabilized samples.

5.4.2 Relationship of Volume Change with Water Content

The relationships between volumetric strain δv (%, based on the specimen dimension at the optimum condition) and gravimetric water content w (%) of Carnisaw and Eagle Ford are given in Figure 5.5. The resulting data of the two identically prepared specimens were very close and trended along the same polynomial-fitted curve. For clarity therefore, only the polynomial-fitted curves of the results of both specimens are illustrated, having R^2 values in excess of 0.99. In Figure 5.5, point 1 represents the specimen at its initial compacted state.

In general, the cyclic wetting-drying process (from point 1 to 5) shows an accruement of δv in comparing the various paths. For example, at identical water content, the first shrinkage path exhibits a greater magnitude of δv than that of the first swelling path. This finding is in accord with the discoveries of Tripathy et al. (2002) on compacted expansive soils, which experienced oedometeric full swelling-full shrinkage cycles under a surface pressure of 6.25 kPa. The second swelling (3 to 4) and shrinkage paths (4 to 5) of both soils almost overlap with each other, except for the section of the

second shrinkage path (4 to 5) of Carnisaw (Figure 5.5 (a)) at water contents smaller than 12 % where a clear increase of δv relative to the second swelling path (3 to 4) (Figure 5.5 (a)) can be seen. These behaviors will be discussed later.

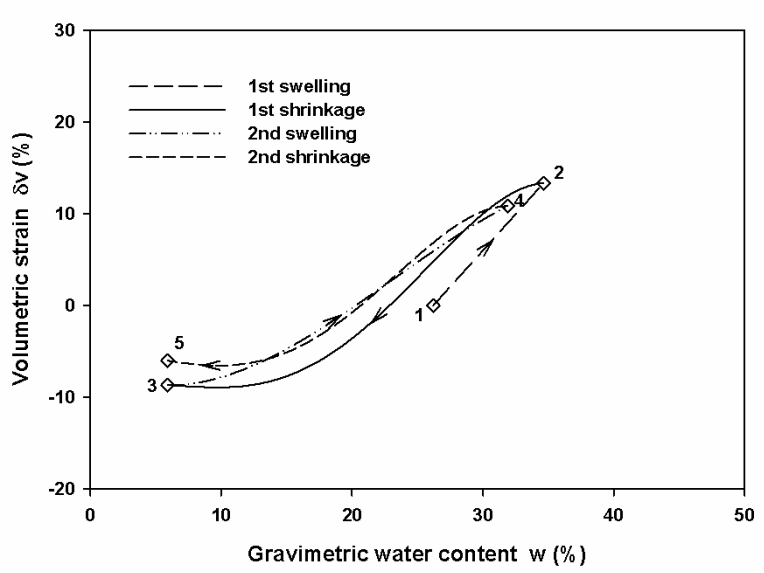

(a)

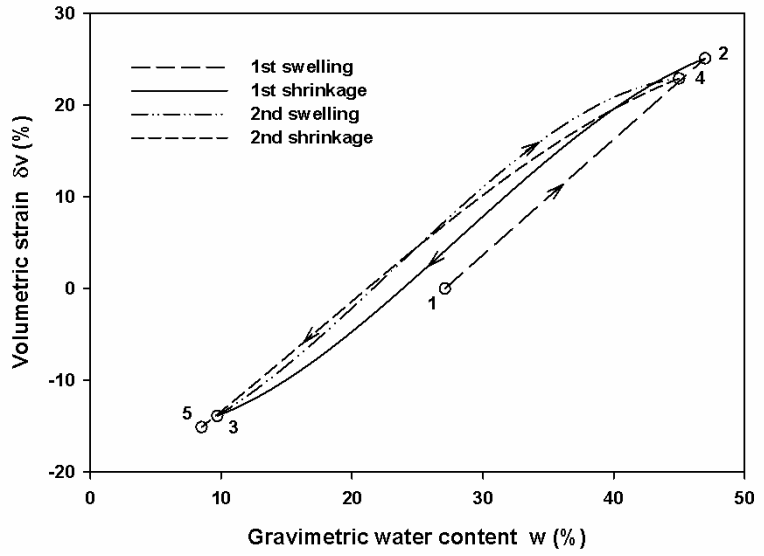

(b)

Figure 5.5 Volumetric strain δv vs. gravimetric water content w

(a) Carnisaw; (b) Eagle Ford

It is desirable to compare the three-dimensional (3D) volumetric assessments with their one-dimensional (1D) counterparts measured from conventional methods. The 1D percents of swell were achieved as the amount of expansion of the sample from its compacted state in an oedometer setup under an overcharge pressure of 1 kPa (method A of ASTM D4546 (1999)). The 1D percents of shrinkage were acquired following British Standard BS-1377 (1990) with which the soil sample was air-dried in a linear bar mold from the liquid limit to residual state. For appropriate comparisons, the 3D swelling was evaluated as the volumetric deformation at the end of swelling (indicated by points 2 and 4 in Figure 5.5) which was calculated based on the initial specimen dimension at the compacted state (the specimen dimension according to point 1). On the other hand, the degree of shrinkage was analyzed based on the specimen dimension at the start of each shrinkage cycle and represented by the percentage of the shrinkage (the amount of volume change from point 2 to 3 over the volume at point 2, or that from point 4 to 5 over the volume at point 4). In this way, both the 1D and 3D results are representative of the specimens undergoing nearly identical hydraulic processes and structural change. That is, the swelling percents represent specimens experiencing full expansion from the compacted state under negligible surcharge; and the shrinkage considers specimens shrinking from the saturated/liquid limit to the residual state. The maximum volumetric deformations in terms of 1D and 3D swelling and shrinkage are listed in Table 5.2.

Table 5.2 Maximum δv from 1D and 3D measurements[*]

Deformation stage	Carnisaw	Eagle Ford
1^{st}_sw_1D[†]	2.3	12.7
1^{st}_sw_3D[†]	13.3	25.1
2^{nd}_sw_3D[†]	10.8	22.9
1^{st}_sh_1D[+]	-13.4	-16.3
1^{st}_sh_3D[+]	-19.4	-31.2
2^{nd}_sh_3D[+]	-15.2	-30.9

[*] sw - swelling; sh - shrinkage; 1D - one dimensional; 3D - three dimensional.
[†]Based on the dimension of the specimen initially compacted at w_{opt} and γ_{dmax}.
[+]Based on the dimension of the specimen at the beginning of the shrinkage.

As revealed in Table 5.2, the studied soils presented significantly larger swelling and shrinkage in the 3D than the 1D measurement. The reasons underlying these phenomena are explicit: the soil expansion was constrained laterally in 1D swelling even though it was fully mobilized in the vertical direction; whereas the lateral shrinkage of the sample in the linear shrinkage test was not accounted for in the shrinkage amount. The traditional evaluation methods (oedometer swelling and linear shrinkage) dramatically underestimate the volume changes of expansive soils under zero/low stress conditions.

5.4.3 Hysteretic SWCCs of Carnisaw and Eagle Ford

By combining the suction results and the volumetric deformation data the HSWCCs of Carnisaw and Eagle Ford, in terms of volumetric water content, can be deduced as depicted in Figure 5.6. The matric suction at the optimum condition (marked by s_{opt}) measured from the filter paper tests were also marked on the graphs. The results of the filter paper test are shown in Figure 5.6 so as to evaluate the role that capillary history plays in determining soil suction.

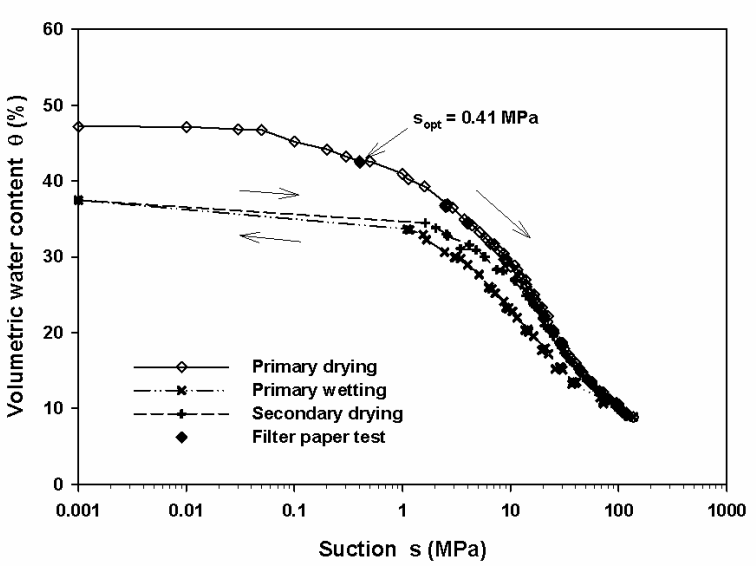

(a)

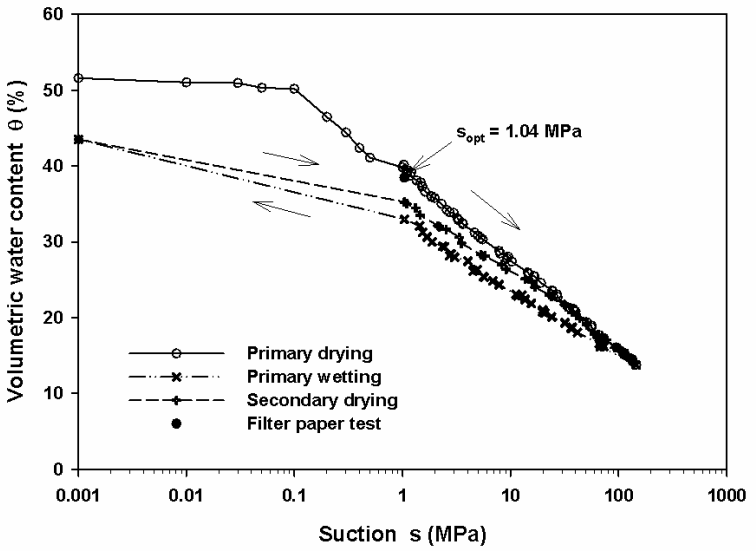

(b)

Figure 5.6 Volumetric water content θ vs. suction s

(a) Carnisaw; (b) Eagle Ford

An assumption underlying the derivation of HSWCCs is that the separated measurements of suction and volume change in the suction range of 1-150 MPa can be combined together, since the specimens for both types of measurements were undergoing the same fabrication and wetting-drying processes. To further justify this

assumption, additional triaxial specimens were prepared along various swell-shrink paths, from which small disk-like chunks were trimmed directly from the specimens and tested by the WP4 (for suctions greater than 1 MPa). The obtained data points precisely matched the HSWCCs in Figure 5.6.

It was found that the suction of the pressure plate test specimens at the optimum condition (w_{opt} and γ_{dmax}) along the primary drying path is close to the magnitude of the directly compacted filter paper test specimens. This is consistent with the conclusion of Vanapalli et al. (1999), which suggests that for fine-grained soils the suction magnitude at a point on the primary drying path can be well represented by the value measured on a directly compacted specimen at the same volumetric water content and identical stress condition. The results in Figure 5.6 show that the capillary history does not seem to control the primary drying path, however beyond the primary drying path, capillary history is important and manifests as the development of the HSWCCs.

In presenting the HSWCCs, three common constitutive models were first attempted in relating suction to water content with respective fitting parameters: Brooks and Corey (1964) model, van Genuchten (1980) model and the model of Fredlund and Xing (1994). However, none of these were able to provide fitted curves that closely matched the tested points. Therefore the points of the HSWCCs were connected by simple straight lines. It must be noted that the section of both the primary wetting and secondary drying paths in the suction range below 1 MPa were not directly measureable due to the inaccuracy of the WP4 test when measuring low suction values as mentioned earlier. The gravimetric water content at which the minimum measurable suction was reached (about 0.25 MPa for Carnisaw and 0.38 MPa for Eagle Ford) in the WP4 tests

was taken as the value corresponding to the token suction (0.001 MPa) and transformed to the volumetric water content accordingly. Even though these suction values (0.25 and 0.38 MPa) were not reliable measurements, they did mark the condition of the WP4 specimens at which further wetting by water vapor resulted in negligible water content increase, indicating that the WP4 specimens along the primary wetting path had almost reached the saturated state (their saturation ratios were estimated to be 96~100 %).

Two stages of hydraulic hysteresis emerged in both soils: 1. the hysteresis between the primary drying and primary wetting curves; 2. the hysteresis between the primary wetting and secondary drying curves. The first stage originates from the behavior of inter-aggregate pores, which decrease upon soil shrinkage during the primary drying process. Right after initial soil expansion, a proportion of free water was stored in macropores between clayey aggregates or bridges while the other portion was confined in intra-aggregate zones (Romero et al. 1999, Fityus and Buzzi 2009). Upon primary drying, the soil specimen experienced significant shrinkage, forcing the aggregates to bind together, which decreased the macroscopic porosity. At the same time, cracks formed at weak connections of soil peds formerly filled with water. During primary wetting, the intra-aggregate micropores expanded upon wetting at the expense of the inter-aggregate macropore volume (i.e., the expanding aggregates encroach into their surrounding macropore space), accompanied by partial collapse of the macropore voids as a consequence of aggregate realignment. The unrecoverable inter-aggregate fabric, as well as the aggregate irregularity, resulted in volume change hysteresis which is illustrated as decreased volumetric water content at a given suction. The maximum decrease of volumetric water content occurs at the low suction range (0.001-1 MPa) as

shown in Figure 5.6, with a magnitude of approximately 11 % for Carnisaw and 14 % for Eagle Ford. When the secondary drying path was initiated, the change of water in the specimen was predominantly governed by the microscopic intra-aggregate zones (Romero et al. 1999), as the volume change behavior showed a high degree of reversible elastic deformability (Delage et al. 1998). This results in a slight hysteresis between the primary wetting and secondary drying curves, attributed mostly to adjustment of particle or aggregate alignments, as the maximum difference of volumetric water content is about 4 % for Carnisaw and 3 % for Eagle Ford (Figure 5.6). Since the remaining macropores will be further closed by aggregate reorganization resulting in a more and more homogeneous structure (Cui et al. 2002), it is postulated that the hysteresis may further decrease for the following wetting-drying cycles (which were not attainable due to significant cracking of Eagle Ford soil specimens in the WP4 tests after secondary drying). Such a postulation is also implied in the following section on the volumetric strain versus suction change relationships.

5.4.4 Evolution of Volumetric Strain Due to Suction Variations

Given the HSWCCs and the cyclic swell-shrink volume change (with water content) relationships acquired, the evolution of volumetric strain caused by suction variations were derived and presented in Figure 5.7. For simplicity, eight critical points (marked as a-h) along the cyclic patterns are employed in depicting the volumetric strain evolution due to suction change, of which the hygroscopic states are narrated as: a-w_{opt} and γ_{dmax} with suction measured from filter paper test; b and f-complete saturation and full expansion denoted by token suction (0.001 MPa); c, e and g-the minimum legitimately measurable suction (slightly higher than 1 MPa) from the WP4

tests; d and h-the maximum measured suction magnitude (110~150 MPa) from the WP4 tests.

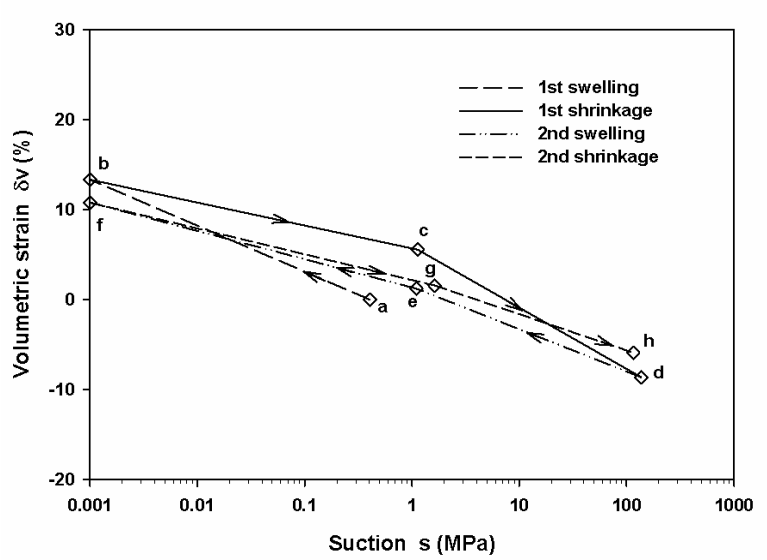

(a)

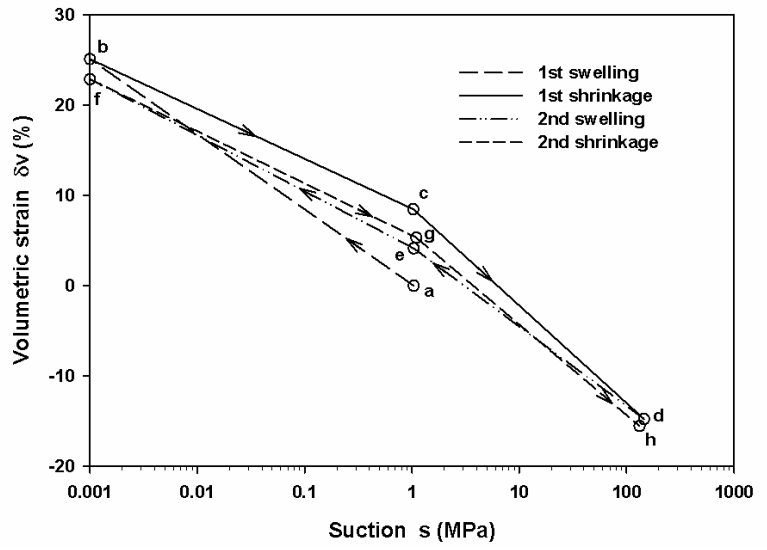

(b)

Figure 5.7 Volumetric strain δv vs. suction s

(a) Carnisaw; (b) Eagle Ford

The swelling behavior of compacted expansive soils can be viewed as the competition between the volume decrease caused by macrostructural aggregate reorganization (or macropore collapse) and the volume increase as a result of microstructural expansion of aggregates (micropore expansion) (Ferber et al. 2004&2006). On the other hand, the shrinkage of expansive soils can be seen as the combined effects of macropore collapse and micropore contraction.

The cyclic volume change behavior of expansive soils is not only dependent on the soil properties but also on the level of stress and the history of hydration (Alonso et al. 1999). In this study, both soils experienced a hygroscopic progress of two full swell-shrink cycles starting from their compacted conditions. These results can be compared with the cases predicted by the Barcelona Expansive Model (BEM) proposed by Alonso et al. (1999&2005). As shown in Figure 5.7, either Carnisaw or Eagle Ford shows a decreased global expansion as the cycle proceeds; in addition, Eagle Ford exhibits slight accumulation of global shrinkage strain (Figure 5.7 (b)). Here global swelling and shrinkage are evaluated based on the initial specimen dimension at the compacted state and can be read directly from the corresponding volumetric strain value on Figure 5.7 This phenomenon accords with the trend of volumetric deformation with cyclic controlled-suction variation (Dif and Bluemel 1991), although the latter case was of a sample tested under a vertical pressure of 0.2 MPa while the samples of this study were under negligible confining stress. The phenomenon can be explained by the BEM model as the plastic strain caused by suction increase (shrinkage) predominates over the plastic strain due to suction decrease (swelling). Moreover, the volume change tended to

stabilize at the end of the second cycle. This tendency is more apparently revealed by Eagle Ford (Figure 5.7 (b)).

An interesting discovery lies in the case of Carnisaw where less shrinkage was observed at the end of the second shrinkage path compared to the first shrinkage path. This provides evidence for the supposition of Alonso et al. (1999) that the build-up of aggregates can induce an increase of macroporosity during strong drying. In other words, upon strong drying, even though the entire sample is doomed to shrink globally, the formulation of macropore invasion may compensate for part of the shrinkage amount, which is implied by less shrinkage strain in the second cycle relative to the first cycle (Figure 5.7 (a)). Note that the case of Eagle Ford, where the reverse occurred, is more common and similar behavior has been presented in the literature (Dif and Bluemel 1991, Alonso et al. 1995&1999) while the behavior seen in Carnisaw soil was not reported until now. This special phenomenon characteristic of Carnisaw may originate from its highly flocculated structure (Figure 3.10 (a)). The increased tensile stresses due to dehydration, manifested by the significant contraction of the meniscus, may tend to strengthen instead of breaking the edge to face or edge to edge contacts (the angle between particles increases) and therefore promote macropore expansion. Conversely, the prevailing face to face contact of Eagle Ford (Figure 3.10 (b)) brings about predominantly intra-aggregate shrinkage in a direction normal to the parallel aligned particles, therefore exhibiting more elastic volumetric deformation with respect to water content or suction.

5.4.5 Discussion on Structural Changes under Various Test Conditions

The structure of soil samples in their compacted states have been approximately visualized through SEM investigations (Figure 3.10) and directly evaluated by looking into electrical anisotropy (Table 4.3). The actual structure of samples along various capillary paths, or under confining circumstances, cannot be explicitly described without application and advancement of the ESEM technology. Instead, the structural evolution can be indirectly reflected by the volume performance and physicochemical changes, as discussed in section 3.2.

The analysis of the 3D swell-shrink behavior suggests the structure of Carnisaw and Eagle Ford evolves in a direction towards eventually a homogeneous, face to face contact-dominant fabric accompanied by diminished inter-aggregate macropores and horizontal clay particle alignment. Such structural evolution of expansive soil has also been supported by both experimental and theoretical works (in a 1D manner) in literature (e.g., Basma et al. 1996, Delage et al. 1998, Romero et al. 1999, and Alonso et al. 1999). During the enforced swell-shrink cycles, however, the two soils maintain in varying degrees their original structure (when initially compacted). In the following chapter physicochemical properties like pH and DDL thickness will be evaluated for their impact on structural change during sample shear. Notice that the isotropic confinement before shear negligibly perturbs sample structure (Wang and Siu 2006b). This is also consistent with Collins' (1978) findings that densification of sample under isotropic shrinkage (similar to the effect of isotropic confinement) does not induce preferred particle reorientation.

5.5 Conclusions and Summary

This section presented a study on the water retention and swell-shrink behavior of expansive soils. Experimental efforts were conducted on deriving and comparing the SWCCs of the six studied soils. A comprehensive investigation of the coupled hysteretic suction-water content-volume change behavior has been carried out on Carnisaw and Eagle Ford. Several conclusions were drawn as follows.

1. Comparison between the SWCCs of the four natural/untreated soils implies that the sample with a higher plasticity has DDL's (mostly lying in intra-aggregate pores) more strongly resistant to surface tension forces, which relates to greater magnitudes of AEV, parameter α, and matric suction at the compacted state. The water retention abilities of the studied samples reduced significantly in response to CFA stabilization as the volumetric water contents decreased up to 7 % in the matric suction range of 1~10,000 kPa. At higher suction values (~10 MPa), both the raw and the stabilized soil SWCCs tend to converge. The decrease in volumetric water contents at lower suction values (< 10 MPa) occurred because the stabilization resulted in enlarged grain sizes, hydrophobic aggregate formation and more open particle arrangement in comparison with the untreated samples.

2. In general, for highly clayey expansive soils under zero/low confining stress, the volume increased with the swell-shrink cycles at the same gravimetric water content. However, the volumetric strain at a specific suction value tended to converge during the second cycle in that the second swelling and shrinkage paths closely approached each other. At the same time, the 3D volumetric measurements generate substantially greater amount of swelling and shrinkage than the 1D estimations based on

conventional evaluation methods. These findings shed light on proper prediction of in situ soil expansion or shrinkage under zero/low confining conditions.

3. Capillary history plays an important role in controlling the water retention characteristics when the soil experiences swell-shrink cycles, narrated by hydraulic hysteresis in between various stages of the wetting/drying process. This role was found to be insignificant, however, in comparing the water retention characteristics between the data points from the saturated specimen dried along the primary drying path and that from directly compacted specimens, provided that both groups of specimens had the same water content, dry density and stress state conditions.

4. Two stages of hydraulic hysteresis were observed in the HSWCCs of Carnisaw and Eagle Ford: hysteresis within the primary drying and primary wetting loop that develops from collapsed inter-aggregate pore space and irregular configuration of clay peds; and hysteresis between the primary wetting and secondary drying curves, which is affected by further realignment of particles, peds or clusters. The decreased volumetric water content difference in the second hysteresis loop suggests a formation of elastic deformability and a tendency toward macrostructural stabilization.

5. The cycles of volumetric deformation versus suction illustrate decreasing global expansion for both soils and accumulating global shrinkage in the case of Eagle Ford due to greater plastic strain decrease during shrinkage than plastic strain increase in swelling. The less plastic soil Carnisaw showed an unusual decrease of global shrinkage possibly because of macropore invasion during strong drying accompanied by remarkable meniscus contractions in a flocculated structure that strengthened the edge to face or edge to edge contacts.

Chapter 6: Shear Strength and Shear-induced Volume Change

6.1 Introduction

The shear strength of unsaturated fine-grained soils has been investigated from a variety of laboratory experiments with the most common being direct shear tests (Donald 1956, Escario 1980, Escario and Saez 1986, Escario and Juca 1989, Gan 1986, Gan and Fredlund 1988, Oloo and Fredlund 1996, Vanapalli et al. 1996, Feuerharmel et al. 2006, Zhan and Ng 2006, Miller et al. 2008, Khoury 2010) and triaxial tests (Gibbs et al. 1960, Bishop et al. 1960, Satija 1978, Escario 1980, Ho and Fredlund 1982, Peterson 1988, Toll 1990, Blatz et al. 2002, Futai et al. 2006, Pereira et al. 2006, Thu et al. 2006, Houston et al. 2008). In these studies, the specimens were compacted to the same dry density, in order to minimize differences in soil structure, after which, shearing was conducted on these specimens controlled at different suctions and net normal stresses. In general, suction can be imposed on the sample through one of the four suction-controlled approaches: axis-translation technique, air circulation method, osmotic method and vapor equilibrium technique (VET). Alternatively, specimens of a desired suction can be prepared on the basis of predetermined SWCCs. The introduction of the suction-controlled approaches, as well as the reason to adopt the alternative suction-prepared method in this study, is presented as follows.

The first approach, commonly known as the axis-translation technique, involves placement of a sample on a high air entry ceramic disk under the control and measurement of both pore-air and pore-water pressures. This makes examination of unsaturated shear strength of sand/silt possible at matric suctions up to 750 kPa using direct shear tests (Escario and Saez 1986, Zhan and Ng 2006, Miller et al. 2008, Khoury

2010), and up to 725 kPa for silt/lean clay in a triaxial testing program (Ho and Fredlund 1982, Thu et al. 2006, Houston et al. 2008). There are three major drawbacks associated with the axis-translation technique. First of all, specimen equilibration usually requires a long period of time that can vary from weeks to months, and in some cases become impossible from a time standpoint (e.g., highly plastic clay). The direct shear test possesses the advantage of faster equilibrium of pore air and water pressures since the thickness of the specimen can be small, however, the test has all the shortcomings inherent in the state of stresses in a direct shear box (Escario and Saez 1986). Secondly, for long-term tests, the dissolved air in the specimen can diffuse through the water in the ceramic disk and collect as air bubbles at the bottom, which need to be flushed away to prevent inaccurate measurement of pore water pressure (Ho and Fredlund 1982, Fredlund and Rahardjo 1993, Houston et al. 2008). This adds a flushing system as a necessary component to the testing apparatus and further requires appropriate calibration of the system, which can be challenging. Last but not least, the capacity of the ceramic disk provides a range of controlled suction up to 1.5 MPa, leaving the study of shear strength of soil at higher suctions (e.g., up to 100 MPa) unfeasible.

The second approach was developed by Cunningham et al. (2003), which incorporated an air-circulation method into triaxial equipment for the shear strength measurement of a clayey silt. Dry air was supplied to the test sample imposing a controlled suction up to 1.2 MPa while suction probes undertook independent measurements of suction at the top and lower part of the sample. For highly plastic soils

especially those that are expansive, development of significant and wide range of suction is expected.

The third and fourth suction-controlled approaches, osmotic and VET, respectively, could be implemented in the shear strength studies on unsaturated clays enabling a suction range up to 8.5 MPa for the former and from 10 to several hundred MPa for the latter. The osmotic method has been implemented in an osmotic shear box (Boso et al. 2005) or osmosis-controlled triaxial apparatus (Cui and Delage 1996), which allows for water exchange between the tested sample and polyethylene solution (PEG) via a semi-permeable membrane. The implementation of the VET involves a closed triaxial system where the relative humidity is kept constant by a saturated saline solution (Blatz and Graham 2000).

When combined in use, the osmotic method and the VET provide a suction control range of 0~300 MPa for highly plastic soils. However, even though a pump can be added to speed up the water/vapor exchange processes, both applications face limitations and disadvantages, including, susceptibility of semi-permeable membranes to microbial attack in the osmotic method, long equilibrium time and rigid temperature control for the VET (Blatz et al. 2008), as well as requiring an excessively large number of specimens to define the three dimensional state boundary surfaces (τ-σ-s) or (q-p-s). Here τ is shear stress, σ is net normal stress, s is suction, p is the net mean stress ($p = (\sigma_1 + 2\sigma_3)/3 - u_a$) and q is deviator stress ($q = \sigma_1 - \sigma_3$). The air phase of the specimen is atmospheric in this study. At failure, there exists a relationship of $p_f = p_c + q_f/3$ in which p_c is confining stress. For the configuration of one boundary surface, at least nine specimens are desired with test conditions in variations of three suctions and three

confinements. This renders the two techniques extremely expensive, as long time periods are required for moisture and suction equalization at sample equilibrium, confinement and deformation phases. Moreover, as independent suction control and measurement are of vital importance in these two suction control techniques, what was reported by Blatz and Graham (2000) and Boso et al. (2005) remained largely in the calibration phase instead of producing stress-strain relationships. These techniques show considerable potential in exploring shear strength behavior of unsaturated clayey soils; nevertheless, their practicability and effectiveness are yet to be examined.

An alternative method to the four discussed previously, that was adopted in this study, was to predetermine the HSWCC of the soil and prepare the triaxial specimens at suction values based on the HSWCC. To achieve this goal, both stress and capillary histories are important. The detailed procedure of specimen preparation and testing is given in section 6.2. Conventional triaxial undrained compression tests (CIUC) were also conducted on the specimens compacted in much the same way as the ones for unsaturated compression tests.

6.2 Sample Preparation and Triaxial Test Program

6.2.1 Sample Preparation Procedure

Since the HSWCCs were used to deduce suction, preparation of the specimens for the triaxial tests followed exactly the same initial compaction as well as identical stress and capillary history of those for the achievement of HSWCCs. For either Carnisaw or Eagle Ford, 27 specimens were prepared at suction, s, close to 2 MPa, 5 MPa and 10 MPa and sheared at confining stress, $p_{c,}$ of 0.1 MPa, 0.2 MPa and 0.4 MPa. A suction range of 2-10 MPa was chosen to cover a wide range of moisture fluctuations

expansive soil could experience in the field in response to drought and flooding. Another reason for choosing these suction values is the HSWCCs from the WP4 measurement were acceptable at suctions higher than 1MPa while Carnisaw specimens began to exhibit severe cracking beyond suction of about 15 MPa. In the meantime, the confining pressure up to 0.4 MPa (400 kPa) is representative of most in-field stress scenarios (equal to the pressure at a depth of 20 m assuming a wet soil density of 2 Mg/m^3). When used as buffer material in barriers for nuclear waste disposal, the depth can be as much as 240 m (Blatz et al. 2002). However, artificial sand-bentonite mixture is usually used as the buffer material, whereas natural expansive soil is more frequently encountered in common construction sites. It's worth mentioning here that when used as nuclear waste containing buffer, the macrostructure (inter-aggregate zones) of expansive soil largely disappears owing to the very high compactive effort, leading to high volumetric reversibility after several drying-wetting cycles (Delage et al. 1998).

The specimens were air-dried or wetted following exactly the same procedure used during the 3D swell-shrink volumetric measurements as narrated in section 5.3.2. No drainage assistance using filter paper or geotexile was applied due to the reasons mentioned earlier (section 5.3.2). It is worth mentioning that Blatz and Graham (2000) applied such drainage (with geotextile) on a compacted 50:50 sand-bentonite mixture in suction-controlled triaxial tests. However, their specimen was compacted initially at a saturation of about 85 % and a suction of 3.0-3.5 MPa and then equilibrated for the target suction using the VET method; therefore, initial saturation and expansion of the specimen was avoided.

Once a specimen reached the volumetric water content corresponding to a desired suction (based on the HSWCCs) it was sealed and stored in a 100 % humidity room for moisture equalization for 2-4 months. Difficulties were encountered in preparing a specimen exactly at target suction. Instead, specimens were produced with suctions slightly larger or smaller than desired from the volume-mass calculation and the HSWCCs. The initial suction estimated from the HSWCCs was expected to closely represent the actual. Evenly distributed suction and moisture throughout the specimen was also desired. To verify these prerequisites, additional specimens were prepared and equalized for 2 months after which small chunks were carefully trimmed from every one-fifth of the specimen height and tested for suction. Some results from Carnisaw (CA) and Eagle Ford (EF) samples are presented in Figure 6.1 (Note: PD - Primary Drying, PW - Primary Wetting and SD - Secondary Drying).

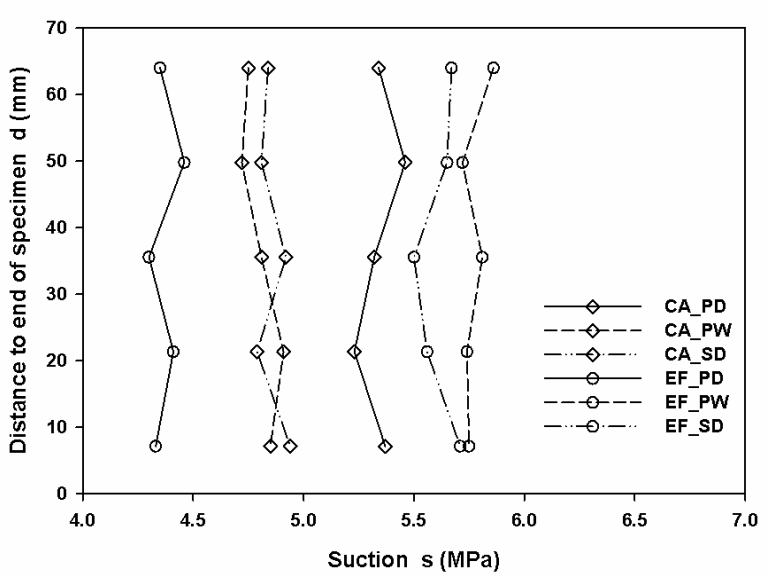

Figure 6.1 Suction distribution after moisture equilibrium

According to Figure 6.1, suction distribution throughout the samples were not exactly homogenous, and deviated slightly from the target suctions obtained from either

the drying or wetting path. In general, the suction variance along the specimen height varied from 0.2 MPa for specimens of low suction (< 6 MPa) to 0.6 MPa for specimens of high suction (> 10 MPa); while the corresponding moisture content varies within 0.5 %. The difference in magnitude in between the averaged measured suction and the estimated value based on the HSWCCs was found below 0.3 MPa. This consistency indicates an excellent homogeneity of the specimens produced by a uniform preparation procedure. Moreover, the total suction of an unconfined sample of highly clayey soil (clay size fraction ≥ 50 %) is exclusively determined by moisture content when relatively dry (e.g., s > 1 MPa) and independent of initial dry density (Wan et al. 1995, Miller et al. 2002, Tang et al. 2002). In the unsaturated triaxial specimens being investigated here, the influence of dry density on initial suction was found negligible.

6.2.2 Triaxial Test Program

Constant-mass confined compression tests were performed on unsaturated triaxial specimens of Carnisaw and Eagle Ford. These tests contain two stages: confining and shearing, both with a drained air phase and an undrained water phase. A schematic diagram of the triaxial test setup was presented in Figure 6.2. Two brass porous disks, each covered with two sheets of Teflon filter membrane, were placed at both the top and bottom of each specimen. The small pore size of the Teflon (PTFE) filter membrane (< 5 μm) makes it relatively impervious to water (with substantially low flow rate) while maintaining permeability to air so that the air phase of the specimen was drained (with the drainage valves open) throughout the test procedure, whereas the water phase remained undrained. The first membrane in immediate contact with the specimen functioned as a waterproof layer, while the second was used to

prevent atmospheric vapor from entering the specimen. The porous disk served as a buffer zone to relieve potential air pressure buildup on the top or bottom of the specimen during shearing. A layer of Whatman filter paper (with pore size of 20-25 μm) was added in between the cap/pedestal and the filter membrane in order to prevent the latter from being torn apart by the edge of the notch on the cap/pedestal surface (this did occur in some trial tests). The filter paper also benefits air flow on membrane surfaces since the paper has a much greater permeability to air, and it was further perforated in the middle area aligned with the cap/pedestal notch so as to assist air flow.

After the specimen was installed on the pedestal, a second Latex membrane was applied to prevent any leakage of the first Latex membrane. Special inspection must be taken on the soundness of part of the first Latex membrane that stretched beyond the specimen and attached to the cap/pedestal. The long specimen preparation time (drying-wetting plus 2-4 month equilibrium) could lead to membrane degradation that would create tiny fissures and bring about small water leakage, even with the use of a second (new) membrane and sealing "O" rings. In at least three tests, this specific leaking problem increased moisture content of the samples by up to 3.5 % after shearing. Unfortunately, the specimens had to be discarded. The problem was solved by cutting off the part of the first membrane that stretches beyond the specimen length once such fissures were detected.

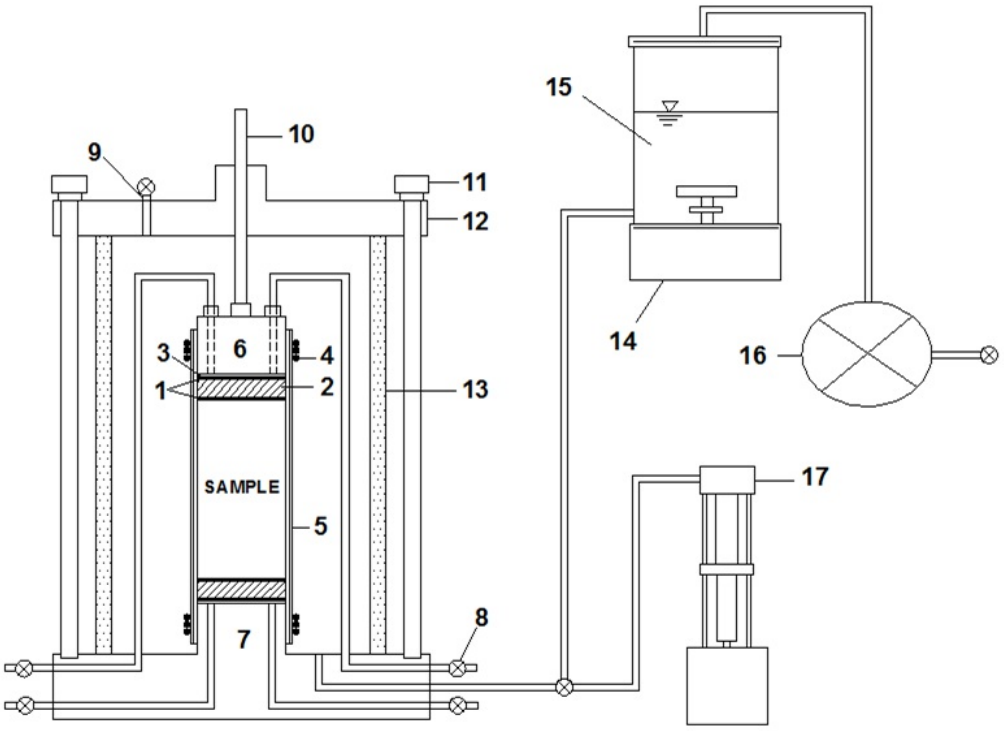

Figure 6.2 Schematic diagram of the triaxial test setup*

*1- Teflon filter membrane, 2- brass porous disk, 3- filter paper, 4- "O" ring, 5- Latex membrane, 6- cap, 7- pedestal, 8- valve, 9- vent port, 10- piston, 11- fastening rod, 12- top frame, 13- acrylic cell, 14- de-air device, 15- water, 16- vacuum pump, 17- cell pump; not to scale

The cell pump and the triaxial cell were integrated with a Sigma-1 automated load test system (manufactured by GEOTAC Inc.) which was able to control and record the stress-strain-volume data on an automated stress-path triaxial software platform. An evaluation of volumetric strain during shear is important when prediction of movements such as settlement is required. In Figure 6.2, the volume change monitored through the cell pump is not able to accurately represent the amount of specimen consolidation because the acrylic cell, flow tubes and Plexiglas pedestals also deform and creep under confining stress. This phenomenon leads to the volume change hysteresis that renders the calibration difficult (Lawrence 2004). A detailed discussion on issues associated

with volume measurement of unsaturated soils in a triaxial test is provided in APPENDIX B.

A slightly higher position of the de-air device above the top of the triaxial cell allowed the de-aired water to flow slowly to and gradually fill the cell chamber, after which the desired confining pressure was immediately applied by the cell pump (Figure 6.2). The specimen confining process was terminated and shearing was initiated when the rate of volumetric change decreased below 0.01 cm^3/hour, usually after 1-3 hours. Under this circumstance, it was assumed that the cell deformation had completed and the creep had stabilized during shear, and the shear-induced volume change as monitored by the cell pump was approximated as the specimen volume evolution. However, the volume change in the confinement stage was unobtainable without implementation of advanced double wall cell and volume monitoring system. Hence, the dimension of the specimen before confinement was taken as the basis for the foregoing volume evolution during shear. In this context, the deformation was slightly underestimated due to the high stiffness of the specimen (as demonstrated later). On the other hand, the overestimation of deformation caused by system creep during shear tends to offset this underestimation.

6.2.3 Selection of an Appropriate Strain Rate

To ensure the equalization and dissipation of induced pore pressures in the constant mass tests, the strain rate was carefully selected for the strain-controlled test. The constant water content (CW) tests run by Bishop et al. (1960) on Boulder clay, Bishop and Donald (1961) on Braehead silt, Gulhati and Satija (1981) on Dhanauri clay reported strain rates of 3.5×10^{-5}, 4.7×10^{-4} and 6.7×10^{-4} %/s, respectively. Vinayagam

(2004) performed CW tests on Minco silt at a strain rate of 5×10^{-5} %/s. Georgetti and Vilar (2010) used a strain rate of 3.3×10^{-4} %/s for the CW triaxial compression tests on a clayey fine sand. Feuerharmel et al. (2006) carried out constant-mass compression test on two unsaturated clayey soils using a conventional direct shear testing equipment at a strain rate of 1×10^{-3} %/s. It should be pointed out that the aforementioned CW tests were conducted under a suction-controlled condition, whereas no suction control was implemented in the constant-mass tests in Feuerharmel et al. (2006) and this study.

Oh et al. (2008) studied the undrained shear strength of unsaturated kaolin with suction up to 3 MPa using undrained triaxial compression tests (constant-mass tests). Drainage of air was allowed before shearing to enable equilibrium of specimens with respect to suction and volume change. The specimens were then sheared at two shear rates (2.5×10^{-4} and 1.3×10^{-5} %/s) under undrained conditions of both air and water. It was discovered that the shear strength increased with decreasing strain rate.

Here, two strain rates, 1.4×10^{-4} %/s and 3.5×10^{-5} %/s were evaluated for comparison purposes based on the literature investigation and soil conditions in this study. These two rates result in a time span of 30 and 120 hours to shear one specimen to 15 % axial strain. Carnisaw and Eagle Ford specimens with the medium suction ($s \approx$ 5 MPa) and the medium confining stress ($p_c = 0.2$ MPa) were evaluated relative to these two strain rates. Table 6.1 summarizes the water retention information of the specimens before and after shearing. In Table 6.1, the value following the sample name denotes the number of hours in test duration. For example, "CA_30" represents the specimen sheared for a period of 30 hours. The ε-q and ε-δv curves are presented in Figures 6.3 and 6.4.

Table 6.1 Comparison of specimen states before and after shearing

s and w state	CA_30	CA_120	EF_30	EF_120
s before shearing (MPa)	4.94	4.93	4.08	4.86
s after shearing (MPa)	4.46	3.24	3.66	3.27
s averaged (MPa)	4.78	4.08	3.87	4.07
s variance (%)*	-11.0	**-34.3**	-10.2	**-32.7**
w before shearing (%)	20.7	20.7	22.7	21.8
w after shearing (%)	19.8	20.5	22.0	20.7
w averaged (%)	20.3	20.6	22.4	21.3
w variance (%)†	-0.9	-0.2	-0.7	-1.1

*s variance = (s after shearing – s before shearing) / s before shearing
†w variance = w after shearing – w before shearing

Some interesting facts are discovered in Table 6.1. A slight decrease of moisture content was observed in all the four specimens. This may be partially attributed to the moisture loss during specimen installation (before test) and trimming for the WP4 suction measurements (after shear). Such a moisture loss would have resulted in a higher measured suction. In reverse, the specimens demonstrated a decrease of suction, which is more profound in specimens sheared at a lower strain rate (highlighted in Table 6.1). Even though suction increase after shear is also possible (as shown later), the highlighted suction decreases suggest that shearing may have an impact on the water retention behavior of expansive soils; meanwhile, such an impact may depend on the strain rate selected. The lower strain rate allowed for the clay particles and aggregates sufficient time in readjusting against shearing and filling up the inter-aggregate macropore space. This brought about denser structure after shear, as indicated by the greater volumetric decrease relative to that of the specimens sheared at the higher rate (Figure 6.3), and the subsequent smaller suction magnitude because of a larger degree of saturation.

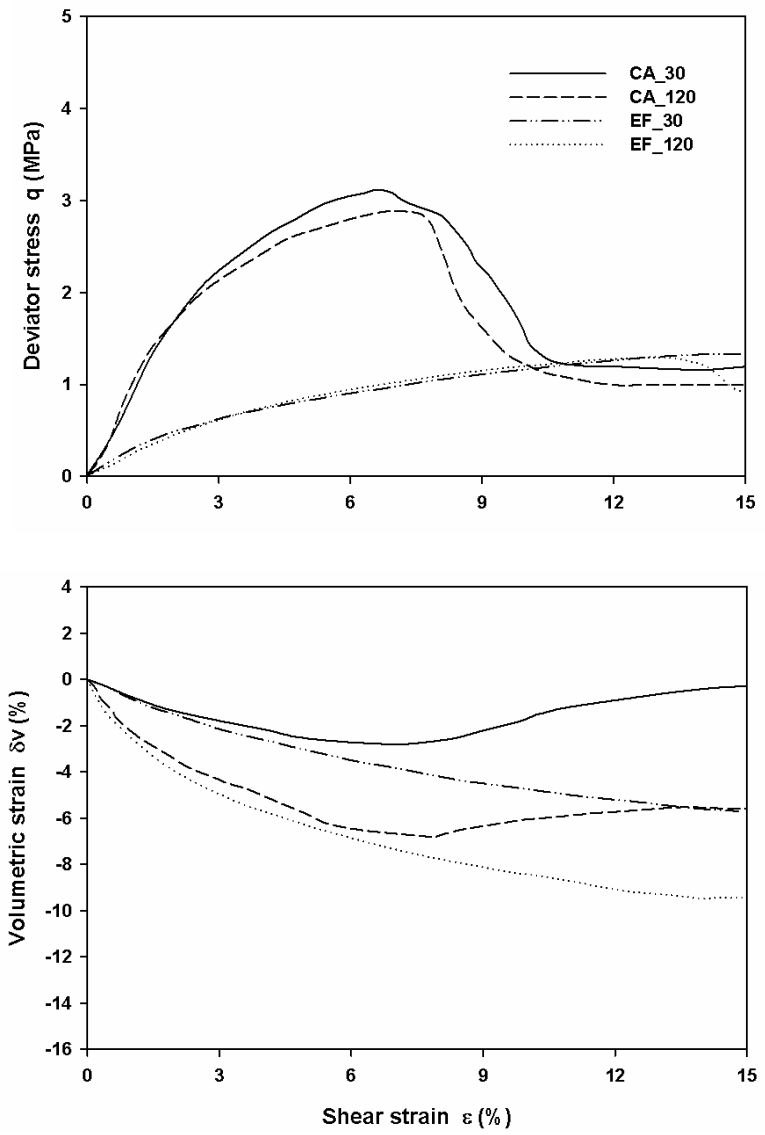

Figure 6.3 ε vs. q and δv curves sheared at different rates

Figures 6.3 and 6.4 indicate that at similar suction magnitudes the strain rate has little impact on the ε-q curve; however, the change of volumetric strain is greater with the lower strain rate and the difference increases as strain proceeds, regardless of soil type. As said, the faster rate (1.4×10^{-4} %/s) introduces lesser suction change following shear; more importantly, this rate allows the test program to be fulfilled in a timely

manner (concerning there are 54 specimens to be tested). Therefore the strain rate s_{r1} was used for the rest of the tests during which the specimens were sheared until $\varepsilon = 15$ % was reached. Conventional consolidated undrained compression tests (CIUC) following ASTM-D4767 (2011) were also conducted on specimens compacted and sheared in much the same way as those for unsaturated triaxial compression tests. The same strain rate (1.4×10^{-4} %/s) used in the CIUC tests is much lower than the suggested magnitude determined by the criterion of ASTM-D4767 (2011). The specimens were sheared after consolidation at effective stresses of 0.05 MPa, 0.1 MPa, 0.2 MPa and 0.3 (or 0.4 MPa) until 15 % vertical strain ($\varepsilon = 15$ %).

6.3 Results and Discussion

6.3.1 Results of the CIUC Tests

The effective stress paths of Carnisaw and Eagle Ford specimens are plotted jointly in Figure 6.4. The critical state lines record slopes of 1.45 and 0.88 for Carnisaw and Eagle Ford, respectively, with the corresponding critical-state friction angle φ_c' of 35.7° and 22.6°. In general, Carnisaw exhibits markedly higher shear strength than that of Eagle Ford. At the same time, the specimens of both Carnisaw and Eagle Ford demonstrate responses of contracting initially and then passing through a phase transformation state.

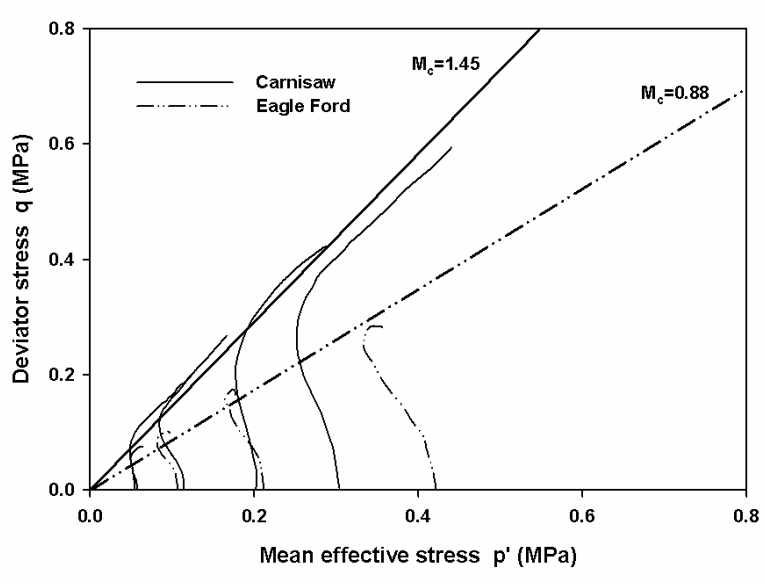

Figure 6.4 Effective stress paths of Carnisaw and Eagle Ford specimens

The low pH of Carnisaw (pH 4.4, Table 2.3) tends to promote a positive charge at the edge site of the clay particle owing to protonation in the acidic environment (Wang and Siu 2006a). This results in strong edge to face particle association (as illustrated by Figure 3.10 (a) and summarized in Table 3.2) caused by strong Coulombian electrostatic forces. On the other hand, the slightly basic acidity of Eagle Ford (pH 7.7, Table 2.3) favors the development of negative charges at the edge site and hence a more dispersive fabric as shown by laminar face to face particle association (Figure 3.10 (b) and Table 3.2) controlled by both van der Waals attraction and DDL repulsion. However, both soils exhibit dilative responses regardless of their distinct structures. This may be attributed to the closely packed fabric and the strong DDL repulsion during shearing. It is desired to compare the results of this study to the work of Wang and Siu (2006b) on two kaolinite samples with similar pH and structure (Figure 6.5). It should be noted that both Carnisaw and Eagle Ford are highly plastic

expansive soils (PI = 27 and 57, CF = 51 % and 66 %; Table 2.2) with more than 95 % of their particles passing the No. 40 U.S. sieve, and no clods greater than a diameter of 1 mm were visualized on the initially compacted specimens (further confirmed by the SEM observations at a low magnification ratio), implying relative homogeneity of soil structure of the specimens at their compacted states.

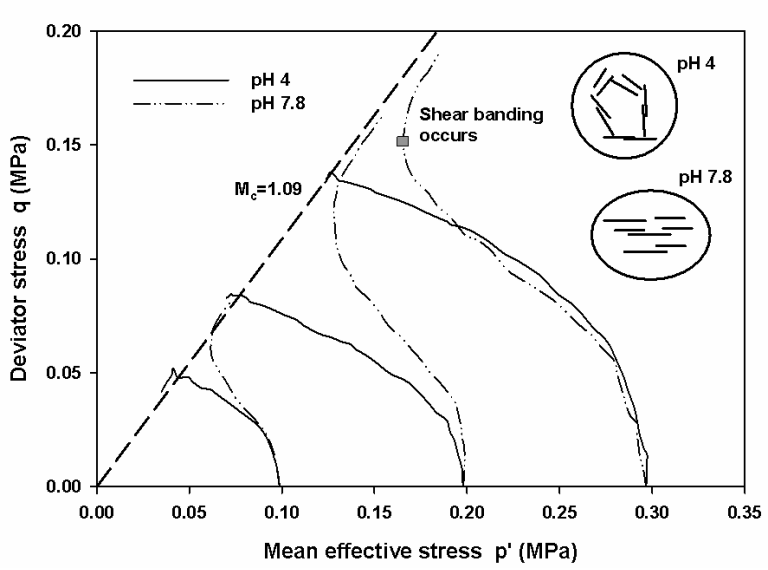

Figure 6.5 Effective stress paths of pH 4 and pH 7.8 kaolinite*

*slightly modified from Wang and Siu (2006b)

In Figure 6.5, the pH 4 specimens showed continuous contraction whereas the pH 7.8 specimens illustrated a phase transformation state and greater shear strength at critical state (Figure 6.5). In contrast, the Carnisaw (pH = 4.4) specimens exhibited dilative behavior despite its flocculated "card house" structure and low pH (same as the pH 4 kaolinite sample). This suggests that mineralogy plays a crucial role in governing the stress-strain behavior of expansive soils. The vermiculite content (Table 3.1) may contribute to the DDL development and repulsion in Carnisaw. Moreover, the trivial salt concentration of Carnisaw further enhanced the development of DDL thickness

(section 4.4), which in turn promoted interparticle repulsion. Such repulsion became significant as the Coulombian attraction deteriorated in response to the gradual destructuring of the edge-face associations when shearing proceeded, rendering Carnisaw even more dilative than Eagle Ford (pH = 7.7). The relatively great salt concentration of Eagle Ford promotes van der Waals attraction to be the prevailing force on the surfaces of face and edge sites as the particles are brought closer. With shearing, the strength gain from DDL repulsion on the face to face contact became progressively intensified, which was similar to that observed in Wang and Siu's (2006b) pH 7.8 kaolinite samples.

6.3.2 Results of the Constant-mass Tests on Unsaturated Specimens

It is necessary to provide the information on the suction before and after shearing (Figure 6.6) in order to evaluate the change of the hygroscopic status in specimens. As mentioned, the suction before shearing was estimated on the basis of the predetermined HSWCCs, while the magnitude after shearing was measured directly by the WP4-T on every one fifth of specimen length and averaged. The graph in Figure 6.6 shows close correspondence of suction before and after shearing, implying little impact of the shearing process on the suction change (with $s > 1$ MPa). These two magnitudes were therefore averaged to give the suction of each specimen in the following analysis.

It is worth noting that the data point deviates from the 1:1 line more significantly at suction greater than 10 MPa (Figure 6.6). This may be related to the degraded accuracy of the WP4-T at high suction measurements (> 10 MPa). Moreover, shearing may affect the water retention behavior of expansive soils with the effect dependent on strain rate, as discussed earlier. The role of such an effect is unclear at present. The

suction distribution throughout the specimen after shearing exhibits high similarity to characteristics depicted in Figure 6.1, indicative of negligible moisture transmission during shearing.

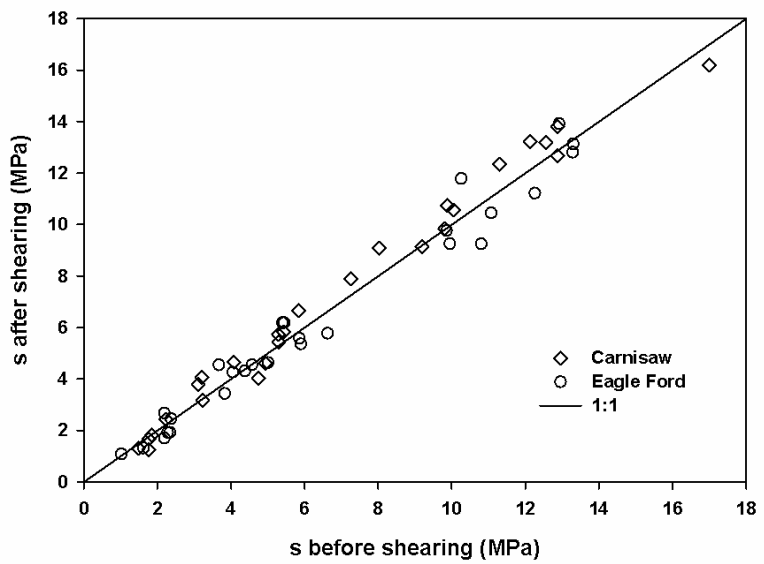

Figure 6.6 Specimen suction before and after shearing

The close correspondence of the suctions before and after shearing as illustrated in Figure 6.6 supports the finding of Tang et al. (2002) which showed recoverable suction changes of a 50:50 sand-bentonite specimen experiencing a process of loading, unloading, shearing and reducing the cell pressure to zero. It should be noted that an increase of confining stress p_c (up to 3 MPa) can induce an increase in the degree of saturation and decrease in suction, s, (Wiebe et al. 1998, Tang et al. 2002, Tang and Graham 2002, Blatz et al. 2002) during confinement. This phenomenon was not evaluated in this study since no independent suction monitoring was implemented during confinement or shearing. Based on the observation of Tang et al. (2002) on the suction changes of a 50:50 sand-bentonite specimen, however, the condition of p_c equal

to 0.4 MPa accounted for s decrease of less than 0.5 MPa due to confinement, even though different soils were studied.

The relationships of deviatoric stress-vertical strain (q-ε) or volumetric strain-vertical strain (δv-ε) when evaluated with respect to suction and confining stress are presented in Figure 6.7 and 6.8, which are representative of specimens on the primary drying (PD) path. The corresponding specimen information is summarized in Table 6.2. The relationships of specimens along the primary wetting (PW) and secondary drying (SD) paths demonstrate similar trends and therefore are not presented here for brevity purposes. It is worth mentioning that duplicate specimens of identical suction were not available because of the preparation process without suction-control implementation. In other words, while it was attempted to make two specimens at identical suction values based on the HSWCCs, the measured suction values both pre- and post- test were slightly different than each other, which is expected due to experimental variability, however, made direct comparisons difficult.

Table 6.2 Information of specimens for q-ε and δv-ε evaluations

Soil specimen	**γ_d[*](kN/m^3)**	**p_c[*](MPa)**	**s[*](MPa)**
CA[*]_L[†]L[+]	15.4	0.10 (L[†])	1.51 (L[+])
CA_HL	15.9	0.40 (H)	1.40 (L)
CA_LH	**16.8**	0.10 (L)	10.31 (H)
EF_LL	14.0	0.10 (L)	1.47 (L)
EF_HL	13.9	0.40 (H)	2.13 (L)
EF_LH	**16.4**	0.10 (L)	10.76 (H)

[*]Note: CA, Carnisaw; EF, Eagle Ford; γ_d, dry unit weight; p_c, confining stress; s, suction;
[†]Confining stress (p_c): L-low; H-high; [+]Suction (s): L-low; H-high

The Carnisaw specimens demonstrate strain-softening behavior (the specimen "CA_LL" shows slight strain softening at ε ≈ 14 %), whereas only the EF specimen of high s but sheared at low p_c (EF_LH) shows such a behavior (Figures 6.7 and 6.8). In

fact, all of the CA specimens (regardless of capillary history) exhibited strain softening behavior, a brittle failure mode with a clear developed failure plane; on the other hand, this brittleness was only seen in EF specimens at relatively large s (around 10 MPa). At lower s (< 10 MPa), the EF specimens experience mostly strain hardening showing a ductile failure mode and a barrel shape after shearing, irrespective of p_c variation. In the quick undrained triaxial tests (3.3×10^{-3} %/s) performed on unsaturated sand-bentonite (50:50) specimens, Blatz et al. (2002) disclosed that the specimen with a lower p_c or higher s tends to be more brittle. In this study, confinement has little effect on the failure mode, which is mainly attributed to the low magnitude of p_c relative to that of s; however, the strain at which the brittle failure manifests does depend on confinement. This is better demonstrated in the CA specimens, for which the strain where softening initiates decreases with the increasing s but increases with increasing p_c (Figure 6.7). At a higher p_c, the specimen (CA_HL) becomes more ductile even though a clear shear plane is still observed.

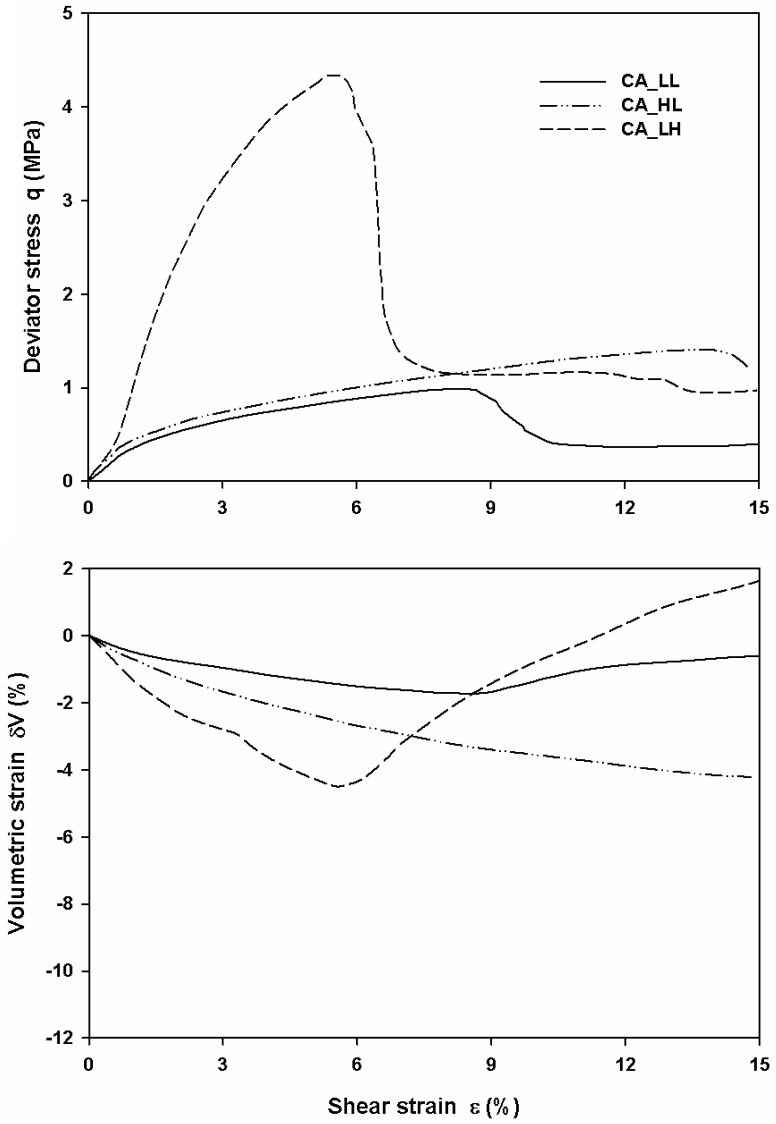

Figure 6.7 Some q-ε and δv-ε curves of Carnisaw

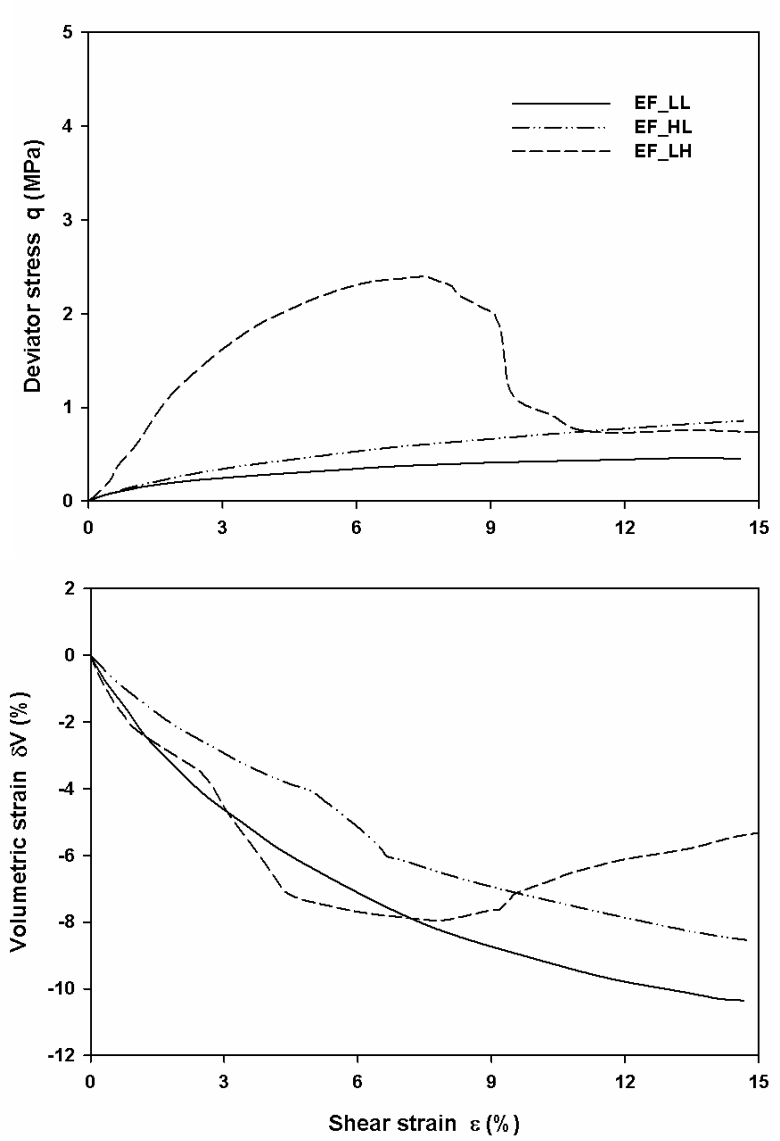

Figure 6.8 Some q-ε and δv-ε curves of Eagle Ford

It appears that an increase in either suction s or confining stress p_c results in enhancement of deviator stress q. The smaller effect of p_c on q compared to that of s is mostly attributed to the lesser change in magnitude of p_c. As shown in Table 6.2, the "H" s is about 8~9 MPa higher than the "L" s whereas an increase of only 0.3 MPa was applied in assessing the effect of p_c. Moreover, the significant increase of s (from "L" to "H", Table 6.2) causes substantial densification of specimen by shrinkage (illustrated by

the highlighted dry unit weight data in Table 6.2). This trend of density change due to the contribution of s is further evaluated on all the test specimens (Figure 6.9). Despite the scattering of data, a clear trend of density increase with increasing s (though it is hard to distinguish the effects of hydraulic hysteresis on the density evolution) can be observed.

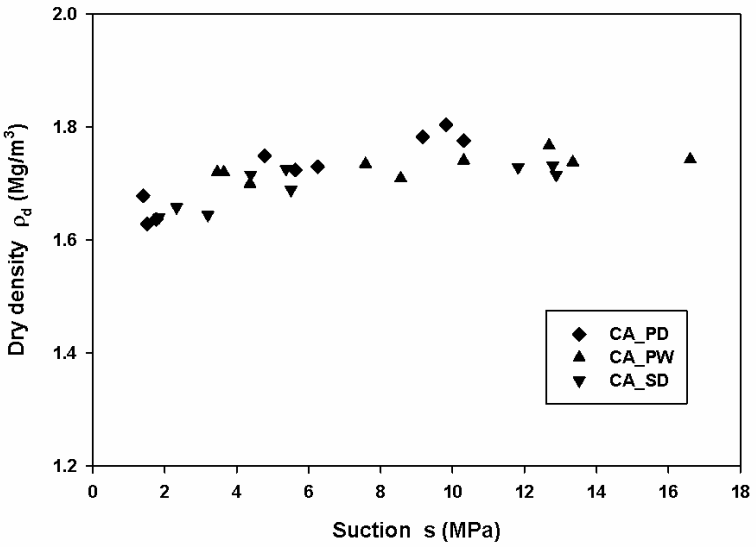

(a)

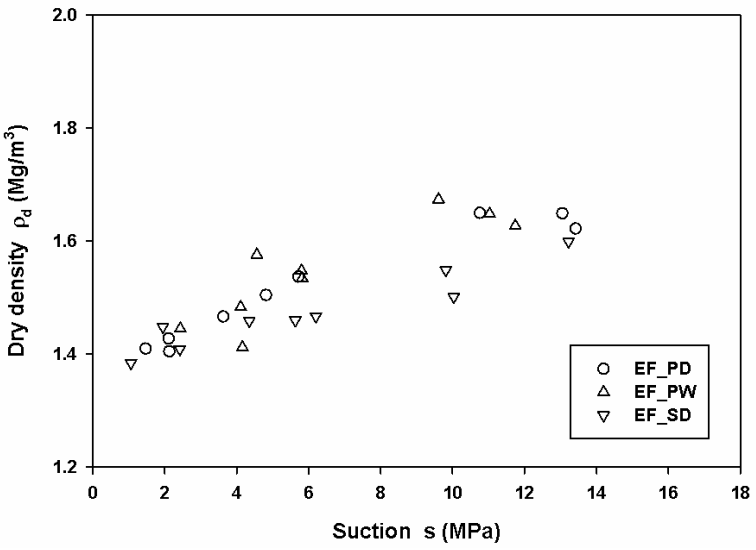

(b)

Figure 6.9 Effect of suction on dry density

(a) Carnisaw; (b) Eagle Ford

Here arises the challenge of how to separate the effects of mean stress p and suction s on the density and shear strength of clayey soils, while at the same time p and s are inter-related. On one hand, augmentation of dry density of an unsaturated specimen can be ascribed to either pressure loading (δp) or shrinkage (δs). On the other hand, an increase of p causes decreasing s as a result of the compression of the air phase

and increasing saturation. On the other hand, suction increase gives rise to higher shear resistance of a specimen; in turn, a specimen with a higher s tends to fail at a larger p ($p_f = p_c + q_f/3$). Hence, it is difficult to experimentally describe the yielding of a highly plastic soil on a constant-p or constant-s plane. Although p and s are commonly accepted as independent stress variables in earlier work on elastic-plastic modeling of highly plastic soils (Alonso et al. 1990, Wheeler and Sivakumar 1995, Delage and Graham 1995, Cui and Delage 1996, Alonso et al. 1999), and recent works (Tang and Graham 2002, Blatz and Graham 2003) conducted research on coupling the effects of p and s on the yielding behavior. However, such a coupling rendered the usage of individual p and s coordinates in constructing the yield surface in a p-s-q space controversial (Blatz and Graham 2003). Moreover, it did not answer the question of how the resulting change in density (in both the confinement and shearing stages) plays in effect. In this sense, future research is needed in evaluating the individual role of p and s in the structure evolution of an unsaturated sample under confinement and shearing.

It is also revealed in Figures 6.7 and 6.8 that the specimen shows stronger resistance to volumetric decrease (or become more dilative) at either a lower p_c (comparison between CA_LL and CA_HL) or a higher s (EF_LL vs. EF_HL). Such trends were reported by Houston et al. (2008) even though soils of lower PI (SM, CL-ML and CL) were investigated. Meanwhile, this resistance depends on the relative change in difference of p and s. For example, specimen EF_HL was sheared with confinement increased by 0.3 MPa but at a suction of 0.66 MPa higher compared to specimen EF_LL, thus showing a stronger resistance. This implies p_c and s may have

similar effect on the shear-induced volume change of unsaturated soils; whichever masks the effect of the other depends on the magnitude in change. Significant increase of s results in apparent dilation when looking into the specimens CA_LH and EF_LH, which is more pronounced in the specimen of lower PI (CA_LH). This same discovery was also reported by Houston et al. (2008) in comparing less plastic soils (SM, CL-ML and CL). From a microscopic point of view, this phenomenon can be attributed to the suction-induced aggregation of particles tightly bound by intra-aggregate surface tension forces. The formulated aggregates experience inter-aggregate meniscus break and roll over each other when shearing proceeds. In the meantime, Carnisaw shows more remarkably dilative behavior because the more flocculated structure and the thicker, smaller particles tend to promote the "ride up" motion of aggregates in response to shearing, whereas the more laminar structure and the thinner, larger clay flakes of Eagle Ford favor the "bend over" effect. No direct visualization of these postulated structure evolutions is available currently, though, due to technological difficulties involved in imaging such evolutions of unsaturated specimens during the confinement and shearing processes.

6.3.3 Specimen Stiffness

Soil stiffness is of interest in assessing the deformational resistance of soil sample in response to shear. Two definitions of secant modulus have been used in this investigation in evaluating soil stiffness: (i) secant modulus $E_{1\%}$ measured from the beginning to 1 % shear strain (Blatz et al. 2002) and (ii) secant modulus E_{50} from the beginning of shearing to 50 % of peak deviator stress (Tang et al. 2002, Blatz et al. 2002). Regardless of the scattering of data, two conclusions can be drawn from Figures

6.10 and 6.11 as: (1) generally both $E_{1\%}$ and E_{50} increases as a function of suction; (2) the moduli appear to be larger along the PD path. The first conclusion, which is mainly related to the increase of dry density with suction (Figure 6.9), is in accordance with the findings of Blatz et al. (2002) on 50:50 sand-benonite specimens at s of 5-42.4 MPa and sheared at p_c of 0.5-3.0 MPa. It was also noticed by Blatz et al. (2002) that the relationship of stiffness with suction is largely independent of p_c. It was observed in this study that the specimen stiffness is slightly strengthened with a higher p_c (up to 0.4 MPa). This leads to the supposition that stiffness (of unsaturated highly plastic soil) increment attributed to the contribution of p_c may degrade at certain high p_c levels. Nevertheless, further research needs to be invested in evaluating the roles of soil type and p_c level on stiffness as a function of p_c.

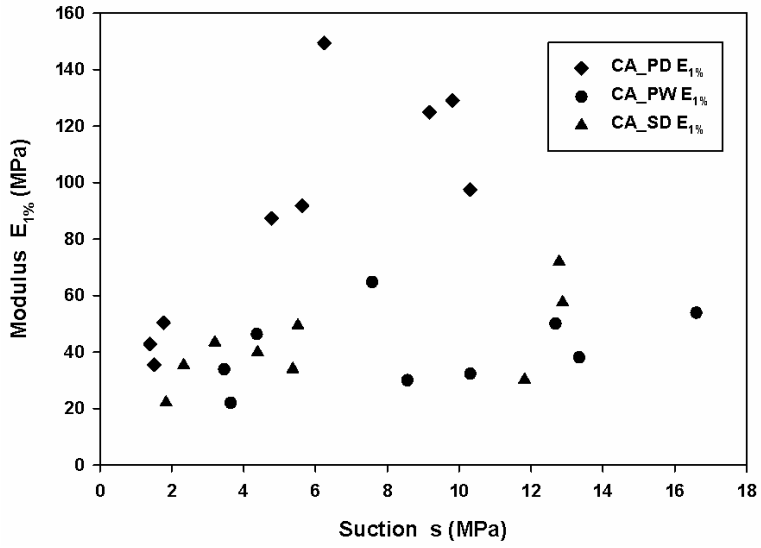

(a)

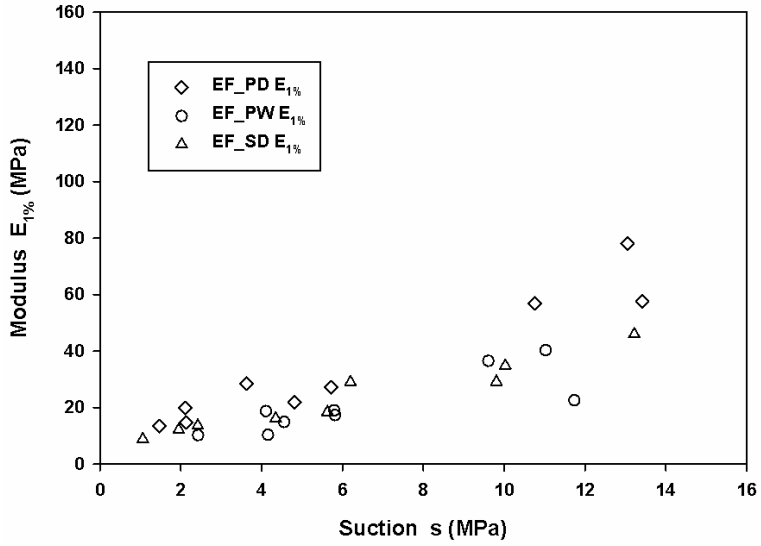

(b)

Figure 6.10 Modulus $E_{1\%}$ with varying suction

(a) Carnisaw; (b) Eagle Ford

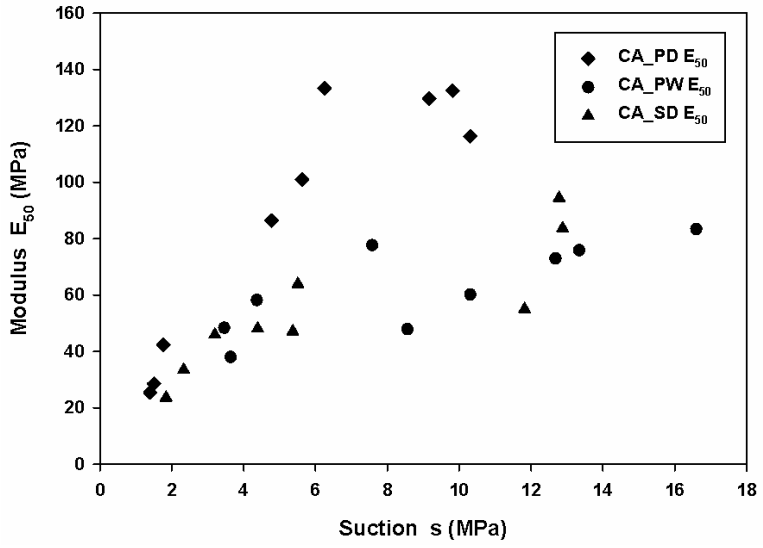

(a)

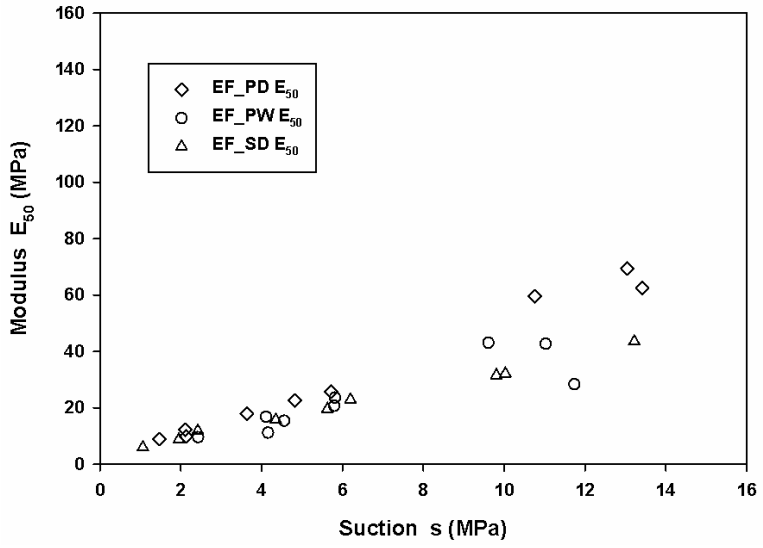

(b)

Figure 6.11 Modulus E_{50} with varying suction

(a) Carnisaw; (b) Eagle Ford

On the other hand, the second conclusion that the moduli $E_{1\%}$ and E_{50} are larger along the PD path is revealed more obviously in Carnisaw (Figure 6.10 (a) and Figure 6.11 (a)). This may be due to the strongly developed Coulombian bonds in Carnisaw specimens of the PD path that deteriorated as drying/wetting proceeded, as discussed

earlier. A lesser important cause can be gradual deterioration of chemical cementation with drying/wetting process arising from redistribution of the chemical agents. This explains the small decrease (with drying/wetting) of moduli in Eagle Ford (Figure 6.10 (b) and Figure 6.11 (b)). No differentiation could be made on the moduli between the PW and SD paths in either Figure 6.10 or 6.11.

6.3.4 Effects of Mean Stress, Suction, Capillary History and Strain Level

Again, since the specimen preparation was carried out based on the HSWCCs instead of equilibrium inside a suction-controlled environment, it is not feasible to evaluate the p-q relationship on a constant-s plane, directly from the test points. However, because the suction values were estimated before shearing from the HSWCCs, and measured by the WP4 afterward and averaged, the p-q relationship can be revealed from the fitted surface of at least nine data points. In this aspect, p-s-q surfaces instead of individual p-q and s-q curves, were numerically fitted based on the tested data points (of both peak strengths q_{pk} and large strain strengths q_{ls}). The surfaces were constructed in a conservative way so as to best represent the test data. These fitting efforts were fulfilled by using a quadratic fitting model (Blatz 2000, Blatz et al. 2002) with the regressions conducted on the *MATHEMATICA* platform. Because constant s planes will be deduced from the fitted surface to represent the actual soil behavior, special care must be focused on defining the boundaries of the surface, as the actual shape of the surface across the entire (p, s) scopes can be misleading with respect to the shapes of the p-q relationships. For instance, a specimen of high suction tends to be relatively strong and is unlikely to fail at a small magnitude of p ($p = p_c + q/3$), thus rendering the part of the surface at locations of low p, high s physically meaningless. In

this regard, the boundaries of p were set as the minimum and maximum p recorded of the test data, and those of s were bounded by the minimum and maximum ratios of (s/p) of the test data. This delimitation resulted in most conservative surfaces that best represent the actual soil behavior. On the basis of the fitted surfaces, constant-p or constant-s planes can be achieved from the regressed surfaces. In order to focus on the effects of the factors like mean stress, suction, capillary history and strain level on shear strength, p_{pk}-q_{pk} and p_{ls}-q_{ls} diagrams at suctions of 2 MPa, 5 MPa and 10 MPa, taken from the fitted surfaces, are presented in Figures 6.12-6.15. The development of peak strength (q_{pk}) and large strain (post peak) strength (q_{ls}) that disclose the shear strength of expansive soil in the field before and after yielding is important to observe. q_{pk} best characterizes the "brittleness" of the test specimens, while q_{ls} is taken to be similar to the "critical state" strength (Blatz et al. 2002), although no measurements have been taken to confirm that state.

The CIUC results are presented for comparison purposes and these points are taken directly from the actual test results (because suction is zero and no fitting is needed). It must be noted that the p-q curves from the CIUC tests are test data and representative of effective stress relationships, whereas the curves from the constant-mass tests are fitted, illuminating total stress relationships.

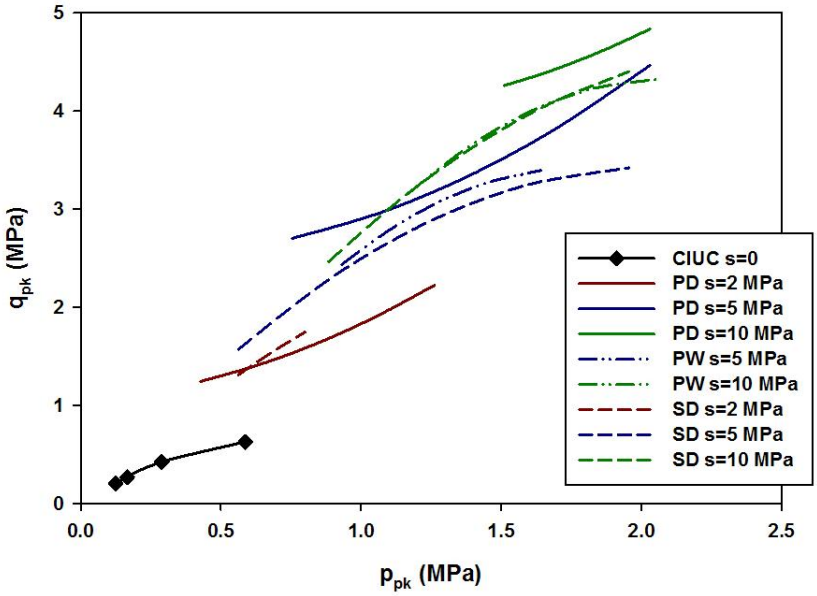

Figure 6.12 Peak strength envelopes of Carnisaw at varying suctions

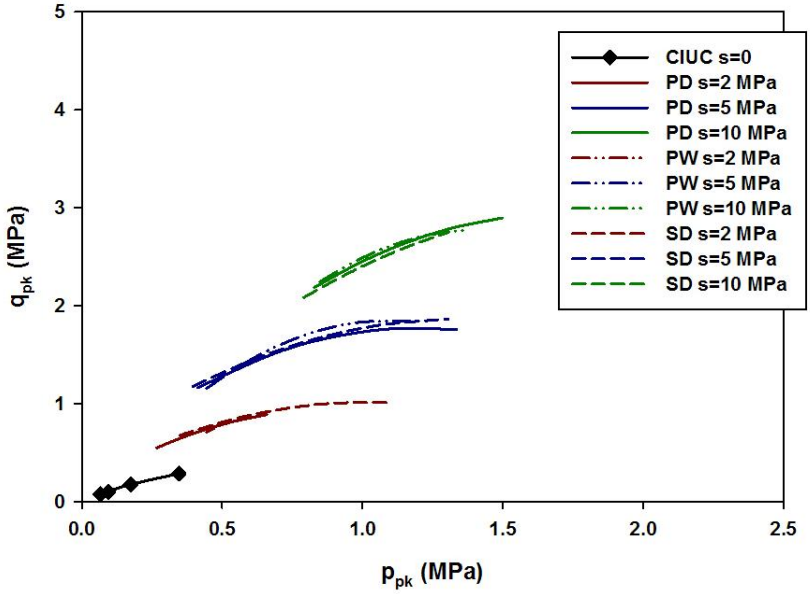

Figure 6.13 Peak strength envelopes of Eagle Ford at varying suctions

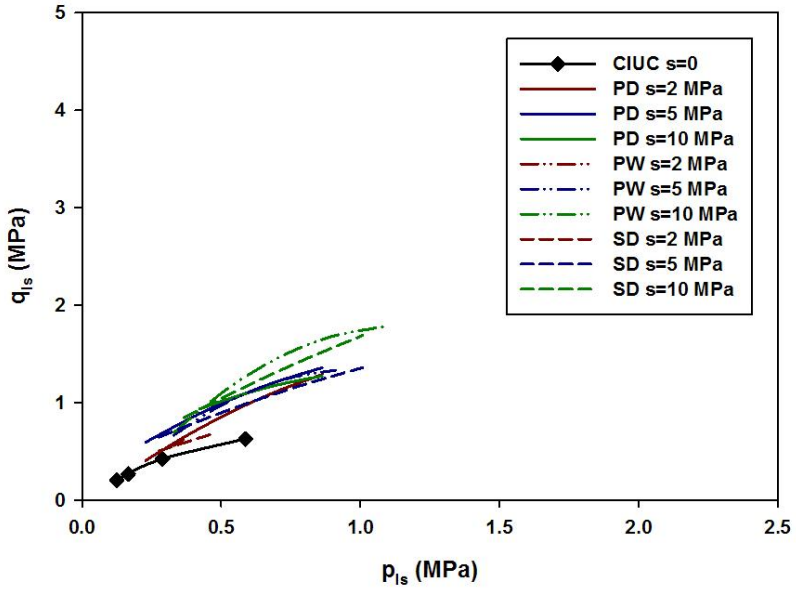

Figure 6.14 Large-strain strengths of Carnisaw at varying suctions

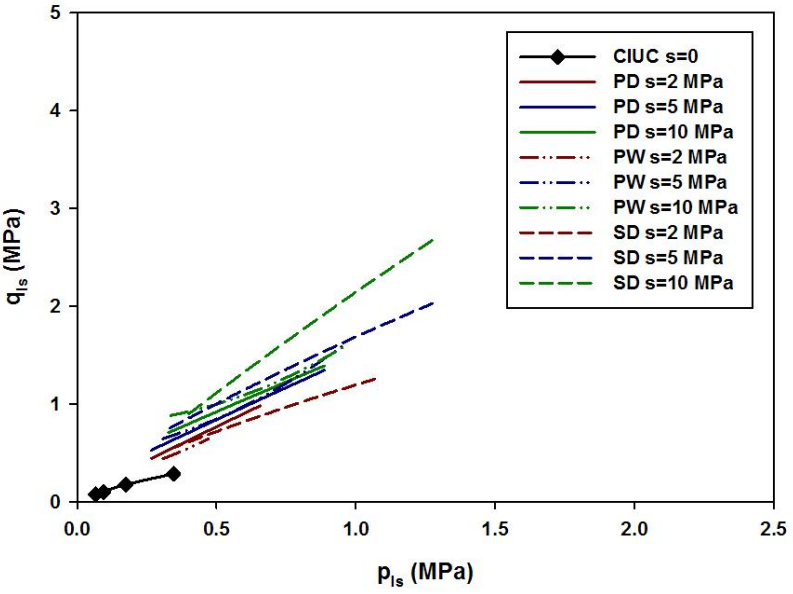

Figure 6.15 Large-strain strengths of Eagle Ford at varying suctions

After close inspection of the p_{pk}-q_{pk} and p_{ls}-q_{ls} diagrams (Figures 6.12-6.15), some interesting findings can be drawn:

1. At an identical p, q increases with increasing suction, regardless of strain level and capillary history. This is expected, as the contraction of meniscus (at higher suction) generates a stronger surface tension (capillary) force that tightens the adjacent particles and strengthens interparticle normal forces. The osmotic part of the suction, however, may decrease q following shrinkage of the DDL and expanding of the macropores. Its influence increases with decreasing degree of saturation (Tang et al. 2002). This does not change the overall impact of total suction on q, implying a lesser influence of osmotic suction.

2. In general, except the p_{pk}-q_{pk} curves representing the PD path of Carnisaw (Figure 6.12), the slopes of the non-linear p-q curves ($\delta q/\delta p$) decrease with increasing p but increase with larger s (Figures 6.12-6.15). This is consistent with Wiebe et al. (1998) and Blatz et al. (2002), though different materials were investigated (50:50 sand-bentonite mixtures in their studies) and no explanations were provided. Tentative efforts are given here to explore the underlying physicochemical mechanisms.

Densification caused by increased p will ultimately reach a critical point that the original specimen is fully destructured where part of the shear resistance contributed by the interlocking between aggregates is gone. At the very moment of this critical point, the resistance comes exclusively from inter-particle slipping carried by the DDL. The soil dilatancy created by DDL repulsion in response to shearing is solely dependent on intrinsic physicochemical characteristics of the soil. After large shear strain, this dilative effect will either increase or decrease (depending on whether the strain-softening or strain-hardening behavior is exhibited) but asymptotically equilibrates (characterized by q_{ls}). This p-q tendency is less obviously illustrated in the large strain case (Figures 6.14

and 6.15), possibly due to the insufficient shear strain implemented (the maximum axial strain was taken at 14~15 %). On the other hand, the increasing suction tends to thwart the destructuring of the specimen and the initiation of the full-developed dilation, due to the stronger interparticle bounding caused by surface tension. In consequence, the p-q slopes increase with increasing suction. It is worth mentioning that part of specimen dilation may also be contributed by the rolling over effect of the clay aggregates similar to the behavior of sand, though more research is needed to justify this mechanism.

3. Capillary history has a dramatic impact on the p_{pk}-q_{pk} envelopes of Carnisaw (Figure 6.12) while playing a much less significant role on its p_{ls}-q_{ls} curves (Figure 6.14). In the case of Eagle Ford, a distinct feature is depicted as the effect of suction history being negligible on the p_{pk}-q_{pk} relationships (Figure 6.13). However, when examining the p_{ls}-q_{ls} curves shown in Figure 6.15, a phenomenon showing the strengthening of q of the SD path relative to the other two paths (PD and PW) is identified. These discoveries are analyzed in the following paragraphs.

The drying/wetting process gradually subjects the volumetric strains of expansive soils to approach an equilibrium elastic stage after a certain number of swell-shrink cycles where macropore collapse that generates irreversible plastic strains progressively decreases (Alonso et al. 1995, Alonso et al. 1999, Romero et al. 1999, Tripathy et al. 2002, Tripathy and Subba Rao 2009, Nowamooz and Masrouri 2008, Romero and Simms 2008). This will eventually result in a dominant soil structure characterized by parallel particle orientation (face to face particle contact) filled mostly with micropores. In other words, the dual-structure of the original sample gradually turns into a single structure of platy clay particles separated by micropores after the

destruction and reorientation of the structural elements of soil aggregate/cluster. Understanding this particular nature of expansive soils, it is not surprising to see the distinct p_{pk}-q_{pk} curve of the PD path of Carnisaw by taking into account the flocculated structure dominated with edge to face particle-to-particle/particle-to-aggregate contacts. The p_{pk}-q_{pk} curves of Carnisaw switch from a shape curving upward to curving downward from the PD to PW path, and the curves representing the SD path remain curved downward (Figure 6.12). Additionally, the corresponding q_{pk} decreases at a given p_{pk}. This is best illustrated in Figure 6.12 from comparing the curves of PD, PW and SD at s equal to 5 MPa. The strength decrease comes from the gradual loss of Coulombian attractive forces at edge to face contacts. In contrary, the laminar structure of Eagle Ford is prone to have almost invariant interparticle forces and therefore renders strength insensitive to capillary paths (Figure 6.13).

Such a coupling of structure and interparticle forces is indirectly demonstrated by Figures 6.14 and 6.15. At large shear strain, the plastic zone of the specimen is completely destructured and thus independent of the original structure. As discussed earlier, the shear strength is at this moment governed by soil dilation from DDL repulsion. An apparent increase in $\delta q_{ls}/\delta p_{ls}$ is noticed on the SD path in Figure 6.15. This specific behavior is likely due to the effect of aging that imparts resistance to compression (Subba Rao and Tripathy 2003). However, why the aging effect is not revealed in the p_{pk}-q_{pk} diagram (Figure 6.13) remains unclear.

6.4 Conclusions and Summary

In this chapter, studies on shear strength and shear-induced volume change of unsaturated Carnisaw and Eagle Ford specimens have been thoroughly conducted. The

approach used in preparation of the unsaturated specimens, which was based on predetermined HSWCCs, has both pros and cons. The main advantages involve the convenience of suction implementation at the range of 1-20 MPa and the avoidance of weaknesses lying in the osmotic and VETs, like biomembrane degradation and rigorous temperature control. In other aspects, there are associated disadvantages considering the long term period spent (4-6 months from the beginning of compaction) and the trouble in achieving multiple specimens of identical suction. Nevertheless, this preparation method seems promising, as the prepared specimens displayed generally consistent suction distribution with the averaged measured suction closely matching the predicted magnitude (from the HSWCCs).

A triaxial test apparatus was set up for the unsaturated test program having air-phase drained and water-phase undrained. Two strain rates were evaluated for their impact on the stress-strain (ε-q) and deformation-strain (ε-δv) relationships. Little difference was found with respect to their influence on the ε-q curves while the lower rate gave rise to greater δv. The higher rate was selected for the rest of the tests by taking into account the less variation of suction before and after shearing and the time expense. Suction measurements using the WP4-T were performed after shear on every one-fifth length of the specimen and the magnitude was averaged, which matched the predicted suction well. The averaged suction and the predicted were averaged again to represent the suction of a specimen. No independent suction control was performed in the confinement and shearing stages.

Conventional CIUC tests were carried out on these two soils. Carnisaw shows a higher strength with a critical-state friction angle φ_c' of 35.7° compared to that of Eagle

Ford (22.6°). The specimens of both soils demonstrated exactly the same style of response of contracting initially, passing through a phase transformation state, and then dilating (increasing in tendency to dilate) with a constant stress ratio. The behaviors can be explored by examining the combined effects of pH, structure, and salt concentration. The interparticle interactions of Carnisaw specimens were initially dominated by strong Coulombian electrostatic attraction but then transformed to intense DDL repulsion due to shear-induced destructuring of the fabric. The Eagle Ford specimens, on the other hand, were first governed by DDL repulsion and van der Waals attraction and then strengthened in the repulsion part that caused dilation in shearing.

The specimen stiffness was investigated in terms of two moduli denoted by $E_{1\%}$ and E_{50}. Both were found to increase as a function of suction, and showed a higher magnitude in the PD path. The effects of mean stress, suction, capillary history and strain level on shear strength were assessed through the studies of the p_{pk}-q_{pk} and p_{ls}-q_{ls} curves with varying suction. The deviator stress q increases with increasing suction, regardless of strain level and capillary history, because of the enhanced surface tension force. In general, the slopes of p-q curves reduce as a function of p and increase with s. The former trend held for the p_{pk}-q_{pk} relationship and was explained by proposing a critical point of soil dilation accompanied by DDL repulsion and particle slipping on surfaces. The trend of the p_{ls}-q_{ls} relationship indicates the equilibration of the dilative effect after large strain failure. For both p_{pk}-q_{pk} and p_{ls}-q_{ls} curves, the strengthened s introduces an enhanced surface tension force and hence restrains the progress of fabric destructuring and specimen dilation in response to shearing. Capillary history shows its maximum impact on the p_{pk}-q_{pk} curves of Carnisaw arising from the significant

structure evolution along the capillary paths. The more homogeneous structure of Eagle Ford renders itself less susceptible to capillary history change in respect to the p_{pk}-q_{pk} curves. The p_{ls}-q_{ls} curves, however, demonstrate little sensitivity to capillary history, regardless of soil type; because of the specimens at this stage are more likely experiencing complete fabric destructuring and equilibrium of DDL repulsion.

Chapter 7: Summary and Conclusions

The primary objectives of this research project include (1) conducting a comprehensive investigation of the carefully selected microscale properties of natural expansive soils; and (2) evaluating the roles of these properties in controlling the macroscopic engineering behavior described as volume change and shear strength. A sequence of experimental works were undertaken to produce results that are insightful for approaching these objectives, associated with specific designs of test equipment and procedure. Inter-disciplinary research endeavors crossing fields of geology, geochemistry, electronics and geomechanics have been explored with the deduced conclusions satisfactorily fulfilling these objectives.

7.1 Summary of Accomplished Tasks

The following tasks have been accomplished in this study:

(1) Testing eleven microscale properties to describe the electro-physico-chemical processes occurring in natural expansive soils and evaluating each property relating to the three key variables (mineralogy, structure and pore fluid) that govern the surface forces in these processes.

(2) Microscopic investigations on soil mineralogy and structure, and the alterations of these two variables caused by CFA stabilization.

(3) Creation of a two-terminal electrode system integrated in conventional oedometer testing. Construction, calibration and verification of the system adapted with two different test setups have been conducted. The electromagnetic properties of the studied samples were obtained at both their compacted and 1D deforming stages.

(4) Quantifying the DDL of the studied soils in terms of surface conductance and thickness. Limitations of the theoretical basis were proposed.

(5) Exploring the SWCCs of the six studied samples and a coupled cyclic water content change-suction variation-volumetric deformation performance of the two untreated samples, Carnisaw and Eagle Ford. The roles of microscale properties in affecting volumetric evolutions were examined.

(6) Establishing an unsaturated triaxial test program based on the predetermined HSWCCs and the chilled mirror hygrometer tests after shear. The macroscopic behavior of soils depicted in this program (also including the additional CIUC tests) was explored from a microscopic point of view.

7.2 Conclusions

Some conclusions can be summarized as follows:

(1) Among the untreated expansive soils, the more plastic sample tends to have higher S_a, CEC, and surface conductance, exhibiting greater swell potential but lower compressive strength. Chemical stabilization by CFA reduces the magnitude of S_a but increases the pH, CEC and surface conductance, accompanied by reduced plasticity, enhanced compressive strength and diminished swell potential.

(2) Montmorillonite is identified as the primary expansive mineral. The effectiveness of montmorillonite expansion, however, is controlled by exchangeable cations, structure and water content. From a structural standpoint, a sample comprised of thin, large clay flakes associated in face to face contact and aligned in a laminar structure tends to have a high swell potential. In reverse, weak swelling can be expected

in the soil with a turbulent structure consisting of relatively thick, narrow clay platelets interacting in an edge to edge or edge to face style.

(3) CFA stabilization decreases the clay size portion in expansive soils not only by chemical flocculation that creates CSH and CAH cementing agents, but also by Fe oxides coating on the surfaces of some flocculated aggregates that sustains deflocculating agents. Meanwhile, the flocculation decreases S_a while the enhanced negative charge accumulation on CSH and CAH gels increases CEC.

(4) The thickness of the DDL is largely influenced by the dc conductivity of the pore fluid phase. The development of the DDL in a soil sample is suppressed by the interaction from adjacent particles as the sample consolidates and intrusion of air when the sample becomes unsaturated. The effectiveness of surface conduction on the interfacial polarization is influenced by the DDL thickness.

(5) The degree of interfacial polarization can be qualitatively predicted by the difference between surface conductivity and bulk fluid conductivity, among which the latter is used in substitution for pore fluid conductivity that is not experimentally determinable at present. Electrical anisotropy, a direct reflector of structural anisotropy, is more significant for the untreated samples with higher S_a; and less profound for the stabilized samples in comparison with their untreated counterparts.

(6) The specifically defined electromagnetic properties (κ'_{inf} and σ_{dc}) increase in magnitude as a function of sample hydration and anisotropy. This introduces an approach in assessing the hydraulic state and structural anisotropy of expansive soils during one-dimensional hydromechanical deformation.

(7) Expansive soil of higher S_a tends to develop a DDL in the intra-aggregate zone that is more resistant to air intrusion and therefore has a greater air-entry value. CFA stabilization shifts the SWCC downward and lowers the air-entry value resulting from enlarged grain sizes and more open particle arrangement.

(8) Under zero/low confining stress, 3D volumetric measurements produce both swelling and shrinkage that overwhelm those from conventional 1D estimations. Sample volume increases with the swell-shrink cycles but tends to stabilize at the end of the second cycle. Apparent hydraulic hysteresis is found along the cycles, with the effect appearing to decrease as result of macropore collapse and stabilization of particle/aggregate realignment. An unusual decrease of global shrinkage in the case of the less plastic sample (Carnisaw) occurs as result of substantial meniscus contraction at strong desiccation that expands the flocculated structure.

(9) In both saturated and unsaturated triaxial tests, the initial Coulombian electrostatic attraction in the structure of Carnisaw is transformed to DDL repulsion in response to shear-induced destructuring of the flocculated structure. The interparticle forces of Eagle Ford are first dominated by DDL repulsion and van der Waals attraction but strengthened in repulsion during shear that renders the specimen dilative. Volumetric dilation occurs at large strains and high suctions, regardless of capillary path.

(10) The stiffness of unsaturated specimens increases as a function of suction and shows a higher magnitude at the PD path. The peak deviator stress q_{pk} increases with p_{pk} with the rate slowing down until a critical point of dilation accompanied by DDL repulsion and particle slipping on surfaces. An increase of suction tends to

postpone the development of mean stress at which this point initiates owing to enhanced surface tension. At certain large strains, the dilative effect stabilizes as the original structure has been completely destroyed along the sheared zone. In respect to the p_{pk}-q_{pk} curves, capillary history substantially impacts Carnisaw inducing radical structural changes, whereas it minimally affects Eagle Ford due to its more homogeneous structure. For the p_{ls}-q_{ls} relationships, capillary history has negligible influence on both soils.

7.3 Recommendations for Future Research

A good understanding of the microscopic characteristics and their connections with macroscopic behavior in the arena of highly plastic soil like expansive soil can be quite challenging. Comprehensive studies aimed towards this goal have been accomplished. Some potential research efforts that would help in explaining some of the questions raised through this study are:

(1) Advancement in visualization of soil structure evolution in varying hydraulic and mechanical processes is needed to provide a solid experimental background. This involves the potential improvement of the ESEM technology that should be able to accommodate an expanded range of test conditions.

(2) Investigations with the aid of dielectric measurements are promising. The electromagnetic properties can be concurrently achieved with macroscopic parameters characteristic of the hydraulic and mechanical behavior (e.g., vertical strain in this study); therefore, they directly describe the intrinsic soil structure and physicochemical mechanisms from a microscopic point of view. Integration of suction control techniques to the designed two-terminal system is under way. Extension of the system to a variety

of mechanical tests (e.g., triaxial test) is desired. Such embedment of dielectric measurement in a conventional test framework should also include other dielectric systems such as TDR and coaxial probe in order to disclose dielectric responses of soils in a wider range of wave frequencies.

(3) Quantifying the DDL thickness will significantly benefit the understanding of clay behavior. The major obstacle lies in how to accurately model the ion and water molecule distribution adjacent to the surfaces of clay particles with varying mineralogy. The effects of particle-particle/adsorbed water-air interactions must also be accounted for. The widely recognized theory of Derjaguin and Landau (1941) and Verwey and Overbeek (1948), often referred to as the DLVO theory, which is an extended form of the Gouy-Chapman theory, needs to be improved.

(4) This study provide experimental database for verification of the current geophysical and mechanical constitutive models. The coupling of both types of modeling has seen some preliminary success in predicting HSWCC (e.g., Anandarajah and Amarasinghe 2012) through the applications of molecular dynamics and discrete element method. It is believed that the future progress of such coupling will bring about revolutionary advances in explanation and prediction of clayey soil behavior in both saturated and unsaturated conditions.

(5) For a triaxial test sample, the increase of suction is accompanied by volumetric shrinkage and an increase of dry density. This coupling proposes a challenge as how to separate the effects of dry density and suction increase on the shear strength. Similar question also arises on the dry density increase in response to the increased confinement. These remaining questions lead to research on quantitative evaluation of

the individual role of either suction or confinement in determining the part of the strength variation that is independent of the change in dry density.

References

Augs, S.S. and Schanz, T. (2005). "Effect of shrinking and swelling on microstructures and fabric of a compacted bentonite-sand mixture." *Proceedings of International Conference on Problematic Soils*, Geoprob 2005, Famagusta, May 25-27, v2, 543-550.

Agus, S.S. and Schanz, T. (2006). "Drying, wetting, and suction characteristic curves of a bentonite-sand mixture." *Unsaturated Soils 2006*, ASCE, Carefree, Arizona, Apr 2-6, 2006, 1405-1414.

Agus, S.S., Schanz, T. and Fredlund, D.G. (2010). "Measurements of suction versus water content for bentonite-sand mixtures." *Can. Geotech. J.*, 47, 583-594.

Alonso, E.E., Gens, A. and Josa, A. (1990). "A constitutive model for partially saturated soils." *Géotechnique*, 40(3), 405-430.

Alonso, E.E., Lloret, A., Gens, A. and Yang, D.Q. (1995). "Experimental behavior of highly expansive double-structure clay." *Unsaturated soils 1995*, 11-16.

Alonso, E.E., Vaunat, J. and Gens, A. (1999). "Modeling the mechanical behavior of expansive clays." *Eng. Geol.*, 54, 173-183.

Alonso, E.E., Romero, E., Hoffmann, C., and García-Escudero, E. (2005). "Expansive bentonite-sand mixtures in cyclic controlled-suction drying and wetting." *Eng. Geol.*, 81, 213-226.

Al-Rawas, A, (1999). "The factors controlling the expansive nature of the soils and rocks of northern Oman." *Eng. Geol.*, 53, 327-350.

Al-Rawas, A.A., and McGown, A. (1999). "Structure of Omani expansive soils." *Can. Geotech. J.*, 36, 272-290.

Amarasinghe, P.M. and Anandarajah, A. (2011). "Influence of fabric variables on clay-water-air capillary meniscus." *Can. Geotech. J.*, 48, 987-995.

Anandarajah, A. and Amarasinghe, P.M. (2012). "Microstructural investigation of soil suction and hysteresis of fine-grained soils." *J. Geotech. Geoenviron. Eng.*, 138(1), 38-46.

Arulanandan, K. (1991). "Dielectric method for the prediction of porosity of saturated soils." *J. Geotech. Eng.*, 117(2), 319-330.

Arulanandan, K. (2003). Soil Structure: In-situ Properties and Behavior. Department of Civil and Environmental Engineering, University of California, Davis, California, 352p.

Arulanandan, K. and Muraleetharan, K.K. (1988). "Level ground soil-liquefaction analysis using in-situ properties." *J. Geotech. Eng. Div.*, ASCE, 114(7), 771-790.

Arulanandan, K. and Smith, S. S. (1973). "Electrical dispersion in relation to soil structure." *J. Soil Mech. Found. Div.*, ASCE, 99 (SM12), 1113-1133.

Arulanandan, K. and Yogachandran, C. (2000). "Dielectric dispersion method for non-destructive characterization of soil composition." *GeoDenver 2000*, ASCE Geo-Institute, ASCE special publication.

Arulmoli, K., Arulanandan, K., and Seed, H.B. (1985). "New method for evaluating liquefaction potential." *J. Geotech. Eng. Div.*, ASCE, 111(1), 85-114.

ASTM (1999) 1999 Annual book of ASTM standards. Volume 04.08, soil and rock (I): D420–D4914, West Conshohocken, Pennsylvania

ASTM. (2011). 2011 Annual Book of ASTM Standards. Volume 04.08 Soil and Rock (I): D420-D5876 and Vol. 4.09 Soil and Rock (II): D5877 – latest. West Conshohocken, Pennsylvania.

Avsar, E., Ulusay, R. and Sonmez, H. (2009). "Assessment of swelling anisotropy of Ankara clay." *Eng. Geol.*, 105, 24-31.

Azam, S., Abduljauwad, S.N., Al-Shayea, N.A. and Al-Amoudi, O.S.B. (1998). "Expansive characteristics of gypsiferous/anhydritic soil formations." *Eng. Geol.*, 51, 89-107.

Baker, J.C., Grabowska-Olszewska, B., Uwins, J.R. (1995). "ESEM study of osmotic swelling of bentonite from Radzionkow (Poland)." *App. Clay Sci.*, 9, 465-469.

Barden, L. and Sides, G.R. (1971). "Sample disturbance in the investigation of clay structure." *Géotechnique*, 21(3), 211-222.

Basma A.A., Al-Homoud, A.S., Husein Malkawi, A.I. and Al-Bashabsheh, M.A. (1996). "Swelling-shrinkage behavior of natural expansive clays." *App. Clay Sci.*, 11, 211-227.

Birle, E., Heyer, D. and Vogt, N. (2008). "Influence of the initial water content and dry density on the soil-water retention curve and the shrinkage behavior of a compacted clay." *Acta Geotechnica*, 3, 191-200.

Bishop, A.W., Alpan, I., Blight, G.E., and Donald, I.B. (1960). "Factors controlling the shear strength of partly saturated cohesive soils." *In proceedings, American Society of Civil Engineers Conference on Shear Strength of Cohesive Soils*, Boulder, 503-532.

Bishop, A.W. and Donald, I.B. (1961). "The experimental study of partly saturated soil in the triaxial apparatus." *Proceedings of the 5th International Conference on Soil Mechanics and Foundation Engineering*, Paris, France, v1, 13-21.

Blatz, J.A. (2000). "Elastic-plastic modeling of unsaturated high plastic clay using results from a new test with controlled suction." Ph.D. thesis, Department of Civil and Geological Engineering, The University of Manitoba, Winnipeg, MB.

Blatz, J.A. and Graham, J. (2000). "A system for controlled suction in triaxial test." *Géotechnique,* 50(4), 465-478.

Blatz, J.A. and Graham, J. (2003). "Elastic-plastic modeling of unsaturated soil using results from a new triaxial test with controlled suction." *Géotechnique,* 53(1), 113-122.

Blatz, J.A., Graham, J. and Chandler, N.A. (2002). "Influence of suction on the strength and stiffness of compacted sand-bentonite." *Can. Geotech. J.*, 39, 1005-1015.

Blatz, J.A., Cui, Y.J. and Oldecop L. (2008). "Vapor equilibrium and osmotic technique for suction control." *Geotech. Geol. Eng.*, 26, 661-673.

Bordi, F., Camitti, C. and Gili, T. (2001). "Reduction of the contribution of electrode polarization effects in the radiowave dielectric measurements of highly conductive biological cell suspensions." *Bioelectrochemistry*, 54, 53-61.

Bosbach, D. and Enders, M. (1998). "Microtopography of high-calcium fly ash particle surfaces." *Adv. Cem. Res.*, 1, 17-23.

Boso, M., Tarantino, A., and Mongiovì, L. (2005). "A direct shear box improved with the osmotic technique." *Proceedings of advanced experimental unsaturated soil mechanics*, Trento, 85-91.

Bredenkamp, S. and Lytton, R.L. (1994). Reduction of Sulfate Swell in Expansive Clay Subgrades in the Dallas District. Texas Transportation Institute, Research Report 1994-5, 124p.

Brooks, R.H. and Corey, A.T. (1964). "Hydraulic properties of porous media." Colorado State University Hydrology Paper, 27(3), 22-27.

Brown, G. and Brindley, G.W. (1980). "X-ray diffraction procedures for clay mineral identification." in Crystal Structures of Clay Minerals and their X-ray Identification. Mineral. Soc. Monogr. 5. Mineralogical Society, London, 305-359.

Brunauer, S., Emmett, P. H., and Teller, E. (1938). "Adsorption of gases in multimolecular layers." *J. Am. Chem. Soc.*, 60, 309-319.

BS 1377 (1990). British Standard Methods of Testing for Soils for Civil Engineering Purposes. British Standards Institution, London.

Buhler, R. and Cerato, A.B. (2007). "Stabilization of Oklahoma expansive soils using lime and class C fly ash." *GeoDenver*: New Peaks in Geotechnics. GSP 162: Problematic Soils and Rocks and In Situ Characterization. Denver, CO, Feb. 18-21, 2007.

Campbell, J.E. (1990). "Dielectric properties and influence of conductivity in soils at one to fifty megahertz." *Soil Sci. Soc. Am. J.*, 54, 332-341.

Cerato, A.B. and Lin, B. (2012). "Dielectric Measurement of Soil-electrolyte Mixtures in a Modified Oedometer Cell Using 400kHz to 20MHz Electromagnetic Waves." *Geotech. Test. J.*, 35(2), 1-9.

Cerato, A.B. and Lutenegger, A.J. (2002). "Determination of surface area of fine-grained soils by the ethylene (EGME) method." *Geotech. Test. J.*, 25(3), 315-321.

Cerato, A.B. and Lutenegger, A.J. (2004). "Determining intrinsic compressibility of fine-grained soils." *J. Geotech. Geoenviron. Eng.* 130(8), 872-877.

Cerato, A.B. and Lutenegger, A.J. (2005). "Activity, relative activity and specific surface area of fine-grained soils." *Proceedings of the 16th International Conference on Soil Mechanics and Foundation Engineering*, Osaka, Japan. Sep. 12-16. v2, 325-328.

Chen, F.H. (1988). Foundations on Expansive Soils. *Elsevier Science Pub. Co.* New York, 463p.

Chen, L.X., Miller, G.A., Kibbey, T.C.G. (2007). "Rapid pseudo-static measurement of hysteretic capillary pressure-saturation relationships in unconsolidated porous media." *Geotech. Test. J.*, 30(6), 1-10.

Choquette, M., Berube, M.A. and Locat, J. (1987). "Mineralogical and microtextural changes associated with lime stabilization of marine clays from eastern Canada." *App. Clay Sci.*, 2, 215-232.

Cokca, E. (2001). "Use of class C fly ash for the stabilization of an expansive soil." *J. .Geotech. Geoenviron. Eng.*, 127(7), 568-573.

Collins, K. (1978). "A scanning electron microscopy study of natural engineering soils." PhD thesis, University of Strathclyde, Glasgow, U.K.

Cui, Y.J. and Delage, P. (1996). "Yielding and plastic behavior of an unsaturated compacted silt." *Géotechnique*, 46(2), 291-312.

Cui, Y.J., Loiseau, C. and Delage, P. (2002). "Microstructure change of a confined swelling soil due to suction controlled hydration." *Unsaturated Soils 2002*, 593-598.

Cui, Y.J., Mantho, A.T., Cui, K. and Audiguier, M. (2006) "Water retention properties and volume change behavior of natural Romainville clay." *Unsaturated soils 2006*, Carefree, Arizona, Apr 2-6, 2006, 873-882.

Cunningham, M.R., Ridley, A.M. and Burland, J.B. (2003). "The mechanical behavior of a reconstituted unsaturated silty clay." *Géotechnique*, 53(2), 183-194.

Delage, P. and Graham, J. (1995). "Understanding the behavior of unsaturated soils requires reliable conceptual model state of the art report." *Proceedings of 1st Int. Conf. on unsaturated soils*, Paris, France, 1223-1256.

Delage, P., Howat, M. and Cui, Y.J. (1998). "The relationship between suction and swelling properties in a heavily compacted unsaturated clay." *Eng. Geol.*, 50(1-2), 31-48.

Derjaguin, B.V. and Landau, L. (1941). "Theory of the stability of strongly charged lyophobic sols and the adhesion of strongly charged particles in solutions of electrolyte." *Acta Physicochimica (URSS)*, 14, 633-662.

Dermatas, D., Chrysochoou, M., Pardali, S. and Grubb, D.G. (2007). "Influence of X-ray diffraction sample preparation on quantitative mineralogy: Implications for chromate waste treatment." *J. Environ. Qual.*, 36, 487-497.

Dif, A.E., Bluemel, W.F. (1991) "Expansive soils under cyclic drying and wetting." *Geotech. Test. J.*, 14(1), 96-102.

Donald, I.B. (1956). "Shear strength measurements in unsaturated non-cohesive soils with negative pore pressures." In *Proceedings, 2nd Australian and New Zealand Conference on Soil Mechanics and Foundation Engineering*, 200-205.

Ebadi, T. and Elektorowicz, M. (1999). "Investigation on the moisture retention characteristics of Lowland expansive soils." In *Proceedings, 9th International Offshore and Polar Engineering Conference*, Brest, France, May 30-Jun 4, 1999, 447-450.

England, B.M. (1991). "The state of the science: scanning electron microscopy." *The Mineralogical Record*, 22, 123-132.

Escario, V. (1980). "Suction controlled penetration and shear tests." *Proc., 4th Int. Conf. on Expansive Soils*, v2, Denver, 781-797.

Escario, V., and Juca, J.F.T. (1989). "Strength and deformation of partly saturated soils." In *Proceedings, 12th International Conference on Soil Mechanics and Foundation Engineering*, Rio de Janeiro, v2, 43-46.

Escario, V., and Saez, J. (1986). "The strength of partly saturated soils." *Géotechnique*, 36(3), 453-456.

Ferber, V., Auriol, J.C. and David, J.P. (2004). "Micro-structure and swelling behavior of compacted clayey soils: a quantitative approach." *Engineering Geology for Infrastructure Planning in Europe*, Springer, Berlin, 275-284.

Ferber, V., Auriol, J.C., Magnan, J.P., Cui, Y.J., Laure, E.De. and Gerente, C. (2006). "A microstructural model for the volume changes of unsaturated clayey soils due to wetting." *Unsaturated soils 2006*, Carefree, Arizona, Apr 2-6, 2006, v1, 861-872.

Fernando, M.J., Burau, R.G., and Arulanandan, K. (1977). "A new approach to determination of cation exchange capacity." *Soil Sci. Soc. of Am. J.*, 41(4), 818-820.

Feuerharmel, C., Pereira, A., Gehling, W.Y.Y. and Bica, A.V.D. (2006). "Determination of the shear strength parameters of two unsaturated colluviums soils using the direct shear test." *Unsaturated soils 2006*, Carefree, Arizona, Apr 2-6, 2006, v1, 1181-1189.

Fityus, S. and Buzzi, O. (2009). "The place of expansive clays in the framework of unsaturated soil mechanics." *App. Clay Sci.*, 43, 150-155.

Fleureau, J.M., Kheirbek-Saoud, S., Soemitro, R. and Taibi, S. (1993). "Behavior of clayey soils on drying-wetting paths." *Can. Geotech. J.*, 30, 287-296.

Fleureau, J.M., Verbrugge, J.C., Huergo, P.J., Correia, A.G. and Kheirbek-Saoud, S. (2002). "Aspects of the behavior of compacted clayey soils on drying and wetting paths." *Can. Geotech. J.*, 39, 1341-1357.

Franzmeier, D.P. and Ross, S.J. (1968). "Soil swelling: laboratory measurement and relation to other soil properties." *Soil Sci. Soc. Am. Proc.* 32, 573-577.

Fredlund, D.G., and Rahardjo, H. (1993). Soil Mechanics for Unsaturated Soils. *John Wiley and Sons*, INC., New York, 517p.

Fredlund, D.G., and Xing, A. (1994). "Equations for the soil water characteristic curve." *Can. Geotech. J.*, 31, 521-532.

Frost, J.D., and McNeil, S. (1998). "Imaging technologies; techniques and applications in civil engineering." *Proceedings of the 2nd International Conference*, ASCE, Reston, VA.

Frost, J.D., and Wright, J.R. (1993). "Digital image processing; techniques and applications in civil engineering." *Proceedings of a Conference*, Kona, Hawaii, Feb 28-Mar 5, 1993, ASCE, New York. 312p.

Futai, M.M., Almeida, M.S.S. and Lacerda, W.A. (2006). "The shear strength of unsaturated tropical soils in Ouro Preto, Brazil." *Unsaturated soils 2006*, Carefree, Arizona, Apr 2-6, 2006, 1200-1211.

Gallage, C.P.K., and Uchimura, T. (2006). "Effects of wetting and drying on the unsaturated shear strength of a silty sand under low suction." *Unsaturated soils 2006*, Carefree, Arizona, Apr 2-6, 2006, 1247-1258.

Gan, J.K.M. (1986). "Direct shear strength testing of unsaturated soils." M.Sc. thesis, University of Saskatchewan, Kaskatoon.

*Géotechnique*Gan, J.K.M., and Fredlund, D.G. (1988). "Multistage direct shear testing of unsaturated soils." *Geotech. Test. J.*, 11(2), 132-138.

Garbulewski, K. and Zakowicz, S. (1995). "Suction as an indicator of soil expansive potential." *Proceedings of the 1st International Conference on Unsaturated Soils*, Paris, 2, 505-512.

Georgetti, G.B., and Vilar, O.M. (2010). "Constant water content triaxial compression tests with a compacted soil." *Unsaturated soils 2010*, Barcelona, Spain, Sep. 6-8, 247-252.

Gibbs, H.J., Hilf, J.W., Holtz, W.G., and Walker, F.C. (1960). "Shear strength of saturated soils." *In Proceedings, American Society of Civil Engineers Conference on Shear Strength of Cohesive Soils*, Boulder, Colorado, 33-162.

Glasser, F.P. (2004). "Coal combustion wastes: characterization, reuse and disposal." *Energy, Waste, and the Environment: a Geochemical Perspective*. Geological Society, London, Special Publications, 236, 211-222.

Grabowska-Olszewska, B. (1988). "Physical properties of clay soils as a function of their specific surface." *Proceedings of the 1st International Congress of the International Association of Engineering Geology: Engineering Problems of Regional Soils*, 405-410.

Gulhati, S.K. and Satija, B.S. (1981). "Shear strength of partially saturated soils." *Proceedings of the 10th Conference on Soil Mechanics and Foundation Engineering*, Stockholm, Jun 15-19, v1, 609-612.

Gutiérrez, A. (2006). "Determination of Atterberg limits: uncertainty and implications." J. *Geotech. Geoenviron. Eng.*, 132(3), 420-424.

Hallberg, G.R. (1977). "The use of COLE values for soil engineering evaluation." *Soil Sci. Soc. Am. J.*, 41, 775-777.

Hammitt, G.M. II (1966). "Statistical analysis of data from a comparative laboratory test program." Sponsored by ACIL. Miscellaneous Paper No. 4-785, U.S. Army Engineer Waterways Experiment Station, Vicksburg, MS.

Han, K.K., Rahardjo, H., and Broms, B.B. (1995) "Effect of hysteresis on the shear strength of a residual soil." *Proceedings of the first international conference on unsaturated soils*, Paris, 2, 499-504.

Hillel, D. (1998). Environmental Soil Physics. *Academic Press*, London, 771p.

Hillier, S. (2003). "Quantitative analysis of clay and other minerals in sandstones by X-ray powder diffraction (XRPD)." *Int. Assoc. Sedimentol. Spec. Publ.*, 34, 213-251.

Ho, D.Y.F., and Fredlund, D.G. (1982). "Multistage triaxial tests for unsaturated soils." *Geotech. Test. J.*, 5, 18-25.

Holtz, W.G. and Gibbs, H.J. (1956). "Engineering properties of expansive clays." *Transact.*, ASCE, 121, 641-677.

Hong, S.Y. and Glasser, F.P. (2002). "Alkali sorption by C-S-H and C-A-S-H gels: Part II. Role of alumina." *Cement Concrete Res.*, 32, 1101-1111.

Houston, S.L., Perez-Garcia, N. and Houston, W.N. (2008). "Shear strength and shear-induced volume change behavior of unsaturated soils from a trixial test program." *J. Geotech. Geoenviron. Eng.*, 134, 1619-1632.

Ito, M., and Azam, S. (2010). "Determination of swelling and shrinkage properties of undisturbed expansive soils." *Can. Geotech. J.*, 28, 413-422.

Johnston, M.M. and Strohm, W.E., Jr. (1968). Results of Second Division Laboratory Testing Program on Standard Soil Samples. Miscellaneous paper No. 3-978, U.S. Army Engineer Waterways Experiment Station, Vicksburg, MS.

Juang, C., and Holtz, R. (1986). "A probabilistic permeability model and the pore size density function." *Int. J. Numer. Anal. Met.*, 10(5), 543-553.

Katti, D.R. and Shanmugasundaram, V. (2001). "Influence of swelling on the structure of expansive soils." *Can. Geotech. J.*, 38, 175-182.

Khoury, C. (2010). "Influence of hydraulic hysteresis on the mechanical behavior of unsaturated soils and interfaces." Ph.D. thesis, University of Oklahoma, 295p.

Khoury, N., and Khoury, C. (2005). "New laboratory methods for characterization of compaction in fine-grained soils." Internal report (revised in 2008). School of Civil Engineering and Environmental Science, the University of Oklahoma.

Klein, K. (2004). "Permittivity measurements of high conductivity specimens using an open-ended coaxial probe – measurement limitations." *J. Environ. Eng. Geoph.*, 9(4), 191-200.

Klein, K. and Santamarina, J.C. (1996). "Polarization and Conduction of Clay-Water-Electrolyte Systems - Discussion by K.Klein and J.C. Santamarina." *J. Geotech. Eng.*, Nov, 954-955.

Klein, K. and Santamarina, J. C. (1997). "Methods for broad band dielectric permittivity measurements (soil-water mixtures, 5Hz to 1.3GHz)." *Geotech. Test. J.*, 20(2), 168-178.

Klein, K. and Santamarina, J. C. (2003). "Electrical conductivity in soils: underlying phenomena." *J. Environ. Eng. Geoph.*, 8(4), 263-273.

Koester, J.P. (1992). "The influence of test procedure on correlation of Atterberg Limits with liquefaction in fine-grained soils." *Geotech. Test. J.*, 15(4), 352-361.

Koliji, A., Vulliet, L., and Laloui, L. (2010). "Structural characterization of unsaturated aggregated soil." *Can. Geotech. J.*, 47, 297-311.

Komine, H. and Ogata, N. (1999). "Experimental study on swelling characteristics of sand-bentonite mixture for nuclear waste disposal." *Soils Found.*, 39(2), 83-97.

Komine, H. and Ogata, N. (2004). "Predicting swelling characteristics of bentonites." *J.Geotech. Geoenviron. Eng.*, 130(8), 818-829.

Konyai, S., Sriboonlue, V., Trelo-ges, V. and Muangson, N. (2006). "Hysteresis of water retention curve of saline soil." *Unsaturated Soils 2006*, ASCE, Carefree, Arizona, Apr 2-6, 2006, 1394-1404.

Laird, D.A. (2006). "Influence of layer charge on swelling of smectites." *App. Clay. Sci.*, 34, 74-87.

Langroudi, A.A. and Yasrobi, S.S. (2009). "A micro-mechanical approach to swelling behavior of unsaturated expansive clays under controlled drainage conditions." *App. Clay Sci.*, 45, 8-19.

Last, W.M. (2001). "Mineralogical Analysis of Lake Sediments in W. M. Last & J. P. Smol (eds.), 2001." Tracking Environmental Change Using Lake Sediments. Volume 2: Physical and Geochemical Methods. Kluwer Academic Publishers, Dordrecht, The Netherlands.

Lawrence, C.A. (2004). "Development of a closed-loop, hydraulically actuated testing system and methodologies for unsaturated soils." Ph.D. Dissertation, Arizona State University, Arizona, USA, May 2004.

Ledbetter, R.H. and Krinitzsky, E.L. (1982). Earthquake Resistance of Damsite 1, Reelfoot-Indian Creek Watershed, Obion County, Tennessee. Report to U.S. Department of Agriculture, Soil Conservation Service.

Leong, E.C., Tripathy, S. and Rahardjo, H. (2003). "Total suction measurement of unsaturated soils with a device using the chilled-mirror dew-point technique." *Géotechnique*, 53(2), 173-182.

Leong, E.C., Agus, S.S. and Rahardjo, H. (2004). "Volume change measurement of soil specimen in triaxial test." *Geotech. Test. J.*, 27(1), 47-56.

Li, X., and Zhang, L.M. (2009). "Characterization of dual-structure pore-size distribution of soil." *Can. Geotech. J.*, 46, 129-141.

Likos, W. and Lu, N. (2002). "Water vapor sorption behavior of smectite-kaolinite mixtures." *Clay. Clay Miner.*, 50(5), 553-561.

Likos, W. and Lu, N. (2006). "Pore-scale analysis of bulk volume change from crystalline interlayer swelling in Na^{+}- and Ca^{2+}- smectite." *Clay. Clay Miner.*, 54(4), 515-528.

Lin, C.P. (2003a). "Analysis of nonuniform and dispersive time domain reflectometry measurement systems with application to the dielectric spectroscopy of soil." *Water Resour. Res.*, 39(1), 1012, doi:10.1029/2002WR001418.

Lin, C.P. (2003b). "Frequency domain versus travel time analyses of TDR waveforms for soil moisture measurements." *Soil. Sci. Soc. Am. J.*, 67(3), 720-729.

Lin, B., and Cerato, A.B. (2012a). "Prediction of expansive soil swelling based on four micro-scale properties." *B Eng. Geol. Environ.*, 71, 71-78.

Lin, B., and Cerato, A.B. (2012b). "Investigation on soil water characteristic curves of untreated and stabilized highly clayey expansive soils." *Geotech. Geol. Eng.*, 30(4), 803-812.

Lin, D.F., Lin, K.L., Hung, M.J. and Luo, H.L. (2007). "Sludge ash/hydrated lime on the geotechnical properties of soft soil." *J. Hazard. Mater.*, 145, 58-64.

Liu, N. (2007). "Soil and site characterization using electromagnetic waves." Ph.D. thesis, Virginia polytechnic institute and state university, Blacksburg, Virginia, 255p.

Liu, N. and Mitchell, J.K. (2009a). "Modeling electromagnetic properties of saturated sand and clay." *Geomechanics and Geoengineering*, 4(4), 253-269.

Liu, N. and Mitchell, J.K. (2009b). "Effects of structural and compositional factors on soil electromagnetic properties." *Geomechanics and Geoengineering*, 4(4), 271-285.

Liu, Z.B., Shi, B., Inyang, H.I. and Cai, Y. (2005). "Magnification effects on the interpretation of SEM images of expansive soils." *Eng. Geol.*, 78, 89-94.

Lyklema, J. (1995). Fundamentals of interface and colloid science volume II: Solid-liquid interfaces, Academic press, New York.

Lytton, R.L. (1994). "Prediction of movement in expansive clays." Vertical and Horizontal Deformations of Foundations and Embankments, A.T. Yeung and G.Y. Felio, eds, ASCE, New York, 1827-1845.

Lytton, R.L. (1995). "Foundations and pavements on unsaturated soils." *Proceedings of the 1st International Conference on Unsaturated Soils*, International Society of Soil Mechanics and Foundation Engineering, Paris, v3, 1201-1210.

Lytton, R.L. (1997). "Engineering structures in expansive soils." Solos Nao Saturados, Rio de Janeiro, Brazil.

Maison, T., Laouafa, F. and Fleureau, J.M. (2010). "Volume change of swelling clayey soils at microscopic scale level." *Unsaturated soils 2010*, Barcelona, Spain, Sep 6-8, 525-530.

Man, A. and Graham, J. (2010). "Pore fluid chemistry, stress-strain behavior, and yielding in reconstituted highly plastic clay." *Eng. Geol.*, 116, 296-310.

Martinez-Nistal, A., Veniale, F., Setti, M. & Cotecchia, F. (1999) "A scanning electron microscopy image processing method for quantifying fabric orientation of clay geomaterials." *App. Clay Sci.*, 14, 235-243.

McBride, M.B. (1994) Environmental Chemistry of Soils. Oxford University Press, 406p.

McKeen, R.G. (1992) "A model for predicting expansive soil behavior." *Proceedings of the 7th International Conference on Expansive Soils*, Dallas, 1, 1-6.

McManus, D. A. (1991). "Suggestions for auth-ors whose manuscripts include quantitative clay mineral analysis by X-ray diffraction." *Mar. Geol.*, 98, 1-5.

Meegoda, N.J., King, I.P., and Arulanandan, K. (1989). "An expression for the permeability of anisotropic granular media." *Int. J. Numer. Anal. Methods Geomech.*, 13(6), 575-598.

Miller, C.J., Yesiller, N., Yaldo, K. and Merayyan, S. (2002). "Impact of soil type and compaction conditions on soil water characteristic." *J. Geotech. Geoenviron. Eng.*, 128(9), 733-742.

Miller, G.A., Khoury, C.N., Muraleetharan, K.K., Liu,C., and Kibbey, T.C.G. (2008). "Effects of solid deformations on hysteretic soil water characteristic curves: experiments and simulations." *Water Resour. Res.*, 44, doi:10.1029/2007WR006492.

Mitchell, J.K. and Soga, K. (2005). Fundamentals of Soil Behavior. 3rd Edition. *John Wiley and Sons*, Inc. New Jersey. 577p.

Mojid, M.A. and Cho, H. (2006). "Estimating the fully developed diffuse double layer thickness from the bulk electrical conductivity in clay." *App. Clay. Sci.*, 33, 278-286.

Monte-H, G., Duplay, J., Martinez, L., Mendoza, C. (2003a). "Swelling-shrinkage kinetics of MX80 bentonite." *App. Clay. Sci.*, 22, 279-293.

Montes-H, G., Duplay, J., Martinez, L., Geraud, Y. and Rousset-Tournier, B. (2003b). "Influence of interlayer cations on the water sorption and swelling-shrinkage of MX80 bentontie." *App. Clay Sci.*, 23, 309-921.

Monte-H, G., Duplay, J., Martinez, L., Escoffier, S., Rousset, D. (2004). "Structural modification of Callovo-Oxfordian argillite under hydration/dehydration conditions." *App. Clay Sci.*, 25, 187-194.

Moore, D.M., and Reynolds., R.C. (1997). X-Ray Diffraction and the Identification and Analysis of Clay Minerals, 2nd ed., *Oxford University Press*, New York. 400p.

Munns, R. (2004). "Salinity stress and its impact." *Plant Stress Website. Blum A.(ed).* http://www.plantstress.com/Articles/index.asp

Muraleetharan, K.K., Liu,C., Wei, C., Kibbey, T.C.G., and Chen, L. (2009). "An elasto-plastic framework for coupling hydraulic and mechanical behavior of unsaturated soils." *Int. J. Plasticity*, 25, 473-490.

Nalbantoglu, Z. and Tuncer, E.R. (2001). "Compressibility and hydraulic conductivity of a chemically treated expansive clay." *Can. Geotech. J.*, 38, 154-160.

Nelson, J.D., and Miller, D.J. (1992). Expansive Soils: Problems and Practice in Foundation and Pavement Engineering. *John Wiley and Sons*, New York, 253p.

Ng, C.W.W., Zhan, L.T. and Cui, Y.J. (2002). "A new simple system for measuring volume changes in unsaturated soils." *Can. Geotech. J.*, 39, 757-764.

Nowamooz, H. and Masrouri, F. (2008). "Hydromechanical behavior of an expansive bentonite/silt mixture in cyclic suction-controlled drying and wetting tests." *Eng. Geol.*, 101, 154-164.

Nowamooz, H. and Masrouri, F. (2009). "Density-dependent hydromechanical behavior of a compacted expansive soil: experimental and analytical aspects." *Eng. Geol.*, 106, 105-115.

OHD L-49 (2005). "Method of test for determining soluble sulfate content in soil." Oklahoma Department of Transportation, Oklahoma.

Oh, W.T., Garga, V.K. and Vanapalli, S.K. (2008). "Shear strength characteristics of statically compacted unsaturated kaolin." *Can. Geotech. J.*, 45, 910-922.

Oloo, S.Y., and Fredlund, D.G. (1996). "A method for determination of f^b for statically compacted soils." *Can. Geotech. J.*, 33, 272-280.

Omotoso, O. (2006). "Some successful approaches to quantitative mineral analysis as revealed by the 3rd Reynolds Cup contest." *Clay Clay Miner.*, 54(6), 748-760.

Padilla, J.M., Houston, W.N., Lawrence, C.A., Fredlund, D.G., Houston, S.L., and Perez, N.P. (2006). "An automated triaxial testing device for unsaturated soils." *Unsaturated Soils 2006*, Carefree, Arizona, 2006, v2, 1775-1786.

Pansu, M. and Gautheyrou, J. (2006). Chapter 18: "Soluble Salts", Handbook of Soil Analysis-Mineralogical, Organic and Inorganic Methods, *Springer*, 1012p.

Parkhomenko, E.I. (1967). Electrical properties of rocks, *Plenum Press*, New York, 314p.

Pereira, A., Feuerharmel, C., Gehling, W.Y.Y. and Bica, A.V.D. (2006). "A study on the shear strength envelope of an unsaturated colluviums soil." *Unsaturated soils 2006*, Carefree, Arizona, 2006, v1, 1191-1199.

Peterson, R.W. (1988). "Interpretation of triaxial compression test results on partially saturated soils." *Advanced Triaxial Testing of Soil and Rock,* American Society for Testing and Materials, Special Technical Publication, 977, 512-538.

Peterson, L.W., Moldrup, P., Jacobsen, O.H. and Rolston, D.E. (1996). "Relations between specific surface area and soil physical and chemical properties." *Soil Sci*., 161(1), 9-21.

Phani Kumar, B.R. and Sharma R.S. (2004). "Effect of fly ash on engineering properties of expansive soils." *J. Geotech. Geoenviron. Eng.*, 130, 764-767.

Poppe, L.J., Paskevich, V.F., Hathaway, J.C. and Blackwood, D.S. (2001). "A Laboratory Manual for X-Ray Powder Diffraction." *USGS Open-File report 01-041.* http://pubs.usgs. gov/of/2001/of01-041/htmldocs/intro.htm

Puppala, A.J., Kadam, R., Madhyannapu, R., Hoyos, L.(2006a). "Small strain shear moduli of chemically stabilized sulfate bearing cohesive soils." *J Geotech. Geoenviron. Eng.*, 132(3), 322-336.

Puppala, A.J., Punthutaecha, K., and Vanapalli, S.K. (2006b). "Soil water characteristic curves of stabilized expansive soils." *J. Geotech. Geoenviron. Eng.*, 132(6), 736-750.

Raman, V. (1967) "Identification of expansive soils from the plasticity index and the shrinkage index data." *Indian Eng. Calcutta.*, 11(1):17–22.

Raythatha, R. and Sen, P.N. (1986). "Dielectric properties of clay suspensions in MHz to GHz range." J. Colloid Interf. Sci., 109(2), 301-309.

Rhoades, J.D. (1982) "Cation exchange capacity." In: Page AL et al (eds) Methods of soil analysis, agronomy 9, 2nd edn. American Society of Agronomy, Madison, 159–165.

Richards, B.G., Peter, P. and Martin, R. (1984). "The determination of volume change properties in expansive soils." *Proceedings of the 5th International Conference on Expansive Soils*. Adelaide, Australia, 179-186.

Rinaldi, V.A. and Francisca, F.M. (1999). "Impedance analysis of soil dielectric dispersion (1MHz-1GHz)." *J. of Geotech. Geoenviron. Eng.*, 125(2), 111-121.

Romero, E., Gens, A. and Lloret, A. (1999). "Water permeability, water retention and structure of unsaturated compacted Boom clay." *Eng. Geol.*, 54, 117-127.

Romero, E. and Simms, P.H. (2008). "Microstructural investigation in unsaturated soils: a review with special attention to contribution of mercury intrusion porosimetry and environmental scanning electron microscopy." *Geotech. Geol. Eng.*, 26, 705-727.

Ross, G.J. (1978). "Relationships of specific surface area and clay content to shrink-swell potential of soils having different clay mineralogic compositions." *Can. J. Soil Sci.*, 58, 159-166.

Santamarina, J. C., Klein, K. and Fam, M. (2001). Soils and Waves: Particle Materials Behavior, Characterization and Process Monitoring. *John Wiley and Sons*, Chichester, UK, 488p.

Satija, B.S. (1978). "Shear behavior of partly saturated soils." Ph.D. thesis, Indian Institute of Technology, New Delhi.

Schofield, R.K. (1947). "Calculation of surface areas from measurements of negative adsorption." *Nature* (London), 160, 408-410.

Seed, H.B., Woodward, R.J. and Lundgren, R. (1962). "Prediction of swelling potential for compacted clays." *J. Soil Mech. Found. Div.*, Am. Soc. Civil Eng. 88(SM3):53-87.

Selig, E.T. and Mansukhani, S. (1975). "Relationship of soil moisture to the dielectric property." *Geotech. Eng. Div. Eng. Div.*, Am. Soc. Civil Eng. Proc. 101 (GT8), 755.

Shang, J.Q., Rowe, R.K., Umana, J.A., and Scholte, J.W. (1999). "A complex permittivity measurement system for undisturbed compacted soil." *Geotech. Test. J.*, 22(2), 165-174.

Shi, B. and Jiang, H. (2002). "Engineering geological characteristics of expansive soils in China." *Eng. Geol.*, 67, 63-71.

Shi, B. and Li, S. (1995). "Quantitative approach on SEM images of structure of clay soils." *Sci. China Ser. B-Chem.*, 38(6), 741-748.

Shi, B., Liu, Z., Cai, Y. and Zhang, X. (2007). "Micropore structure of aggregates in treated soils." *J. Mater. Civil Eng.*, 19(1), 99-104.

Shi, B., Murakami, Y., and Wu, Z.S. (1998). "Orientation of aggregates of fine-grained soil: quantification and application." *Eng. Geol.*, 50(1-2), 59-70.

Silva, J.A., and Uchida, R. (2000). Plant Nutrient Management in Hawaii's Soils, Approaches for Tropical and Subtropical Agriculture, University of Hawaii at Manoa, 158p.

Simmes, P.H., and Yanful, E.K. (2002). "Predicting soil-water characteristic curves of compacted plastic soils from measured pore-size distributions." *Géotechnique*, 52(4), 269-278.

Simms, P.H., and Yanful, E.K. (2005). "A pore-network model for hydromechanical coupling in unsaturated compacted clayey soils." *Can. Geotech. J.*, 42, 499-514.

Smart, P. (1967). "Particle arrangements in kaolin." *Proceedings of the 15th national conference on clays and clay mineral*, v15, 241-254.

Smart, P. and Leng, X. (1993). "Present developments in image analysis." *Scanning Microscopy*, 7(1), 5-16.

Smart, P. and Tovey, N.K. (1982). "Electron microscopy of soils and sediments: technique." *Clarendon Press*, Oxford, 264p.

Smith, C.W., Hadas, A., Dan, J., and Koyumdjisky, H. (1985). "Shrinkage and Atterberg limits relation to other properties of principle soil types in Israel." *Geoderma*, 35, 47-65.

Snyder, R.L. and Bish, D.L. (1989). "Quantitative Analysis in Modern Powder Diffraction." *Reviews in Mineralogy*, v20, Bish and Post (eds.).

Srodon, J., Drits, V.A., McCarty, D.K., Hsieh, J.C.C. and Eberl, D.D. (2001). "Quantitative X-ray diffraction analysis of clay-bearing rocks from random preparations." *Clay. Clay Miner.*, 49(6), 514-528.

Subba Rao, K.S. and Tripathy, S. (2003). "Effect of aging on swelling and swell-shrink behavior of a compacted expansive soil." *Geotech. Test. J.*, 26(1), DOI: 10.1520/GTJ11100J

Suryanarayana, C. and Norton, M.G. (1998). X-rays and Diffraction in X-ray Diffraction: A Practical Approach, *Plenum Press*, New York.

Tang, G.X. and Graham, J. (2002). "A possible elastic-plastic framework for unsaturated soils with high-plasticity." 39, 894-907.

Tang, G.X., Graham, J., Blatz, J., Gray, Malcolm., and Rajapakse, R.K.N.D. (2002). "Suctions, stresses and strengths in unsaturated sand-bentonite." *Eng. Geol.*, 64, 147-156.

Thakur, V.K.S., Sreedeep, S. and Singh, D.N. (2005). "Parameters affecting soil-water characteristic curves of fine-grained soils." *J. Geotech. Geoenviron. Eng.*, 131(4), 521-524.

Thakur, V.K.S., Sreedeep, S. and Singh, D.N. (2006). "Laboratory investigations on extremely high suction measurements for fine-grained soils." *Geotech. Geol. Eng.*, 24, 565-578.

Thevanayagam, S. (1993). "Electrical response of two-phase soil: theory and applications," *J. Geotech. Eng.*, 119(8), 1250–1275.

Thu, T.M., Rahardjo, H., and Leong, E.C. (2006). "Effects of hysteresis on shear strength envelopes from constant water content and consolidated drained triaxial tests." *Unsaturated soils 2006*, Carefree, Arizona, Apr 2-6, 2006, 1212-1222.

Tinjum, J. (1995). "Soil water characteristic curves for compacted fine-grained soils." MS thesis, Department of Civil and Environmental Engineering, University of Wisconsin-Madison, Madison, Wisconsin.

Tinjum, J.M., Benson, C.H. and Blotz, L.R. (1997). "Soil-water characteristic curves for compacted clays." *J. Geotech. Geoenviron. Eng.*, 123(11), 1060-1069.

Tishmack, J.K., and Burns, P.E. (2004). "The chemistry and mineralogy of coal and coal combustion products." *Energy, Waste, and the Environment: a Geochemical Perspective*, Geological Society, London, Special Publications, 236, 223-246.

Toll, D.G. (1990). "A framework for unsaturated soil behavior." *Géotechnique*, 40(1), 31-44.

Tovey, N.K. (1970). "Electron microscopy of clays." Ph.D. thesis, Cambridge University, Cambridge, U.K.

Tovey, N.K. and Hounslow, M.W. (1995). "Quantitative microporosity and orientation analysis in soils and sediments." *J. Geol. Soc. London*, 152, 119-129.

Tripathy, S., Bag, R. and Thomas, H.R. (2010). "Desorption and consolidation behavior of initially saturated clays." *Unsaturated soils 2010*, Barcelona, Spain, Sep. 6-8, 381-386.

Tripathy, S. and Subba Rao, K.S. (2009). "Cyclic swell-shrink behavior of a compacted expansive soil." *Geotech. Geol. Eng.*, 27, 89-103.

Tripathy, S., Subba Rao, K.S.S. and Fredlund, D.G. (2002). "Water content-void ratio swell-shrink paths of compacted expansive soils." *Can. Geotech. J.*, 39, 938-959.

USGS Open-File Report 01-041 (2001). A laboratory manual for X-ray powder diffraction. http://pubs.usgs.gov/of/2001/of01-41/

van der merwe, D.H. (1964). "The prediction of heave from the plasticity index and the percentage clay fraction of soils." *Civil Eng. South Africa*, 6,103-107.

van Genutchen, M.T. (1980). "A closed form equation for predicting the hydraulic conductivity of unsaturated soils." *Soil Sci. Soc. Am. J.*, 44, 892-898.

Vanapalli, S.K., Fredlund, D.G. and Pufahl, D.E. (1999). "The influence of soil structure and stress history on the soil-water characteristics of a compacted till." *Géotechnique*, 49(2), 143-159.

Vanapalli, S.K., Fredlund, D.G., Pufahl, D.E. and Clifton, A.W. (1996). "Model for the prediction of shear strength with respect to soil suction." *Can. Geotech. J.*, 33, 379-392.

Varghese, S. (1996). Use of Electrical Measurements to Determine Soil Properties and Identify the Presence of Contaminants in Soils. A project report for the *School of Civil Eng. and Environ. Sci.*, the University of Oklahoma, 48p.

Verwey, E.J.W. and Overbeek, J. Th.G. (1948). Theory of the Stability of Lyophobic Colloids. Elsevier, Amsterdam.

Vinayagam, T. (2004). "Understanding the stress strain behavior of unsaturated Minco silt using laboratory testing and constitutive modeling." Master thesis, University of Oklahoma, 132p.

Viola, R., Tuller, M., Or, D. and Drasdis, J. (2005). "Structure of clay-sand mixtures at different hydration states." *Proceedings of International Symposium on Advanced Experimental Unsaturated Soil Mechanics*, Trento, Italy, June 27-29, 437-442.

Wan, A.W.-L., Gray, M.N., and Graham, J. (1995). "On the relations of suction, moisture content, and soil structure in compacted clays." *Proc. of 1st Int. Conf. on Unsat. Soils*, Paris, France. Balkema, Rotterdam, 215-222.

Wang, X. and Benson, C. (2004). "Leak-Free Pressure Plate Extractor for Measuring the Soil Water Characteristic Curve." *Geotech. Test. J.*, 27(2), 1-10.

Wang, Y.H. and Sui, W.K. (2006a). "Structure characteristics and mechanical properties of kaolinite soils. I. Surface charge and structural characterization." *Can. Geotech. J.*, 43, 587-600.

Wang, Y.H. and Sui, W.K. (2006b). "Structure characteristics and mechanical properties of kaolinite soils. II. Effects of structure on mechanical properties." *Can. Geotech. J.*, 43, 601-617.

Webb, A. and Orr, C. (1997). "Analytical methods in fine particle technology." Micromeritics Instr. Corp., Norcross, GA, USA.

Wheeler, S.J. and Sivakumar, V. (1995). "An elasto-plastic critical state framework for unsaturated soil." *Géotechnique*, 45(1), 35-53.

Wiebe, B., Graham, J., Tang, G.X. and Dixon D. (1997). "Influence of pressure, saturation, and temperature on the behavior of unsaturated sand-bentonite." *Can. Geotech. J.*, 35, 194-205.

Wilson, M.J. (1987). "X-ray powder diffraction methods." in A Handbook of Determinative Methods in Clay Mineralogy. Wilson MJ (ed.), Chapman and Hall, NY.

Yong, R.N. (1999). "Soil suction and soil-water potentials in swelling clays in engineered clay barriers." *Eng. Geol.*, 54, 3-13.

Zevenbergen, C., Bradley, J.P., Piet van Reeuwijk, L., Shyam, A.K., Hjelmar, O., and Comans. R.N.J. (1999). "Clay formation and metal fixation during weathering of coal fly ash." *Environ. Sci. Tech.*, 33, 3405-3409.

Zhang, G., Germaine, J.T., Whittle, A.J. and Ladd, C.C. (2004). "Soil structure of a highly weathered old alluvium." *Géotechnique*, 54(7), 453-466.

Zhan, T.L.T., and Ng, C.W.W. (2006). "Shear strength characteristics of an unsaturated expansive clay." *Can. Geotech. J.*, 43, 751-763.

Appendix A

The fitted parameters k_i, m_i and n_i for the calibration factors α and β are listed in Table A.1 and Table A.2 given below. The calibration was performed on several pairs of electrodes with size and spacing varying at each of the 43 testing frequencies. De-ionized water (κ' = 80 at 25°C) was chosen as the standard liquid for determining the calibration factor α. Potassium chloride (KCl) solution with a dc conductivity of 1413 μS/cm (at 25°C) was selected in achieving the calibration factor β. A detailed presentation of the procedure can be referred to Cerato and Lin (2012).

Table A.1 Fitted parameters k_1, m_1 and n_1 with change of frequency

Frequency	k_1	m_1	n_1	R^2	Frequency	k_1	m_1	n_1	R^2
400 kHz	1.00	0.63	0.93	0.94	**8 MHz**	0.96	0.61	0.86	0.93
455 kHz	1.00	0.63	0.93	0.94	**9 MHz**	0.96	0.61	0.86	0.94
500 kHz	1.00	0.63	0.94	0.94	**10 MHz**	0.96	0.61	0.87	0.94
600 kHz	1.00	0.63	0.93	0.94	**12 MHz**	0.96	0.60	0.88	0.94
700 kHz	1.00	0.63	0.92	0.93	**14 MHz**	0.96	0.60	0.88	0.94
800 kHz	1.00	0.64	0.92	0.94	**16 MHz**	0.96	0.59	0.89	0.94
900 kHz	1.00	0.63	0.93	0.94	**18 MHz**	0.96	0.59	0.90	0.94
1 MHz	1.00	0.63	0.93	0.94	**20 MHz**	0.96	0.58	0.91	0.95
1.2 MHz	1.00	0.63	0.93	0.93	**23.33 MHz**	0.96	0.58	0.91	0.97
1.4 MHz	1.00	0.63	0.93	0.94	**26.66 MHz**	0.96	0.59	0.92	0.97
1.6 MHz	1.00	0.62	0.94	0.94	**30 MHz**	0.95	0.57	0.95	0.97
1.8 MHz	1.00	0.62	0.94	0.94	**35 MHz**	0.90	0.55	1.00	0.97
2 MHz	1.00	0.62	0.94	0.94	**40 MHz**	0.90	0.45	1.16	0.95
2.333 MHz	0.96	0.61	0.87	0.94	**45 MHz**	0.60	0.63	0.89	0.96
2.666 MHz	0.96	0.61	0.87	0.94	**50 MHz**	0.60	0.63	0.91	0.96
3 MHz	0.96	0.61	0.87	0.94	**60 MHz**	0.60	0.50	1.08	0.95
3.5 MHz	0.96	0.61	0.87	0.94	**70 MHz**	0.40	0.58	1.04	0.93
4 MHz	0.96	0.61	0.87	0.93	**80 MHz**	0.20	0.67	0.98	0.92
4.5 MHz	0.96	0.61	0.86	0.93	**90 MHz**	0.20	0.61	1.04	0.94
5 MHz	0.96	0.61	0.86	0.93	**100 MHz**	0.00	0.74	0.99	0.94
6 MHz	0.96	0.61	0.86	0.94	**110 MHz**	0.00	0.71	1.02	0.92
7 MHz	0.96	0.61	0.86	0.94					

Table A.2 Fitted parameters k_2, m_2 and n_2 with change of frequency

Frequency	k_2	m_2	n_2	R^2	Frequency	k_2	m_2	n_2	R^2
400 kHz	1.00	0.37	0.78	0.95	**8 MHz**	1.01	0.38	0.79	0.95
455 kHz	1.00	0.37	0.77	0.95	**9 MHz**	1.01	0.38	0.79	0.95
500 kHz	1.00	0.37	0.77	0.95	**10 MHz**	1.01	0.37	0.80	0.95
600 kHz	1.00	0.37	0.77	0.95	**12 MHz**	1.01	0.37	0.81	0.94
700 kHz	1.00	0.37	0.78	0.95	**14 MHz**	1.01	0.37	0.83	0.93
800 kHz	1.00	0.37	0.77	0.95	**16 MHz**	1.01	0.37	0.83	0.93
900 kHz	1.00	0.37	0.78	0.95	**18 MHz**	1.00	0.38	0.83	0.92
1 MHz	1.00	0.37	0.77	0.95	**20 MHz**	1.00	0.38	0.84	0.92
1.2 MHz	1.00	0.37	0.77	0.95	**23.33 MHz**	1.00	0.38	0.80	0.99
1.4 MHz	1.00	0.37	0.77	0.95	**26.66 MHz**	1.00	0.38	0.81	0.98
1.6 MHz	1.00	0.37	0.77	0.95	**30 MHz**	1.00	0.38	0.86	0.97
1.8 MHz	1.00	0.37	0.77	0.95	**35 MHz**	0.70	0.57	0.71	0.93
2 MHz	1.00	0.37	0.77	0.95	**40 MHz**	0.60	0.72	0.74	0.92
2.333 MHz	1.01	0.37	0.77	0.95	**45 MHz**	0.40	0.83	0.60	0.92
2.666 MHz	1.01	0.37	0.77	0.95	**50 MHz**	0.40	0.85	0.63	0.93
3 MHz	1.01	0.38	0.77	0.95	**60 MHz**	0.30	0.91	0.64	0.92
3.5 MHz	1.01	0.37	0.77	0.95	**70 MHz**	0.10	1.07	0.62	0.94
4 MHz	1.01	0.38	0.77	0.95	**80 MHz**	0.00	1.18	0.63	0.94
4.5 MHz	1.01	0.38	0.77	0.95	**90 MHz**	0.00	1.23	0.64	0.92
5 MHz	1.01	0.38	0.78	0.95	**100 MHz**	0.00	1.41	0.64	0.92
6 MHz	1.01	0.37	0.78	0.95	**110 MHz**	0.00	1.58	0.75	0.92
7 MHz	1.01	0.38	0.78	0.95					

Appendix B

Monitoring the volume change of an unsaturated soil specimen in a single-wall acrylic cell can be challenging due to the following problems: (1) air compressed in the water filling the cell; (2) hysteretic response of cell wall in expansion/contraction; (3) deformation of flow tubes and connections; (4) creep of membranes and acrylic parts; (5) cell pressure and temperature fluctuations; (6) permeation and diffusion of water into outside atmosphere through membrane or acrylic parts. Initial attempts were made to calibrate the test system in order to possibly measure the volume change of unsaturated specimens. To address problem (1), a deaired device was installed beside the triaxial testing frame with the bottom of the de-air chamber slightly higher than the top of the triaxial cell so that the de-aired water can flow slowly to the cell. Moreover, the temperature was monitored and controlled to be 25 ± 0.5 °C and the cell pressure was applied through a software-controlled automated pump so that the pressure fluctuation was also minimized. A calibration test (without soil specimen placed) was designed to calibrate the other four problems. The test was set up with both top and bottom flow tubes open to the outside atmosphere. The calibration process was undertaken following three loading-unloading cycles of cell pressure as illustrated by the schedules in Figure B.1.

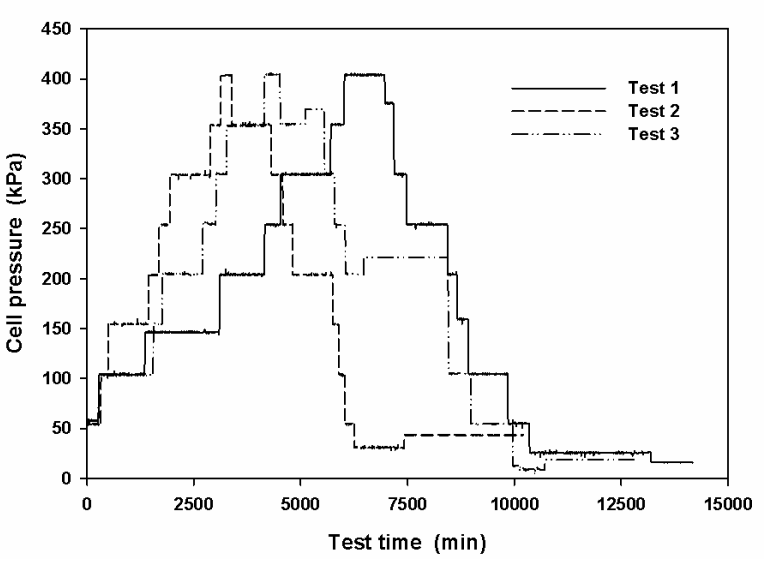

Figure B.1 Schedules of the three loading/unloading cycles

The relationship between the volume change contributed by the abovementioned problems and the cell pressure is presented in Figure B.2.

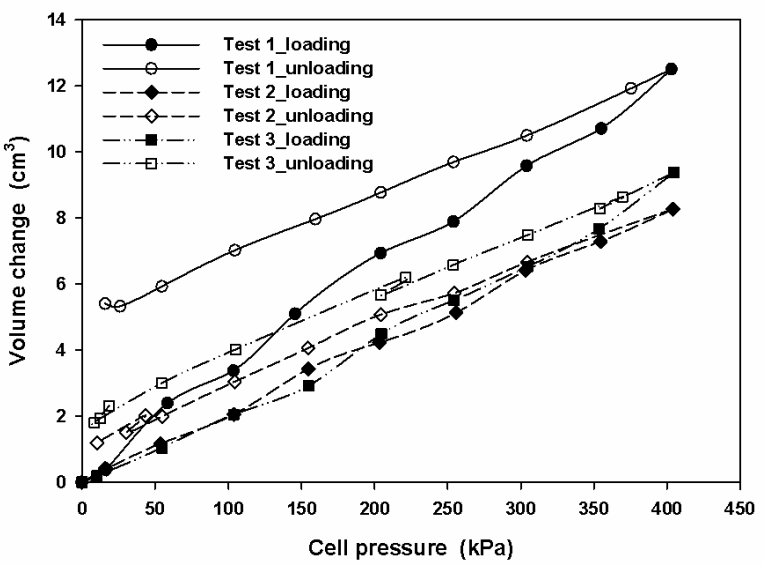

Figure B.2 Calibration of the test system for volume change

As can be observed from Figure B.2, no legitimate calibration scheme can be reasonably applied for specimen volume monitoring during a triaxial test. The hysteresis in each loading/unloading cycle exhibits a maximum volume change difference of about 5 cm^3. Moreover, the increase of cycles does not show any tendency of change, which implies the loading/unloading schedules have certain impact on the volumetric response of the test system. Lawrence (2004) showed similar phenomena of calibration curves on a single-wall test system while increasing the cell pressures up to 1000-1600 kPa. The volume change observed at 400 kPa, however, was around 30-65 cm^3, which is much greater than the magnitude in this study (7-12.5 cm^3), possibly due to the different acrylic cell used and no de-airing of water that filled the cell.

Problems associated with the calibration of a conventional single-wall system have been addressed by several researchers through adoption of a complex and specific test system (Ng et al. 2002, Leong et al. 2004, Padilla et al. 2006). Common features among these systems include a combined use of an advanced double-wall triaxial cell and the corresponding cell volume monitoring apparatus. Aluminum cell and bronze fixed tubes can be utilized to minimize deformation and creep (Ng et al. 2002) while a temperature sensor immersed in a reference cell can be used to adjust for the temperature effect (Leong et al. 2004). Automatic flushing device can be integrated for depleting accumulated diffused air in the high-air entry disks (Padilla et al. 2006). With the abovementioned approaches, no cell calibration is needed in regards to volume measurement of the unsaturated specimen. However, these systems require advanced design and machinery that are not immediately accessible.